Curative N-1 Security Restoration of Transmission Systems

A thesis submitted for the academic degree of

Doktor der Ingenieurwissenschaften (Dr.-Ing.)

at the

Faculty of Electrical Engineering and Information Technology

TU Dortmund Universsity

by

Dipl.-Ing. Martin Matthias Lindner

Supervisor: Univ.-Prof. Dr.-Ing. Christian Rehtanz, TU Dortmund University
Co-Advisor: Univ.-Prof. Dr.-Ing. Dirk Westermann, Technische Universität Ilmenau

Day of Oral Examination: 08.05.2026

Abstract

Congestion Management (CM) is a key task for German grid operators in light of the increasing integration of renewable energy sources and the simultaneous delay in grid expansion. To ensure N–1-secure operation, grid operators implement costly Remedial Actions (RAs) such as redispatch to resolve congestion.

Curative system operation promises to reduce these costs by implementing RAs not only preventively, i. e., before, but also curatively, i. e., after the occurrence of an N–1 contingency. The selection of suitable RAs is supported by numerical optimization models aiming to minimize CM costs.

This work presents a preventive-curative-restorative CM strategy (PrevCurRest) that extends existing approaches by including the restoration of N–1 security after an N–1 contingency. The resulting grid state is curatively N–1–1-secure. The modeling is based on a graph-based approach, which enables an intuitive coupling of various preventive and curative grid states within a mixed-integer linear program. To reduce complexity, approaches were developed to decrease the number of grid states to be considered.

A particular focus is placed on the integrated consideration of thermal reserves of overhead line conductors in two consecutive curative time windows within the optimization model.

Using the RTS-GMLC test system, various CM strategies are compared. The results show that the PrevCurRest strategy only slightly reduces the redispatch volume compared to a purely preventive approach, but comes with significantly higher model complexity. Nevertheless, it enables the restoration of N–1 security, which has, to the knowledge of the author, so far not been addressed in an integrated approach.

Kurzfassung

Engpassmanagement (EPM) ist eine zentrale Aufgabe deutscher Netzbetreiber angesichts des zunehmenden Ausbaus erneuerbarer Energien und des gleichzeitig verzögerten Netzausbaus. Um einen N–1-sicheren Betrieb zu gewährleisten, setzen Netzbetreiber kostenintensive EPM-Maßnahmen wie Redispatch ein, um Engpässe zu beheben.

Kurative Systemführung verspricht eine Senkung dieser Kosten, indem Maßnahmen nicht nur präventiv, d. h. vor, sondern auch kurativ, d. h. nach Eintritt eines N–1-Ereignisses, ergriffen werden. Die Auswahl geeigneter EPM-Maßnahmen erfolgt mithilfe numerischer Optimierungsmodelle mit dem Ziel, die EPM-Kosten zu minimieren.

Diese Arbeit stellt eine präventiv-kurativ-restorative EPM-Strategie (PrevCurRest) vor, die bestehende Ansätze um die Wiederherstellung der N–1-Sicherheit nach einem N–1-Ereignis erweitert. Der so erhaltene Netzzustand ist kurativ N–1–1-sicher. Die Modellierung erfolgt über einen graphenbasierten Ansatz, der eine intuitive Verknüpfung verschiedener präventiver und kurativer Netzzustände innerhalb eines gemischt-ganzzahligen Optimierungsmodells ermöglicht. Zur Komplexitätsreduktion wurden Ansätze entwickelt, die die Anzahl der zu berücksichtigenden Netzzustände verringern.

Ein Schwerpunkt liegt auf der integrierten Berücksichtigung thermischer Reserven von Freileitungsseilen in zwei aufeinanderfolgenden kurativen Zeitfenstern im Optimierungsmodell.

Am Beispiel des RTS-GMLC-Testsystems werden verschiedene EPM-Strategien verglichen. Die Ergebnisse zeigen, dass die PrevCurRest-Strategie das Redispatchvolumen im Vergleich zu rein präventiven Ansätzen nur geringfügig reduziert, jedoch mit einer deutlich höheren Modellkomplexität einhergeht. Dieser Nachteil wird teilweise ausgeglichen durch ein höheres Sicherheitsniveau gegenüber bisherigen N–1-sicheren Ansätzen.

Preface

This dissertation was written during my time as a research associate at the Institute of Energy Systems, Energy Efficiency and Energy Economics (ie³) at TU Dortmund University. The concluding phase coincided with the beginning of my employment at 50Hertz Transmission GmbH, which has contributed a practical perspective that is reflected throughout the thesis.

I would like to express my sincere gratitude to my doctoral advisor, Prof. Dr.-Ing. Christian Rehtanz, for his outstanding professional guidance and continuous support throughout my doctoral studies. My time at the institute has been highly instructive, offering valuable insights into the world of energy economics as well as numerous opportunities for personal and professional growth. I would also like to thank Prof. Dr.-Ing. Dirk Westermann for kindly agreeing to serve as the second reviewer.

I am profoundly grateful to my colleagues at the ie³-institute, especially Charlotte Biele, Dr. Marcel Klaes, Dr. Alexander Engelmann, Dr. Gösta Stomberg, for their invaluable guidance, thoughtful structuring of ideas, and for always asking the right questions. I also appreciate the stimulating discussions on curative congestion management and the collaborative spirit within the MILES working group, including Milijana Teodosic and Nils Offermann. My sincere thanks extend to the colleagues from the InnoSys 2030 project, in particular Dr. Andreas Wasserrab and Dr. Robert Schwerdfeger from TenneT, as well as Katharina Kollenda, Alexander Schrief, and Dr. André Hoffrichter from RWTH Aachen, for their constructive feedback and fruitful exchange of ideas. I am also thankful to my colleagues at 50Hertz, especially Roman Sikora, for providing valuable opportunities to discuss and refine concepts from a practitioner's perspective. I would also like to thank Prof. Dr.-Ing. Sven Cichos for his valuable feedback and thorough proof-reading of the manuscript.

I would like to extend my deepest thanks to my family, especially my wife Diana, for her unwavering support, patience, and encouragement throughout every stage of my doctoral journey. I am also deeply grateful to my parents and parents-in-law for their continuous support during this time.

Dortmund, September 2025

Martin Lindner

Contents

List of Figures

List of Tables

1. Introduction

1.1. Relevance

The energy transition in Germany has led to a significant change in the distribution of generators and loads. The increased share of Renewable Energy Sources (RES) has led to a more decentralized generation and a more volatile feed-in. The former grid infrastructure was mainly designed to connect conventional coal-fired and nuclear power plants to the load centers. RES, however, are often located in regions with a high potential for wind or solar power, which are often far away from the load centers. This leads to a higher utilization of the existing transmission grid. Grid expansion was significantly delayed in the past decade, especially for High Voltage Direct Current (HVDC) links between the north and south of Germany. Still, grid expansion will be an ongoing process for the next years to keep up with the increasing electrical demand and generation.

As a result, the increased utilization of the transmission grid leads to frequent congestion in the German transmission grid. In 2024, the redispatch volume in Germany amounted to 30.3 TWh at a cost of 2.9 billion Euro [1].

In this context, it is important to note that the European electricity sector is organized in a zonal market design, in which each bidding zone is a separate market area. Each market area is connected to neighboring bidding zones via interconnectors. During the market coupling process, the available transmission capacities of interconnectors are implicitely considered when clearing the individual zonal markets. Thus, while inter-zonal transmission capacities are implicitely considered in the market result, the intra-zonal transmission capacities are not considered in the market coupling process. This is to incentivice Transmission System Operators (TSOs) to extend their grid infrastructure accordingly and support cross-zonal trading. However, in a large bidding zone, such as Germany, in which the distribution of generation and load is rapidly changing, grid expansion is a time-consuming process.

To address the operational challenges that arise from delayed grid expansion, elaborated CM processes on national and European level aim at identifying and mitigating congestion. As for all grid operation processes, the TSO has to balance the trade-off between the security of supply, cost-effectivenes, and sustainability. Whereas the security of supply is usually handled by adhering to the N–1 security criterion, the cost-effectiveness is adressed by using

Security-Constrained Optimal Power Flow (SCOPF) methods that minimize the costs of RAs to mitigate congestion. The sustainability aspect is considered by carefully evaluating the costs and benefits of grid expansion and prioritizing RES infeed.

Different strategies of CM are applied to mitigate congestion in the transmission grid. The most common strategy is to use only preventive RAs, denoted as the Prev strategy, followed by a combination of preventive and curative RAs, denoted as the PrevCur strategy. In addition to the term "curative", the terms "corrective" and "post-fault" are also used in the literature to express that RA are carried out after the occurence of a contingency event.

In 2024, 85 % of the redispatch volume in Germany was caused by current limitations of transmission assets [1], which reflects the thermal asset constraints. The steady-state limit is imposed by the so-called Permanently Admissible Transmission Loading (PATL), whereas temporary limits are referred to as Temporarily Admissible Transmission Loading (TATL). By monitoring the ambient conditions and conductor temperatures of Overhead Lines (OHLs) conductors with Dynamic Line Rating (DLR) systems important developments were made to increase PATL limits.

The application of TATL is especially important for curative CM. In constrast to preventive CM, which ensures that PATL limits are not exceeded for any potential contingency, curative CM allows for a temporary exceedance of PATL limits due to the thermal inertia of grid assets. Immediate curative RAs must lower the currents in the affected assets below the PATL limits to avoid damage. By responding to each contingency individually, curative CM can reduce security margins that reduce the transmission capacity in the base case. Thus, curative CM can increase the utilization of grid assets and reduce the need for preventive CM.

However, increasing the overall loading of transmission assets can increase the system's vulnerability towards multiple, subsequent contingencies. Even if preventive curative RAs act adequately to a first contingency, the system may still be vulnerable to a subsequent contingency that occurs before N–1 security was fully re-established. Due to reduced security margins in the combined preventive-curative CM approach (PrevCur) compared with the preventive approach (Prev), the so-called restoration of N–1 security becomes more important, but even more challenging if to be handled by operators in real-time. Given the risen awareness for grid resilience, the restoration of N–1 security is a crucial aspect of curative CM that has not been addressed adequately so far. The associated preventive-curative-restorative CM strategy will be denoted as PrevCurRest in the following.

1.2. Research Problem

The TSOs are responsible for ensuring that the physical limitations of the grid are not violated in the base case (i. e. without contingency) and in the case of single-mode (N–1) and selected exceptional contingencies (N–k) [2]. The need for optimized RAs arises from complex task of maintaining the security of supply while minimizing the CM costs considering a large number of generation units, transmission assets and contingency scenarios. Without optimization, operators would have to manually assess the grid situation and decide on the most cost-effective RAs. Given the high costs, it appears reasonable to use optimization methods to minimize the costs of CM.

The optimization of RAs can be conceived as a notion of an Optimal Power Flow (OPF) problem. The objective is to minimize adjustments to Power Flow Controlling Devices (PFCs) and market schedules subject to the physical constraints of the grid and unit-specific constraints of market participants. Considering contingencies in the optimization problem leads to a so-called SCOPF formulation. While the preventive SCOPF has decision variables for the base case only, the curative SCOPF formulation has sets of decision variables for the base case and each contingency case. Preventive and curative decision variables are coupled as they act on the same set of PFCs and generators that are being optimized. Additionally, the preventively established base case loading of assets influences the thermal reserves during curative timeframes.

The research project InnoSys 2030 [3] investigated the potential of curative CM to lower the costs of CM in the German transmission grid while maintaining a high security of supply. The project developed detailed models for CM optimization and layed out the path for a future implementation of curative CM in the German transmission grid. The works published in [4], [5], [6] implemented the afforementioned properties of PrevCur strategy in a detailed SCOPF model. The authors proved that curative CM can lower the costs of CM in Germany significantly compared to Prev strategy. To consider different lead times of curative RAs, the authors introduced a distinction between slow and fast curative measures, which become fully effective after 2 min and 15 min after the contingency, respectively. The question of how to consider the thermal reserves in two consecutive curatives timeframes was not satisfactorily adressed. This work closes the gap by introducing polyhedral TATL constraints in the CM model.

A conceptual contribution of the InnoSys 2030 project is the System Operation Process that systemizes the stages of curative CM. Fig. 1.1 shows a derived version of the process from

[7] and [8].

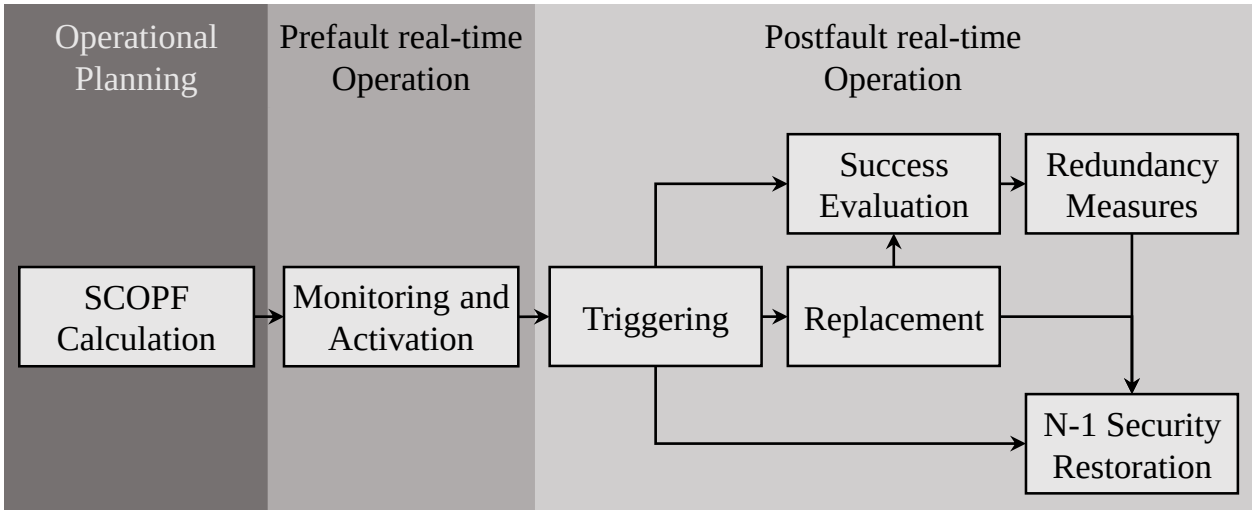

Figure 1.1.: InnoSys System Operation Process derived from [7], [8]

A description of the process is as follows: The initial operation planning phase conducts the SCOPF calculation and determines optimal preventive and curative RAs based on forecasted grid situations. To avoid unwanted triggering of curative RAs, the "Monitoring and Activation" phase enables the Supervisory Control and Data Acquisition (SCADA) system to monitor the triggering conditions of curative RAs. As soon as a triggering event occurs, the "Triggering" stages updates setpoints of all affected PFCs and units to the curative schedules. The "Success Evaluation" monitors, if the curative RAs were successful in avoiding grid overloads. In case of malfunction, redundancy measures are activated to avoid damage to grid assets. The "Replacement" phase ensures that temporary curative RAs, as in the case of Battery Energy Storage Systems (BESSs), are replaced by permanent measures. The final stage is the "N–1 Security Restoration". The scope of InnoSys 2030 stretched from the initial operation planning phase to the "Replacement" phase, in which the grid would be in an N–0 secure state. The restoration of N–1 security was to be handled by the TSO in real-time operation. This work incorporates the restoration of N–1 security in the CM optimization model allowing for a more accurate evaluation of the benefits of curative CM in terms of costs and grid resilience. The associated preventive-curative-restorative CM strategy will be denoted as PrevCurRest in the following.

By imposing N–1 security constraints on the system state after the implementation of curative RAs, the grid achieves so-called N–1–1 security. This means the system is not only able to withstand a primary contingency, but is also capable of handling a subsequent, secondary

contingency without violating operational limits. It is important to note that N–1–1 security is distinct from N–2 security, which requires the grid to withstand any two contingencies occurring *simultaneously*.

This work splits the overall SCOPF formulation into subproblems, called "grid situations", defined by their timestamps and sets of active contingencies. The grid situations are structured in a graph representation, in which the transitions between grid situations are defined by time and contingency events. The graph representation allows for intuitive modeling and visualization of internal and coupling constraints of the subproblems. Although, this work solves the overall SCOPF centrally, the graph representation allows for a future distributed solving approach, in which the subproblems are solved in parallel.

A focus of this work lies on the integration of BESSs in the curative CM optimization model. So far, TSOs assumed that curative CM would use dedicated BESSs "grid boosters") with predefined State of Charges (SoCs) and guaranteed flexibility potentials. The rising amount of BESS installations in the upcoming years provides the opportunitiy to use the flexibility potential of market-driven units for curative CM. Due to their fast response time, BESSs can be applied for fast curative RAs with almost no lead-time. The limited energy capacity, however, requires a replacement of the BESS by other measures after the curative timeframes. It is thus crucial to properly align the timing of subsequent RAs. Moreover, an accurate modeling of the SoC of BESSs is important to reliably estimate their flexibility potential. This work considers the time-coupling nature of BESSs in preventive and curative timeframes allowing for an accurate modeling of the SoC, which increases the potential combinations of curative and replacement measures.

In summary, the objectives of this work are:

1. Graph-based model of the CM optimization program under N–1–1 security requirements
2. Examplary comparison of preventive, preventive-curative, and preventive-curative-restorative CM strategies
3. Integration of polyhedral TATL constraints in the CM optimization model

1.3. Research Approach

So far, curative operation concepts strongly focus on the immediate responses to specific contingencies. The consequent utilization of redundancy measures shall prevent damage to grid assets in case of failed curative measures. However, the impact of an overall increased base case loading on the restorability of N–1 security has not been addressed so far.

To investigate the interplay between cost-efficient CM and grid security this work extends existing approaches for SCOPF with a focus thermal constraints and BESSs operation during curative timeframes. The proposed graph-based model lays the foundation for a future distributed optimization approach, in which the subproblems are solved in parallel. The simulation results of this work are based on a modified RTS-GMLC test grid [9]. The results prove the potential of curative RAs to lower the costs of CM and increase the preparedness towards subsequent contingency events.

1.4. Thesis Structure

Chapter 2 introduces key concepts of operational security and grid resilience, and situates CM within the framework of European regulations. In Chapter 3, the fundamentals of OPF and SCOPF are revisited, and the rationale behind the adopted Direct Current (DC) power flow approximation is discussed. The thermal behavior of OHL conductors and their incorporation into the SCOPF model for the PrevCurRest strategy are explored in Chapter 4. Modeling details and implementation aspects are detailed in Chapter 5. Finally, Chapter 6 analyzes simulation results based on a modified RTS-GMLC test grid, comparing the outcomes for different CM strategies. The work concludes with a summary and an outlook on future research topics in Chapter 7.

2. State of the Art of Congestion Management

This chapter explores the role of CM in ensuring the reliable and efficient operation of the power system. To provide context, the concepts of resilience, reliability, security, and robustness are first defined and distinguished. Subsequently, the present work is positioned within the framework of these concepts. The second part of the chapter reviews the state of the art in CM. It begins with an overview of the regulatory framework, followed by a discussion of various approaches to congestion handling, with a particular emphasis on curative CM.

2.1. Operational Security and Resilience

The purpose of this section is to position the present work within the context of operational security and resilience. Although definitions of these terms vary, the terms security, resilience, reliability, and robustness have distinct meanings in the context of power systems. The IEEE PES Task Force on "Methods for Analysis and Quantification of Power System Resilience" elaborated the right study designs for investigating each term [10].

The *robustness* of a system is perceived as an embedded and scenario-independent property to withstand disturbances in its environment without any active response of the system. Translated to power systems, robustness relates to the system components' design, e. g. the physical ability to withstand short-circuit currents. [10]

Reliability studies cover high-probability events with low to average impacts, that can happen regularly such as equipment failures. The reliability term is further divided into *adequacy* and *operational reliability*. Adequacy refers to the system's ability to meet the demand for energy incorporating supply uncertainties, while operational reliability refers to the system's ability to operate even if equipment is lost. Metrics such as System Average Interruption Duration Index (SAIDI), System Average Interruption Frequency Index (SAIFI), Loss of Load Expectation (LOLE), and Expected Energy Not Served (EENS) allow for retrospective reliability evaluation. Still, the metrics hide the underlying assumptions on the nature of the disturbances and the system's response. [10]

Resilience scenarios are characterized by low-probability events with high impacts, that are extremely rare and specific to the system under consideration, e. g. natural disasters. In ad-

dition to the internal system scope, resilience also considers the external environment, e. g. the impact and response of the society and other infrastructures. The authors of [10] characterize the relationship between reliability and resilience as a "feedback structure", where reliability studies provide metrics for day-to-day operation and resilience studies cover the response to extraordinary events. This means, that measures to enhance resilience can impact requirements for reliability and vice versa. [10]

The resilience definition of [10] is:

Definition 1 (Resilience)

> *"Power system resilience is the ability to limit the extent, system impact, and duration of degradation in order to sustain critical services following an extraordinary event. Key enablers for a resilient response include the capacity to anticipate, absorb, rapidly recover from, adapt to, and learn from such an event. Extraordinary events for the power system may be caused by natural threats, accidents, equipment failures, and deliberate physical or cyber-attacks."*
>
> *— Stankovic et al. [10]*

This resilience definition is sufficiently specific to be applied to power systems and broad enough to cover a wide range of extraordinary events.

The term *Security* refers to the system's ability to withstand a set of predefined contingencies without violating operational limits. The focus is on maintaining continuous operation at the same level of service, which distinguishes security from operational reliability. The N–1 criterion is a well-known example of a security measure. The power system is N–1 secure, if it remains within operational security limits after the occurence of a single contingency [2].

Definition 2 (Contingency) *"A 'contingency' means the possible or real loss of any grid element or a significant grid user, or […] any element of the distribution system which is relevant for the transmission system's operational security. This loss cannot be predicted in advance […]."*

> *— Methodology for Coordinating Operational Security Analysis (CSAM) [11]*

Operational limits are defined thermal, short-circuit current, voltage, protection and emission constraints of assets. In addition system limitations can be considered such as stability constraints and frequency limits.

The N–1 criterion has an overlap with the robustness definition when designing a grid layout, however, as the system conditions change permanently, N–1 security is not an inherent property but is achieved by operational measures. The popularity of the N–1 criterion is due to the fact that the list of potential contingencies consists only out of physical assets that are part of the system. It is therefore possible to continously verify and quantify the compliance with the N–1 criterion in real-time operation by means of Contingency Analyses (CAs). N–k criteria with $k > 1$ are less common, as the number of scenarios increases exponentially with k. The authors of [10] argue, that N–k security is economically inviable and that observed values for k in resilience events are higher than what can be covered by N–k evaluations. Still, N–k-constrained SCOPF and Unit Commitment (UC) methods are being under research [12], [13] with $k \leq 4$.

It should therefore be stated, that the N–1 criterion can only be regarded as an indicator for operational security under normal conditions, but not for resilience, as it does not cover extraordinary events and the system's ability to respond to them. Nevertheless, predefined reactions to contingencies, such as in curative CM, can be incorporated into security analyses.

The corresponding rulesets that require system operators to operate their grid according to the N–1 criterion are defined by the the North American Electric Reliability Corporation (NERC) standard TPL-001-5.1 on Transmission System Planning Performance Requirements [14] in North America and the System Operation Guideline 17/1485 (SOGL) [2] in Europe. The European regulatory framework will be further discussed in Section 2.3.1.

The SOGL applies the term *operational security* which is defined as

Definition 3 (Operational Security)

> *"'Operational security' means the transmission system's capability to retain a normal state or to return to a normal state as soon as possible, and which is characterised by operational security limits."*
>
> *— SOGL [2]*

In the *normal state*, all operational limits are satisfied both for the current system state and for all contingency scenarios. The definition of operational security is similar to the N–1 criterion but can also be applied to other security criteria such as N–2 or N–k. The reference to the system's capability to return to a normal state forms a transition to the resilience definition, making the concept of operational security an interface between security and resilience.

An attempt to include the system response into the N–1 criterion is the so-called N–1–1 criterion. The NERC standard TPL-001-5.1 [14] defines system conditions under which the power system shall operate reliably. The event categories P3 and P6 are defined by consecutive losses of a generator and a transmission asset, or two transmission assets, respectively. After the primary contingency the system shall continue to operate without iterrupting supply. After the secondary contingency the system shall remain stable but forced interruptions and load losses are acceptable. The time between the two contingencies can be used to take curative measures. This option distinguishes N–1–1 events from N–2 events, where two assets are lost at the same time.

Definition 4 (N–1–1 criterion) *The power system is N–1–1 secure, if it remains within operational security limits after the occurence of a primary and a secondary contingency. The time span between the primary and secondary contingency may be used to apply curative measures.*

The N–1–1 analyses according to TPL-001-5.1 are conducted annually, so they are not a part of daily operational planning processes. A framework to asses N–1–1 compliance is outlined in [15]. The authors of [16] point out, that TPL-001-5.1 does not specify a time span between the primary and secondary contingency. The authors propose a nested security-constrained UC method that considers the time span between the primary and secondary contingency to apply curative measures. In their case studies for a modified IEEE 118-bus system the authors of [16, P. 14] consider time spans of $2\,\mathrm{h}$ to $6\,\mathrm{h}$ between the primary and the secondary contingency.

Likewise, the European SOGL does not define a time span during which N–1 security must be re-established after the occurrence of a contingency. Article 35 of the SOGL requires a restoration of the normal state, in which N-1 security is maintained,"as soon as possible" [2]. Setting a time span would require the TSO to conduct N–1–1 analyses and prepare restorative RAs which is not common practice in Europe.

This is justified by current monitoring indicators: Regarding the annual Incidident Classification Scale Report [17], there is apparently no need for increased preparedness towards contingencies. The report lists 58 N–1 violations in 2023 in Central Europe, of which 37 where caused by generation and load forecasts errors but none by tripped grid elements [17, P. 21]. All N–1 violations were resolved within 10 h, 33 of them within 2 h, and 22 of them within 1 h [17, P. 35].

Given the apparent flexibility in real-time operations to resolve N–1 violations, the question arises as to the necessity of a provably N–1–1 secure operation. The authors of [17] argue, that N–1 violations mainly originate from uncertainties in generation and load forecasts and therefore underline the importance of accurate forecasts especially for extreme weather events. Both arguments are valid, but they do not address the question of whether the system is capable of adapting to a new power flow situation due to uncertainties or contingencies. The N–1–1 criterion can answer this question at least for ordinary N–1 contingencies. During extreme weather events, that potentially cause multiple simultaneous contingencies, the N–1–1 criterion is not applicable.

Still, an N–1–1 secure operation reduces the operational risks in case of subsequent single contingencies as restorative RAs are already prepared and can be applied immediately. Current operational procedures first try to handle the present situation before re-establishing a new N–1 secure state. The assessment and implementation of RAs in the new grid state is a highly manual process that requires the operator's attention and expertise. This work's approach spends the time between two contingencies to run another SCOPF for future time stamps and while the prepared restorative RAs establish an N–1 secure state. This reduces the time needed to restore the N–1 secure state and reduces the risk of human errors in the process.

To assess N–1–1 security compliance, commercial software tools are available. The N–1–1 module of the PowerWorld Simulator can run SCOPF calculations to find optimal curative RAs after the occurence of primary contingencies considering all potential secondary contingencies [18, P. 10]. The differentation between [18] and this work is, that the SCOPF in [18] is conducted individually for the primary contingencies, whereas this work's PrevCurRest model considers all base cases, primary and secondary contingencies at once. From the description in [18] it is not clear, if the initially provided input base case is required to be N–1 secure or how the software handles primary contingencies for which the SCOPF cannot determine RAs that create a feasible N–1–1 secure system state.

Fig. 2.1 illustrates the relationship between the security levels. If the system is N–1–1 secure, it is also N–1 secure, but not necessarily N–2 secure. N–1–1 security is a step forward

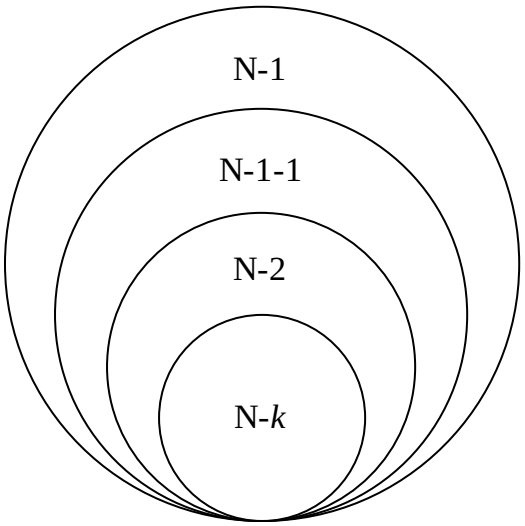

Figure 2.1.: Venn diagram of the security levels (own work)

from pure N–1 security evaluation to a more detailed analysis of the system's capabilities to recover from single contingencies. These capabilities remain in the context of reliability assessment and can only be regarded as one part of the resilience evaluation.

Table 2.1.: Comparison of Robustness, Reliability, Security, and Resilience

	Event Type	**Operator Activities**
Robustness	Unspecified disturbances	No active response
Reliability	High-probability, low/medium impact events	Design principles in grid planning and operation
Security	Predefined contingencies (N–1/N–k)	Planned preventive and curative RAs
Resilience	Low-probability, high-impact, extraordinary events	Adaptive, flexible response

2.2. Congestion management approaches

A common distinction between CM approaches is based on the implementation time of RAs. While preventive CM measures are implemented in anticipation of a trigger event that could lead to a limit violation, curative CM measures are executed after the event has occurred. Trigger events are typically contingencies, such as the loss of a transmission line or transformer. Additionally, sudden changes in generation or load can also act as triggers. Figure 2.2 illustrates the distinction between preventive and curative measures.

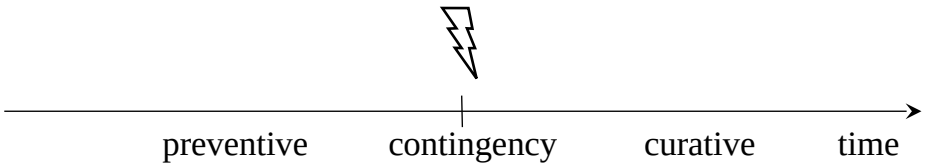

Figure 2.2.: Congestion Management Approaches

The following sections provide definitions and descriptions on congestion management, operational security and remedial actions. If not stated otherwise, the definitions are derived by the author based on his domain knowledge.

2.2.1. Preventive

Preventive RAs ensure that the grid can be operated without violating the operational limits in the normal state (N–0) and any relevant contingency scenario, typically N–1 contingencies. As preventive RAs are implemented in advance to contingency events, they establish a grid state that is robust against a set of potential contingencies. If CM is conducted entirely in the preventive time frame, the post-contingency state is theoretically permissible for indefinite time. Given the low probability of contingencies, preventive RAs decrease the available transmission capacity during normal operation to ensure grid security. Typically, a maximum base case loading of $70\,\%$ is assumed in transmission grids to maintain N–1 security [19]. As preventive RAs are optimized set of contingencies, the most critical contingency determines available transmission capacity under normal operating conditions.

The following definition is used in this work:

Definition 5 (Preventive RA) *Preventive RAs are taken in advance of potential, pre-defined contingencies to ensure grid security for normal operation and all relevant post-contingency scenarios. These measures originate from operational planning processes and are implemented during real-time operation.*

The costs for preventive RA are incurred regardless of whether the contingency occurs. Due to the lead times of thermal power plants, a significant portion of preventive RAs is already requested during day-ahead processes. Considering the high redispatch costs in Germany, efforts are made to further optimize preventive RAs with shorter lead times throughout the business day to account for changing generation conditions. Another approach involves the increased use of curative RAs, which are described in the following section.

2.2.2. Curative

Curative CM leverages the ability of assets to operate temporarily above their permanent operational limits. This approach allows for the adjustment of grid conditions following a (primary) contingency, ensuring that permanent operational limits are restored within the permissible time frame. Curative RAs are optimized alongside preventive RAs during operational planning. Their implementation occurs in real-time operation after the occurrence of predefined trigger criteria. Depending on the level of automation, curative RAs are executed either fully automatically by SCADA systems or on-site controllers (Special Protection Schemes), or manually by operators. For the purposes of this work, it is assumed that curative RAs are implemented fully automatically.

Curative RAs are tailored to individual contingencies, enabling a more efficient deployment of RAs compared to preventive CM. Due to the low probability of contingencies, the frequency of curative RAs deployment is also low. Since the costs of curative RAs are incurred only when a contingency occurs, they are generally more cost-effective than preventive RAs. Additionally, the use of temporary operational limits allows for higher asset utilization during normal operation, thereby increasing transmission capacity.

It is important to note that despite their secondary nature, curative RAs ensure compliance with the N–1 security criterion, as the fundamental principle remains that operational limits must not be exceeded under any circumstances. To distinguish between the two approaches,

the term “preventive N–1 security” is used when only preventive RAs are applied, while “curative N–1 security” refers to scenarios where curative RAs are also employed.

While the beginning of a curative RA is triggered by the occurrence of an event, the endpoint may not be obvious in real-time operation. According to the SOGL the system transitions from the N–1 situation to the new N-situation, when the normal state is restored, which includes N–1 security compliance [2, Art. 35 3.]. This means that, from the moment N–1 security is restored, new RAs are considered preventive.

It is to be mentioned that, the SOGL does not distinguish between curative and preventive RAs. However, the SOGL combines two post-contingency phases here: on the one hand, managing the N–1 situation, and on the other hand, returning to the N–1-secure state. For better conceptual distinction, this work considers *curative* RAs as those aimed at re-establishing an N–0-secure state. RAs beyond this, which aim at returning to the N–1-secure state, are referred to as *restorative* RAs. Note the terminological overlap with the term *restoration* used in the context of recovery from a blackout state. Once N–1 security is re-established and a new operational planning cycle is initiated, new preventive RAs can be applied.

Definition 6 (Curative Remedial Actions) *Curative RAs are automatically implemented following the occurrence of a predefined contingency to re-establish compliance with permanent asset limits in the post-contingency state (N–0 security). During curative RAs, assets may be temporarily operated within increased operational limits. Curative RAs are optimized during operational planning processes and executed in real-time operation.*

Definition 7 (Restorative Remedial Actions) *Restorative RAs are measures implemented after curative RAs to re-establish full compliance with the operational security criteria, specifically restorative the grid from the post-contingency (N–0) secure state back to an N–1-secure state.*

Figure 2.3 illustrates the timeframes of preventive, curative, and restorative RAs.

The curative RAs discussed in this work operate within the thermal time constants of assets, typically a few minutes, and can therefore be considered quasi-static. Beyond this, curative concepts can also be applied to dynamic scenarios to ensure compliance with stability limits. These concepts require different simulation and optimization approaches, which are not considered in this work.

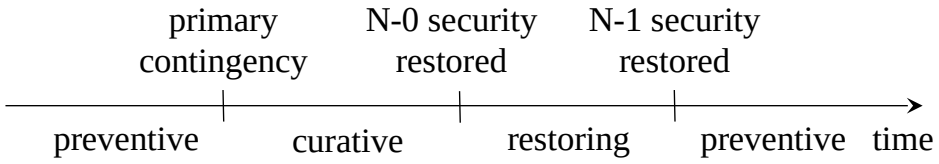

Figure 2.3.: Timeframes of remedial actions (own work)

2.2.3. Ad-hoc

Unlike preventive and curative RAs, ad-hoc RAs are not part of operational planning processes. These measures are determined based on real-time grid conditions. Currently, ad-hoc RAs are typically devised using the operators' experience and validated through simulation runs before manual implementation. Coordination with neighboring grid operators is carried out via telephone or dedicated communication systems. Ad-hoc RAs do not prioritize cost-optimality but address operational uncertainties and events in real-time. This approach forms part of the operators' routine activities and does not rely on extensive SCOPF calculations. This allows it to address the grid situation as-is, independent of forecasts and contingency scenarios. The increased uncertainties caused by fluctuations in generation and load highlight the need for enhanced decision-support tools to assist operators in mitigating critical grid situations. The focus on the existing grid state allows more accurate and less extensive optimization models, as the number of future and potential contingencies scenarios is drastically reduced.

2.3. Regulatory framework and operational processes

This section provides an overview of the regulatory framework and operational processes governing CM in the European and German electricity transmission systems. In the following, the main defintions and operational planning processes at the European and German

levels are outlined, illustrating how TSOs coordinate and implement RAs in practice.

Definition 8 (Congestion) *An asset is considered congested if the grid's power flow situation does not comply with the operational security limits of the asset in the normal state (N–0) and alert state (N–1 / N–k).*

— based on Definitions of Capacity Allocation and Congestion Management (CACM) [20, Art. 2] and SOGL [2, Art. 3]

Operational (security) limits can be imposed by the thermal, voltage, short-circuit, protection and emission constraints of the grid elements. Note, that a congestion does not necessarily mean that limits are surpassed in the current state, but that the grid element is potentially congested in case of a contingency.

The following provides a general definition of CM:

Definition 9 (Congestion Management) *CM bundles the processes required for congestion identification and mitigation. It includes the planning, coordination and execution of RAs to ensure that power flow situations comply with the operational limits of the grid elements.*

The way congestion is managed depends on the market design and the needs of the TSO. In nodal markets, the transmission capacities between grid nodes are respected during the allocation of trading bids. By conducting an OPF or SCOPF, an Independent System Operators (ISO) centrally optimizes the dispatch of generation units to minimize the total system costs. The locational prices create incentives to invest in generation capacities in areas with high demand and low transmission capacities. This reduces the need for grid expansion and also the need for RAs.

In contrast to the nodal market design, the zonal approach divides the power system into bidding zones, each with a uniform price and the assumption of unlimited transmission capacity within the zone. Cross-zonal exchanges are explicitly limited, resulting in identical prices within each zone but potentially different prices between zones. The European Union electricity market exemplifies this zonal design, where bidding zones typically align with national borders. Determining and integrating available cross-zonal transmission capacities into the market clearing process is a key aspect of European regulation, supporting the objective of a single European market that maximizes overall welfare. The regulatory framework governing this process is discussed in the following section.

2.3.1. European and German regulatory framework

The indiscrimantory pricing within bidding zones creates competitive and liquid markets, but lacks incentives for generation investments in the vicinity of high demand areas. The German bidding zone is an illustrative example: Most of on- and offshore wind generation is located in the north, while the load centres mainly located are in the south. The large distance with limited transmission capacities between these areas leads to frequent congestion that is resolved by redispatch measures. This involves the curtailment of generation units in the north and the activation of conventional generation units in the south, which is costly and increases the carbon footprint of the system. Other countries such as Sweden and Italy are split into several bidding zones to handle congestion more efficiently by respecting the transmission capacities between bidding zones in the market clearing process.

This work's focus is on the German CM processes, which are part of the European CM framework. The European CM framework is defined by multiple regulations, also denoted as *guidelines*. The operational implementation, often referenced as *methodologies*, is primarily carried out by the TSOs within the European Network of Transmission System Operators for Electricity (ENTSO-E) and approved by the European Union Agency for the Cooperation of Energy Regulators (ACER). In the following, the relevant regulations and methodologies are briefly described.

The European Regulation (EU) 2015/2022 on Capacity Allocation and Congestion Management (CACM) [20] focuses on the day-ahead and intraday cross-zonal exchanges with the goal of maximizing welfare. Contrary to what the name might suggest, the CACM does not regulate the operational CM but governs the exchanges between bidding zones. It therefore establishes methodologies for a common European grid model methodology, the flow-based capacity calculation, the market coupling, and cross-zonal RAs.

The main regulatory framework for the operational CM is the Regulation (EU) 2017/1485 SOGL [2]. It covers the operational security, operational planning, close to real-time operation, regional security coordination, outage coordination, load-frequency frequency control and reserves, scheduling between control areas, and training of system operator employees [21]. An important implementation of the SOGL is the CSAM [11], [22] according to Art. 75 SOGL.

Art. 18 of the SOGL classifies the five system states. The relevant properties in the context of CM are listed below:

- **Normal state**: Voltage and power flows are within operational limits for the current grid situation and all defined contingency situations after activation of RAs.
- **Alert state**: Voltage and power flows are within operational limits for the current grid situation, but at least for one contingency situation, operational limits are exceeded even after activation of RAs.
- **Emergency state**: Voltage and power flows violate at least one operational limit in the current grid situation.
- **Blackout state**: A TSO loses more than 50 % of its demand or total absence of voltage for at least 3 min in its control area.
- **Restoration state**: The system recovers from an emergency or a blackout state.

Note, that the transition from the normal state to the alert state is not the occurence of a contingency, but a non-compliance with operational limits in a potential contingency situation, which refers to the N–1 security criterion. Art. 25 states voltage, short-circuit current and thermal limits as operational limits. This also encompasses transitory limits, thereby enabling the use of TATL limits within curative RAs. This is further supported by Art. 32. The system state is determined at least every 15 min by a CA, that simulates the grid situation for all contingencies defined in a contingency list.

The contingencies are classified into three categories [22, Art. 7]:

- **Ordinary contingency**: Loss of a single branch or injection
- **Exceptional contingency**: Simultaneous loss of multiple branches or injections due to a common cause
- **Out-of-range contingency**: Simultaneous loss of multiple branches or injections without a common cause

The contingency list consists of ordinary and exceptional contingencies, that the TSO considers relevant for the operational security of its grid.

The operational handling of N–1 contingencies is defined in Art. 35 SOGL. In case of a contingency, the TSO shall activate RAs to restore the system to the normal state “as soon

as possible". The fact that the SOGL does not define a time frame for the restoration process indicates that the TSO has a certain degree of freedom depending on the current grid situation.

The Articles 20 to 23 SOGL cover the application of RAs [2]. Art. 21 SOGL sets out the following requirements to RAs:

- Adequate for ensuring operational security
- Coordinated with neighboring TSOs via Regional Coordination Center (RCC) or Regional Security Coordinator (RSC)
- Effectiveness and economical efficiency
- Activation as close to real-time as possible
- Failure risk assessment
- Keep as much cross-zonal capacity available as possible

Art. 22 SOGL lists different means of RAs to influence power flows and voltages, such as topology changes, Phase-Shift Transformer (PST) tap changes, shunt reactor or capacitor switching, HVDC adjustments, generation redispatch, countertrade, and eventually load shedding.

A detailed specification of measures to maintain operational security is provided by the CSAM [22], which defines preventive, curative, and "restoring" RAs. While preventive and curative RAs are part of the operational planning processes, restoring RAs are subject to operator decisions in real-time operation [11, P. 35].

The German legislation defined in the Energiewirtschaftsgesetz (EnWG) [23] is embedded in the European regulatory context.

2.3.2. Operational planning processes

Operational planning covers all processes that are preventively conducted by the TSOs to ensure a secure operation in Real-time (RT) denoted by the timestamp t. For this work, the Close to real-time (C2RT) activities, which are conducted in the last 30 min before the RT operation, are out of scope of the operational planning processes.

The legislative framework described in Section 2.3.1 is implemented by the European TSOs in multiple processes that are conducted on a daily basis. Both Capacity Calculation (CC) and CM processes are part of the operational planning.

Definition 10 (Operational Planning) *Operational Planning (OP) is conducted by grid operators to prepare RAs that ensure secure and reliable RT operation.*

Definition 11 (Real-time operation) *RT operation denotes all processes conducted and decisions taken by operational staff and automatic installations to operate the grid at any time.*

Sometimes the term C2RT is used to refer to preparational actions that are conducted in the last 30 min before the RT operation. In the context of this work, C2RT is part of the RT operation, as it is conducted outside of the operational planning processes.

The following section outlines the European and German operational planning processes. The implementation of the European processes varies depending on the respective TSO and their associated RCC/RSC, which act as coordinators between several TSOs. The German processes are carried out by the four TSOs Amprion, TenneT, TransnetBW, and 50Hertz. As there is no comprehensive public documentation of the German procedures, the description draws on the author's professional experience and domain knowledge. Figure 2.4 illustrates parts the European and German CM and CC processes for the Business Day D that are relevant in the scope of this work.

The European operational planning processes start at $D-2$ with the Two Days Ahead Congestion Forecast (D2CF), which identifies potential congestion based on forecasted Net Positions (NPs) epresenting the sum of imports and exports for each bidding zone. The purpose of the D2CF is the preparation of the flow-based domain in the Day-Ahead Capacity Calculation (DACC). This process determines the feasible domain of physical cross-zonal exchanges which is provided to the European wholesale markets. The Day Ahead (DA) auction closes at $D-1$ 12:00, after which market coupling is performed to optimally allocate the cross-zonal capacities among the bidding zones.

Once the results of the DA auction are published, market participants submit their generation and load forecasts to the TSOs by $D-1$ 14:30. Each TSO then builds its national Individual Grid Model (IGM) using the submitted forecasts and the latest grid topology. All national IGMs within an RCC are merged by an RSC to form a Common Grid Model (CGM).

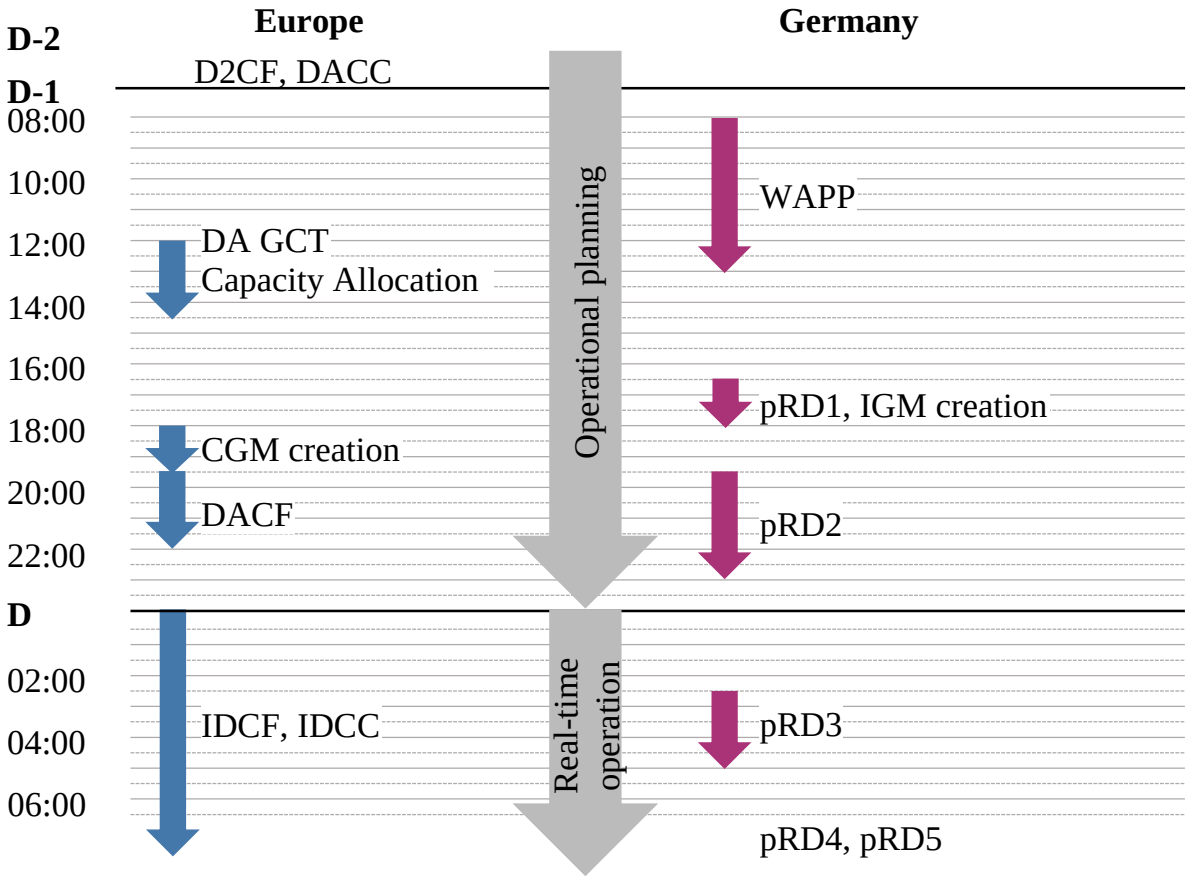

Figure 2.4.: European and German CM processes.

In the subsequent Day-Ahead Congestion Forecast (DACF), the RSC performs a Load Flow and Contingency Analysis (LF/CA) to assess power flows in the base case and all relevant contingency scenarios. At this stage, the CGM may still contain congestions. To resolve these, an iterative process is initiated: national TSOs propose RAs and incorporate them into their respective IGMs. The process of merging the updated IGMs into a new CGM, performing the LF/CA, and coordinating cross-zonal RAs is repeated until the CGM is free of congestion. Depending on the power flow situation, this process can take several hours.

The four German TSOs (Amprion, TenneT, TransnetBW, and 50Hertz) have established national operational planning processes. The Week-ahead Planning Process (WAPP) entirely relies on prognosis data as it is conducted before the European processes. The process identifies power plants with long lead times that must be activated before the European processes. The same applies to the Preventive Redispatch Process (pRD) pRD1, which acts on the basis of the DA auction results but lacks a CGM. The pRD2 process finally interacts with the DACF process to determine the final set of RAs for the Business Day.

The intraday processes on European level, Intraday Capacity Calculation (IDCC) and Intraday Congestion Forecast (IDCF), are similiar to the DA processes and are repeatedly conducted throughout the day. The IDCF is conducted hourly.

On a national level, the German TSOs run the pRD processes pRD3, pRD4 and pRD5 which are distributed over the day, to adjust the preventive RAs based on the latest generation and load forecasts.

Depending on the particular TSO, the degree of automation of the operational planning processes is very different. In Germany, the determination of RAs is supported by numerical optimization tools. To unify the national TSO processes across Europe, Art. 76 SOGL requires the TSOs to propose a methodology for the regional operational security coordination. For the Central European CORE Capacity Calculation Region, this is done by the CORE-ROSC methodology [24]. The Regional Operational Security Coordination (ROSC) consists of one day-ahead and multiple intraday Coordinated Regional Operational Security Analysiss (CROSAs). Each CROSA consists of multiple steps [24]:

- **CGM building**: The national IGMs are combined into a regional CGM containing the latest grid topology, generation and load forecasts.
- **Load flow and security analysis**: The CGM is used to calculate the power flows in the base case and all relevant contingency scenarios. The security analysis checks the compliance with the operational security limits.

- **Remedial Action Optimization**: A central time-coupled SCOPF is conducted by the RSCs for the hours of the Business Day to determine the optimal set of preventive and curative RAs. The degrees of freedom for the optimization are the generation redispatch, topology changes, and PFCs such as PSTs and HVDC links.
- **Inter-/intra Capacity Calculation Region (CCR) coordination**: The RSCs coordinate the implementation RAs with TSOs within the CCRs and with neighboring CCRs. In this phase, proposed RAs can be modified or rejected by the TSOs based on their local knowledge.

The CORE-ROSC methodology is currently being implemented by the TSOs in the CORE CCR. The optimization goals are ambitious, regarding the size of the CGM and the degrees of freedom. It is expected, that CORE-ROSC will simplify the coordination of RAs between the TSOs, but will not be able to fully replace national operational planning tools and processes.

2.4. Congestion Management strategies in this work

Based on the previously described terminology and the regulatory framework, this section introduces the three CM strategies considered in this work. The focus is on the preventive-curative-restorative strategy (PrevCurRest), which developed in this thesis. The other strategies, Prev, PrevCur, and PrevN2, are subsets of the PrevCurRest strategy and are used for comparison purposes in Chapter 6.

This thesis considers the CM strategies:

1. The *preventive* CM strategy (Prev) uses only preventive RAs and establishes a preventively N–1 secure grid state.
2. The *curative* CM strategy (PrevCur) applies curative RAs, and preventive RAs, to ensure a curatively N–1 secure grid state.
3. The *preventive-curative-restorative* CM strategy (PrevCurRest), which is the focus of this work, establishes an N–1–1 secure grid state. It extends the curative strategy by a restoration phase, which aims at re-establishing an N–1 secure grid state after a primary contingency event.

4. The *preventively N–2 secure* CM strategy (PrevN2) uses only preventive RAs to ensure a preventively N–2 secure grid state. This strategy is used as a benchmark to compare the performance of the PrevCurRest strategy.

2.5. Conclusion of the chapter

CM comprises a set of operational planning and real-time processes regularly conducted by grid operators to ensure secure operation in accordance with the regulatory framework. In the European and German context, CM is characterized by a complex interplay of national and international processes, designed to address the challenges of CM in a zonal market design. This section outlined the rationale behind guidelines (e.g., SOGL) and methodologies (e.g., CSAM). The notions of preventive, curative, and ad-hoc RAs were introduced, highlighting their roles in ensuring different levels of grid security (N–1, N–1–1, N–k).

3. Optimal Power Flow

The minimization of CM costs represents a particular instance of the broader OPF problem, which seeks the optimal operation of a power system subject to constraints such as Power Flow Equations (PFEs), asset limitations, and security requirements. In nodal market structures, OPF is commonly formulated to minimize total generation costs while respecting transmission constraints. The ISO typically solves the OPF, and its results determine generator dispatch and influence market clearing prices. The importance of efficient OPF solutions is underscored by initiatives like the ARPA-E Grid Optimization Competition, which aims to advance solution methodologies [25]. While OPF for CM is especially relevant in zonal markets, its outcomes also significantly affect operational costs and environmental impacts.

This chapter presents an overview of the OPF problem, its key components, and the modeling of PFEs. It further addresses current challenges and developments in OPF research, including the application of approximations and relaxations to enhance tractability.

3.1. Model components of Optimal Power Flow

The OPF problem lies at the intersection of power systems engineering and numerical optimization, and is an active area of research. Fundamentally, OPF seeks to determine optimal operational or planning decisions for power systems, subject to a range of constraints—most notably those capturing the physical laws governing the electrical grid. The generic OPF is a minimization problem with the decision variables $\mathbf{x} \in \mathbb{R}^{N_x}$, an objective function $f(\mathbf{x}) : \mathbb{R}^{N_x} \to \mathbb{R}$, a set of inequality constraints $\mathbf{g}(\mathbf{x}) : \mathbb{R}^{N_x} \to \mathbb{R}^{N_g}$, and equality constraints $\mathbf{h}(\mathbf{x}) : \mathbb{R}^{N_x} \to \mathbb{R}^{N_g}$:

$$\min_{\mathbf{x}} \quad f(\mathbf{x}) \tag{3.1}$$

subject to:

$$\mathbf{g}(\mathbf{x}) \leq 0 \tag{3.2}$$

$$\mathbf{h}(\mathbf{x}) = 0 \tag{3.3}$$

Table 3.1 provides examples of the typical components of OPF formulations. The objective function is typically a cost function that is minimized, but can also be a maximization problem. The variables are divided into decision variables and state variables. Decision variables are the degrees of freedom that can be controlled by the grid operator, whereas state variables are implicitely determined by the resulting power flow. The constraints are divided into fundamental constraints and additional constraints. The fundamental constraints are required to model the physical feasibility of the power flow and ensure compliance with basic asset limits. Depending on the particular OPF formulation, additional constraints can be added to ensure compliance with security, stability, reserve, and intersectoral requirements or consider stochastic uncertainties. Security constraints, which ensure that the system remains within operational limits under contingency conditions, define a class of OPF known as SCOPF. The two surveys of Capitanescu on OPF [26], [27] provide a comprehensive overview of OPF formulations and solution methods.

Among the fundamental constraints, the power flow constraints are of particular interest for all kinds of OPF problems, as the underlying PFEs are nonlinear and nonconvex, which characterizes the overall OPF problem. Section 3.2 describes the PFEs in detail and gives a brief overview of the approximations and relaxations.

Table 3.1.: Typical components of Optimal Power Flow formulations

Objective Functions	
Minimization of:	*Maximization of:*
Generation costs	Social welfare
Network losses	Transmission capacity
Redispatch costs	
Emissions	
Switching actions	
Load shedding	
Variables	
Decision Variables:	*State Variables:*
Generator active/reactive power	Voltage magnitudes and angles
Voltage setpoints	Active and reactive power flows
Transformer tap positions	Currents
HVDC setpoints	
Switching actions	
Setpoints of shunt devices	
Commitment status of generation units	
Constraints	
Fundamental Constraints:	*Additional Constraints:*
Power flow constraints	Intersectoral constraints
Power balance constraints	Stochastic constraints
Thermal asset constraints	Security constraints
Voltage magnitude constraints	Reserve requirements
Generator power constraints	Stability constraints

3.2. Power Flow Modelling

This section gives a brief introduction to the modelling of power flows in OPF formulations. Despite sharing the same branch model (Section 3.2.1), power flow calculation (Section 3.2.2) must be distinguished from branch flow equations used in OPF. Nevertheless, the PFEs are the basis for the DC-approximation (Section 3.2.4) and sensitivity-based approaches, that simplify the OPF problem. A comprehensive survey on representations of the PFEs, including their convex relaxations and approximations, can be found in [28].

3.2.1. Branch Model

Consider a balanced electrical network represented in single-line notation, comprising a set of buses $\mathcal{N} = \{1, \ldots, N_{\text{bus}}\}$ and a set of branches. The branches can be indexed either by $\mathcal{B} = \{1, \ldots, N_{\text{branch}}\}$ or by the ordered set of bus pairs $\mathcal{B}^{\text{E}} \subseteq \mathcal{N} \times \mathcal{N}$, where each branch is identified by the tuple (i, k) connecting bus i to bus k (short notation (ik)).

Each branch is represented by the Π-model shown in Fig. 3.1, which is a common representation used in power system analysis tools such as `MATPOWER` [29] and `PowerModels.jl` [30]. The branch model is suitable for electrically short branches, typically less than 300 km in length. In this section, all values are assumed to be in per unit (p.u.). The branch model and the subsequent equations of this section are derived from [29].

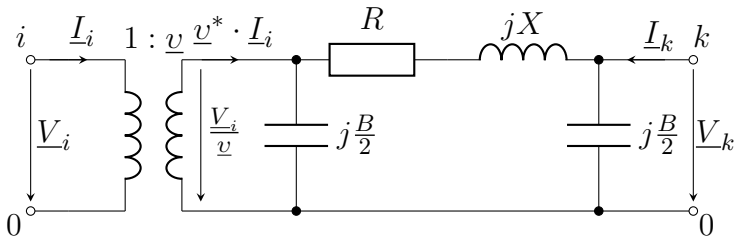

Figure 3.1.: Branch Π-model with all values in p. u.

The branch is represented by an ideal transformer with a complex transformation ratio $\underline{\upsilon} = \upsilon \cdot e^{j\theta}$ and a Π-section with shunt admittances $\underline{Y}_{i0}$ and $\underline{Y}_{k0}$, and a series admittance $\underline{Y}_{ik}$:

$$\underline{Y}_{i0} = \underline{Y}_{k0} = j\frac{B}{2} \tag{3.4}$$

$$\underline{Y}_{ik} = \frac{1}{R + jX} \tag{3.5}$$

The branch admittance matrix $\underline{\mathbf{Y}}_{\text{branch}}$ is defined as:

$$\underline{\mathbf{Y}}_{\text{branch}} = \begin{bmatrix} \frac{\underline{Y}_{i0} + \underline{Y}_{ik}}{\upsilon^2} & -\frac{\underline{Y}_{ik}}{\underline{\upsilon}^*} \\ -\frac{\underline{Y}_{ik}}{\underline{\upsilon}} & \underline{Y}_{k0} + \underline{Y}_{ik} \end{bmatrix}. \tag{3.6}$$

The currents $\underline{I}_i$ and $\underline{I}_k$ at the sending and receiving ends of the branch are related to the complex voltages $\underline{V}_i$ and $\underline{V}_k$ by:

$$\begin{bmatrix} \underline{I}_i \\ \underline{I}_k \end{bmatrix} = \underline{\mathbf{Y}}_{\text{branch}} \cdot \begin{bmatrix} \underline{V}_i \\ \underline{V}_k \end{bmatrix}. \tag{3.7}$$

3.2.2. Power Flow Equations

Following the notation of [28], let $\underline{\mathbf{v}} = \left(\underline{V}_1, \ldots, \underline{V}_{N_{\text{bus}}}\right)^\top \in \mathbb{C}^{N_{\text{bus}}}$ be the complex bus voltages, $\underline{\mathbf{i}} = \left(\underline{I}_1, \ldots, \underline{I}_{N_{\text{bus}}}\right)^\top \in \mathbb{C}^{N_{\text{bus}}}$ the complex bus injection currents, and $\underline{\mathbf{Y}} \in \mathbb{C}^{N_{\text{bus}} \times N_{\text{bus}}}$ be the bus admittance matrix. This leads to the so-called I-V-representation of the PFEs, which is given by:

$$\underline{\mathbf{i}} = \underline{\mathbf{Y}} \cdot \underline{\mathbf{v}}. \tag{3.8}$$

The elements $\underline{y}_{ik}$ of the bus admittance matrix $\underline{\mathbf{Y}}$ are defined as [28]:

$$\underline{y}_{ik} = \begin{cases} \underline{y}_i + \sum\limits_{m:(im)\in\mathcal{B}} \frac{\underline{y}_{i0} + \underline{y}_{im}}{\upsilon^2} + \sum\limits_{m:(m,i)\in\mathcal{B}} \underline{y}_{mi} & \text{if } i = k \\ -\frac{\underline{y}_{ik}}{\underline{\upsilon}^*} & \text{if } (ik) \in \mathcal{B} \\ -\frac{\underline{y}_{ik}}{\underline{\upsilon}} & \text{if } (k,i) \in \mathcal{B} \\ 0 & \text{otherwise} \end{cases} \tag{3.9}$$

with $\underline{y}_i$ being the shunt admittance connected to bus i.

The vector of injected apparent bus powers $\underline{\mathbf{s}} \in \mathbb{C}^{N_{\text{bus}}}$ is:

$$\underline{\mathbf{s}} = \underline{\mathbf{v}} \cdot \underline{\mathbf{i}}^* \tag{3.10}$$

$$= \mathbf{p} + j\mathbf{q} \tag{3.11}$$

Substituting the bus currents $\underline{\mathbf{i}}$ in 3.8 leads to the PFEs for the bus injection model:

$$\underline{\mathbf{s}} = \text{diag}\left(\underline{\mathbf{v}}\right) \cdot \underline{\mathbf{Y}}^* \cdot \underline{\mathbf{v}}^* \tag{3.12}$$

The separation into real and imaginary parts has different possible expressions (see [28]). To derive the DC-approximation in Section 3.2.4, the complex bus voltage is expressed polar and the bus admittance matrix in rectangular coordinates:

$$\underline{\mathbf{v}} = \mathbf{v} \cdot e^{j\phi} \tag{3.13}$$

$$\underline{\mathbf{Y}} = \mathbf{G} + j\mathbf{B} \tag{3.14}$$

This leads to the following PFEs:

$$P_i = V_i \sum_{k=1}^{N_{\text{bus}}} V_k \left(G_{ik} \cdot \cos\left(\phi_i - \phi_k\right) + B_{ik} \cdot \sin\left(\phi_i - \phi_k\right)\right) \tag{3.15}$$

$$Q_i = V_i \sum_{k=1}^{N_{\text{bus}}} V_k \left(G_{ik} \cdot \sin\left(\phi_i - \phi_k\right) - B_{ik} \cdot \cos\left(\phi_i - \phi_k\right)\right) \tag{3.16}$$

$$\forall i \in \mathcal{N}$$

3.2.3. Branch flow equations

In contrast to the PFEs, were a nonlinear system of equations is solved for the bus voltages with given bus injections, OPF formulations employ the branch flow equations to model the power flows resulting from the optimized bus injections. Using the branch model of Fig. 3.1, the branch flows are given by [30]:

$$\underline{S}_{ik} = \left(\underline{Y}_{ik} + \underline{Y}_{i0}\right)^* \frac{V_i^2}{\upsilon^2} - \underline{Y}_{ik}^* \cdot \frac{\underline{V}_i \cdot \underline{V}_k^*}{\underline{\upsilon}} \tag{3.17}$$

$$\forall (i,k) \in \mathcal{B}^{\text{E}}$$

$$\underline{S}_{ki} = \left(\underline{Y}_{ik} + \underline{Y}_{k0}\right)^* V_k^2 - \underline{Y}_{ik}^* \cdot \frac{\underline{V}_i^* \cdot \underline{V}_k}{\underline{\upsilon}^*} \tag{3.18}$$

$$\forall (k,i) \in \mathcal{B}^{\text{E}}$$

The expression in polar coordinates enables a simpler inclusion of the PST's transformation ratio υ and phase shift θ_{ik} compared to rectangular coordinates. Moreover, the polar coordinate expression is the basis for the DC-approximation in Section 3.2.4. The branch flow equations are given by [30]:

$$P_{ik} = (G_{ik} + G_{i0})\frac{V_i^2}{\upsilon^2} - G_{ik}\frac{V_i V_k}{\upsilon}\cos(\phi_i - \phi_k - \theta_{ik}) - B_{ik}\frac{V_i V_k}{\upsilon}\sin(\phi_i - \phi_k - \theta_{ik}) \tag{3.19}$$

$$P_{ki} = (G_{ik} + G_{k0})V_k^2 - G_{ik}\frac{V_i V_k}{\upsilon}\cos(\phi_k - \phi_i + \theta_{ik}) - B_{ik}\frac{V_i V_k}{\upsilon}\sin(\phi_k - \phi_i + \theta_{ik}) \tag{3.20}$$

$$Q_{ik} = -(B_{ik} + B_{i0})\frac{V_i^2}{\upsilon^2} + B_{ik}\frac{V_i V_k}{\upsilon}\cos(\phi_i - \phi_k - \theta_{ik}) - G_{ik}\frac{V_i V_k}{\upsilon}\sin(\phi_i - \phi_k - \theta_{ik}) \tag{3.21}$$

$$Q_{ki} = -(B_{ik} + B_{k0})V_k^2 + B_{ik}\frac{V_i V_k}{\upsilon}\cos(\phi_k - \phi_i + \theta_{ik}) - G_{ik}\frac{V_i V_k}{\upsilon}\sin(\phi_k - \phi_i + \theta_{ik}) \tag{3.22}$$

$$\forall (i,k) \in \mathcal{B}^{\mathrm{E}}, (k,i) \in \mathcal{B}^{\mathrm{E}}$$

3.2.4. DC-Approximation

The PFEs in Eq. (3.12) are inherently nonlinear and nonconvex. This nonconvexity implies that solutions to the PFEs may not be unique. Consequently, the solution to the OPF problem may also not be unique, and only local optimality can generally be guaranteed. To address this challenge, various convex relaxations have been developed that allow for the computation of a global optimum. The solution from a relaxation, however, may not be feasible for the original nonconvex PFEs; rather, it provides a lower bound on the optimal objective value. Relaxed solutions can also be used as initial points for local search methods to obtain feasible solutions. [28]

In contrast to relaxations, approximations simplify the PFEs but typically fail to preserve their physical properties. As a result, the practical feasibility of an OPF solution derived from an approximation is not guaranteed. Moreover, approximations do not provide any information about a lower bound for the optimal solution. Fig. 1.1 in [28] provides a visual comparison of relaxations and approximations.

A commonly used approximation is the DC-approximation, which simplifies the PFEs to

a linear representation and results in a linear OPF program. The DC-approximation assumes:

- Near-nominal voltage magnitudes $|\mathbf{v}| \approx 1\,\mathrm{p.u.}$
- Small voltage angle differences $\sin(\phi_i - \phi_k) \approx \phi_i - \phi_k$
- Neglectable reactive power flows $Q_i \approx 0$
- Neglectable resistance, $X \gg R$, i.e., $B_{ik} \approx \frac{1}{X_{ik}}$ and $G_{ik} \approx 0$

The PFEs Eqs. (3.15) and (3.16) reduce to:

$$P_i = \sum_{k=1}^{N_{\text{bus}}} B_{ik} \cdot (\phi_i - \phi_k) \tag{3.23}$$

$$Q_i = 0 \tag{3.24}$$

The branch flow equations Eqs. (3.19) to (3.22) simplify to:

$$P_{ik} = -\frac{B_{ik}}{\upsilon} \cdot (\phi_i - \phi_k - \theta_{ik}) \tag{3.25}$$

$$P_{ki} = -\frac{B_{ik}}{\upsilon} \cdot (\phi_k - \phi_i + \theta_{ik}) \tag{3.26}$$

$$\forall (i,k) \in \mathcal{B}^{\mathrm{E}}, (k,i) \in \mathcal{B}^{\mathrm{E}}$$

A detailed review of various DC-approximation variants is provided by [31]. The approach used here corresponds to the "cold-start DC model with fixed voltage," which demonstrated acceptable accuracy in the tests reported by the authors. Specifically, deviations between DC and Alternating Current (AC) power flow results were within $\pm 10\,\%$ for base cases [31, Fig. 6] and up to $\pm 14\,\%$ under contingency conditions in extra-high voltage networks [31, Fig. 10]. However, the accuracy of the DC-approximation is strongly influenced by the characteristics of the grid and its operating state. While no general rule exists for its precision, the DC-approximation remains a widely used approach for transmission system studies as it permits for a linear representation of the branch flow equations. The linearity enables the use of efficient optimization algorithms for linear programs (LPs) and Mixed-Integer Linear Programs (MILPs), which is particularly advantageous for large-scale systems.

3.3. Design Aspects of OPF Models

OPF models are used for a wide range of optimizing applications in grid planning and operational contexts. It is therefore common practice to adapt the modeling — which always represents an abstraction of reality — to the specific purpose of the application. In case of security constraints (N–1, etc.) in the formulation, it is common to denote this as a SCOPF. The design of an OPF model involves balancing *complexity* with the ability to represent system behavior with sufficient *accuracy*. The results produced by the optimization are inherently dependent on the model's assumptions and simplifications, and should therefore be regarded as a basis for informed decision-making rather than definitive solutions. This section discusses general design aspects of OPF models, focusing on aspects relevant for their use in operational planning of CM.

Main requirements for OPF/SCOPF models in CM are summarized below:

- *Feasibility*: The model must be able to find a feasible solution for the given grid situation, even if it is not optimal. This is crucial in operational planning, where the primary goal is to ensure system security.
- *Run-time*: The model must be able to solve the optimization problem within a reasonable time frame, typically within minutes, to allow for timely decision-making in operational planning.
- *Optimality*: While global optimality is not the primary goal, it is desirable to find a solution that is close to the global optimum. This is important as even small deviations from the optimal solution can lead to significant cost increases for CM.
- *Interpretability*: The model should be interpretable, allowing system operators to understand and trust the optimization results. This is essential for practical application as interpretability reduces the risk of misinterpretation and reduces the time for decision-making and coordination with neighboring TSOs.
- *Accuracy*: Voltages and currents are the main variables of interest in operational planning and should therefore be considered jointly in the optimization model. Another aspect is the representation of UC constraints.
- *Scalability*: The model should be capable of handling large-scale power systems efficiently, ensuring that solution times remain practical as the system size and complexity increase.

The prioritization of these requirements may vary depending on the specific application and context. Two central design decisions for OPF models in operational planning are the representation of discrete UC decisions and the representation of PFEs. These modeling choices define the resulting optimization problem class and directly influence the selection of appropriate solution algorithms, the choice of available numerical solvers, and the feasibility of leveraging parallel computation.

- **Modeling of discrete UC decisions**: Accurately representing UC is crucial in operational planning, especially for conventional generators whose availability for RAs depends on their commitment status. This is typically achieved using binary decision variables, resulting in a mixed-integer (MI) problem. While alternative linear approaches such as Big-M formulations exist, they can introduce numerical challenges.[28]
- **Modeling of PFEs**: Incorporating the nonlinear AC PFEs leads to a nonconvex, nonlinear program (NLP). To enhance tractability, convex relaxations—such as Semidefinite Program (SDP), Second Order Cone Program (SOCP), Quadratic Program (QP), or LP—are often employed, enabling the use of efficient solvers. However, solutions from relaxations may not always be physically feasible. Alternatively, approximations like the DC-approximation yield a convex linear formulation, allowing for fast solution via linear programming (LP). While this approach improves computational efficiency, it may compromise physical accuracy and feasibility. [28].

These two modeling choices can be generalized as follows: (i) whether the optimization problem includes binary decision variables (such as for discrete transformer tap positions), and (ii) whether nonlinear terms appear in the objective function or constraints.

Table 3.2 illustrates the possible program classes depending on the choice for the representation of UC and PFEs based on the work of [28].

Table 3.2.: Program classes of OPF models depending on the modeling of unit commitment constraints and power flow equations.

		UC	
		Linear	**Binary**
PFEs	**Exact**	NLP	MINLP
	Relaxed	QP / SOCP / SDP	MIQP / MISOCP
	Approx.	LP / SOCP	MILP / MISOCP

The most preferrable variant in terms of accuracy is to use binary decision variables for the UC and the full AC PFEs leads to a nonconvex mixed-integer nonlinear program (MINLP), which is generally difficult to solve.

An approach that uses binary UC variables and nonlinear PFEs, is described in [32], [33]. This approach follows a successive mixed-integer linear programming scheme, where the nonlinear PFEs are linearized around a feasible solution obtained from a previous iteration. This method allows for the inclusion of UC decisions while maintaining a tractable optimization problem. Intermediate power flow calculations enable feasibility checks of the solutions obtained from the MILP, enhancing robustness against poor initializations. While this approach is promising and has been adopted in the German operational planning tool "Redispatch-Ermittlungs-Server" (Redispatch Calculation Server), – from a practitioner's perspective – its performance regarding *run-time* and *scalability* for large-scale systems remains to be an issue, especially due to convergence issues during intermediate power flow calculations.

If binary UC variables are omitted and the nonlinear PFEs are retained, the resulting nonconvex Nonlinear Program (NLP) does not guarantee global optimality, and solutions may be sensitive to the bad initialization. Despite these challenges, large-scale NLP formulations of OPF and SCOPF have been successfully applied in practice [34].

As system size and complexity increase, solving such NLP formulations centrally becomes increasingly challenging due to timing, numerical, and memory limitations. This motivates the exploration of distributed and decentralized optimization techniques, which decompose the original problem into smaller, more manageable subproblems that can be solved in parallel. Decomposition routines such as *Benders decomposition* [35] have been successfully applied to AC SCOPF problems including binary variables [36], [37], [38]. Still, there are no convergence guarantees for nonlinear subproblems, so the *robustness* of the approach is limited. Staying with the aforementioned two-stage approach and focusing on the solving of the NLP part, different solution algorithms in the field of distributed and decentralized optimization are available offering convergence guarantees [39]. The objective of distributed and decentralized optimization is not per-se the reduction of the *run-time* of the optimization by parallelization, but finding an optimal solution to consensus problem in a setup with multiple agents, representing the subproblems, that do not have to share all their data with each other (*privacy* aspect), which is usually not the case in operational planning. The tested algorithms in this thesis include the distributed Augmented Lagrangian Alternating Direction Inexact Newton (ALADIN) method [40] and the decentralized Distributed Sequential

Quadratic Programming (dSQP) method [41]. Both suffered from numerical issues, which may be solved in future work. The popular Alternating Direction Method of Multipliers (ADMM) [42] was not tested, as it formally requires the NLP formulation to be convex, which is not the case for the nonlinear PFEs. Nevertheless, ADMM was successfully applied to AC SCOPF problems, e. g. in [43]. It remains an open question at what problem size the parallelization of the distributed solution outweighs the disadvantages of increased communication overhead compared to a centralized solution. A framework for applying distributed optimization algorithms to OPF problems is provided by [44].

A key consideration of the model design is the optimization *run-time* to find a *feasible* solution. As discussed in Section 2.3.2, the available time for decision-making is limited to a few hours in day-ahead planning processes. Due to the iterative nature of the planning process, the computation time for the optimization is limited to a few minutes. Today, most of the time is spent on data handling, result interpretation, and coordination among TSOs, Distribution System Operators (DSOs), and market participants. The CORE-ROSC methodology [45] aims to streamline these steps, potentially allowing more time for optimization, which is increasingly necessary as the size and complexity of the grid grow. Therefore, *scalability* is a key aspect of the model design. The afforementioned *decomposition* and *parallelization* approaches will gain relevance in practice. In this context, *privacy* concerns when sharing grid data among grid operators is of minor importance, as the optimization model relies on accurate grid data to produce meaningful results for coordination.

LPs are efficiently solvable using well-established algorithms such as the simplex method or interior-point methods, with polynomial-time performance guarantees for the latter. Modern solvers can routinely handle LPs with millions of variables and constraints, delivering globally optimal solutions with high reliability and speed. MILPs, which extend LPs by including integer or binary variables, are inherently more challenging due to their combinatorial nature. MILPs are NP-hard in general, and their solution time can grow exponentially with problem size and complexity. However, advances in solver technology — such as branch-and-bound, cutting planes, and heuristic methods — have significantly improved practical performance. State-of-the-art MILP solvers like Gurobi [46] and CPLEX can efficiently solve large-scale problems, especially when the model structure is exploited, but solution times remain sensitive to the number of integer variables and the tightness of constraints. For operational planning in power systems, MILPs offer a tractable balance between modeling fidelity and computational feasibility, provided that problem sizes remain within the practical limits of current solver capabilities. Alternatively, a relaxed version of

the PFEs may be used, leading to a mixed-integer quadratic program (MIQP), which is more tractable for many solvers, but comes with the afforementioned limitations.

If optimization model is intended to be used in day-to-day operations, it must be *robust* against unfavorable initialization and offer convergence guarantees under predefined conditions. This is particularly important for nonconvex, nonlinear models (e. g. with full AC PFEs), where convergence to a local optimum can depend on the initial values of the decision variables.

Quality aspects of the optimization results are their *interpretability* and *trustworthiness* from the perspective of human operators. In practice, implementing RAs often requires manual adjustments to ensure that the proposed actions are manageable. For example, several small redispatch measures may be aggregated into a single action involving only one generator. While such manual interventions may reduce the optimality of the solution, they enhance its practical feasibility in operations. A formulation of such "operator-friendly" constraints is difficult to achieve in an optimization model, as it usually requires additional binary decision variables and complex constraints to limit the number of redispatch RA actions.

The scope of CM optimization in Germany has traditionally been limited to *current* limits, whereas *voltage* limits are not considered. This is due to the fact that voltage control is primarily a local issue, and the optimization model focuses on the global grid state. However, as reactive power control becomes increasingly important with the phase-out of synchronous generators, it is increasingly important to consider voltage limits in the optimization model to obtain *accurate* results. Neglecting reactive power flows underestimates the thermal loading of assets, which needs to be accounted for by security margins.

As redispatch is the predominant RA in Germany, a key aspect is an accurate representation of the *UC* of generators. This includes the modeling of minimum up- and down-times, as well as the ramping capabilities of generators. Such constraints involve binary decision variables, which requires a mixed-integer formulation of the optimization model. An alternative approach is to use relaxed LP formulations with a penalization of binary constraint violations. This approach is acceptable in grid planning studies, where a multitude of scenarios is considered and LP formulations are sufficiently accurate. However, in operational planning, where the focus is on operational feasibility, the use of binary decision variables is necessary.

Another design aspect is the representation of *stochastic uncertainties* in the optimization model. In practice, uncertainties between the time of optimization and the actual operation

are accounted for by security margins, which are substracted from the physical transmission limits of the grid elements. Depending on the choice of the security margins, this approach may be over-conservative, leading to increased RAs costs, or over-optimistic, leading to increased burdens for real-time operation. Moreover, conservative security margins may lead to a significant reduction of the real thermal reserves available for curative CM in real-world applications. To address uncertainties in operational planning, stochastic models and optimization techniques are necessary, particularly when there are several hours between planning and real-time operation. One way to mitigate these uncertainties is to shorten the lead times of optimization runs, enabling the use of the most recent load and generation forecasts. However, this approach also imposes stricter requirements on the permissible computation times.

3.4. Conclusion of the chapter

OPF is a fundamental optimization problem in power system operation. This chapter has provided an overview of the mathematical formulation of the OPF problem, its typical components, and the modeling of the PFEs, including both the full AC and simplified DC representations. The discussion highlighted the inherent trade-offs between model complexity, computational tractability, and physical accuracy, which are central to the design of OPF models for operational planning.

Key aspects such as the inclusion of discrete UC decisions, the choice between nonlinear and linearized PFEs, and the handling of uncertainties and security constraints were examined. The OPF model's design determines the class of the optimization problem, influencing the selection of solution techniques and the feasibility of real-time applications.

Furthermore, this chapter emphasized the significance of interpretability and scalability in the design of OPF models, especially for operational planning applications that require timely and dependable solutions. Ultimately, the development of OPF models involves balancing feasibility, optimality, computational efficiency, and accuracy to meet the practical needs of power system operation.

4. Thermal degrees of freedom of overhead conductors

The primary constraint on transmission capacity is typically the thermal limit of the asset, which restricts the permissible current to prevent the conductor from exceeding its maximum allowable temperature. Surpassing this temperature accelerates aging and increases the risk of failure due to excessive sag. Additional constraints may arise from system stability, protection equipment, or electromagnetic compatibility, with the most restrictive factor determining the operational current limit. This section examines the thermal behavior of Overhead Line (OHL) conductors and presents an approach for considering temporary current limits in two consecutive timeframes for curative CM.

4.1. Thermal behavior of overhead line conductors

The thermal behavior of OHL conductors is a well-studied subject. The European standard EN 50182 [47] specifies thermally admissible currents $I_{\text{th,max}}$ that ensure the maximum conductor temperature ϑ_{max} is not exceeded. These values are determined for an ambient temperature of $\vartheta_{\text{a}} = 35\,°\text{C}$, a wind speed of $v_{\text{W}} = 0.6\,\text{m/s}$, and global solar radiation of $Q_{\text{se}} = 900\,\text{W/m}^2$, which is a conservative rating for most of the year in Central Europe.

Often, the weather conditions are more favorable, offering better cooling for the OHL conductors. Thus, various Dynamic Line Rating (DLR) methods have been developed to adapt the ampacity of conductors accordingly. At their core, DLR systems use thermal conductor models, as outlined in foundational studies [48], [49], and later refined in standards and guidelines [50] and [51]. These models derive the conductor temperature from its Heat Balance Equation (HBE), which sums up all heating and cooling factors acting on the conductor, including the Joule heating caused by ohmic losses.

In operational settings, the weather data is acquired by forecast or real-time data. For validation or calibration purposes, the conductor temperature can additionally be measured by direct or indirect sensors. Due to additional costs and the complexity of the installation, temperature measurements are only applied in a few cases. For many grid operators, the application of model-based DLR is state of the art in grid planning and operation. The German TSOs incorporate DLR up to $1.5 \cdot I_{\text{th,max}}$ during grid expansion planning [52].

This work applies the definitions and notations of the thermal conductor model of standard IEEE 738-2012 [51]. The equations in the remainder of this section are taken over from [51]. The dynamic HBE is given by Eq. (4.1):

$$\frac{\mathrm{d}\vartheta_{\mathrm{avg}}(t)}{\mathrm{d}t} = \frac{1}{m \cdot C_{\mathrm{p}}} \left(q_{\mathrm{J}} + q_{\mathrm{S}} - q_{\mathrm{C}} - q_{\mathrm{R}}\right) \tag{4.1}$$

In this expression, ϑ_{avg} denotes the average conductor temperature. Note that all variables on the right-hand side are expressed on a per-unit-length base. Here, m signifies the mass of the conductor, C_{p} stands for its specific heat capacity, q_{J} denotes the Joule heating effect, q_{S} corresponds to the solar heating, q_{C} refers to the convective cooling, and q_{R} represents the radiative cooling component.

Joule heating The quadratic relationship between the conductor current I and the Joule heating q_{J} is expressed in Eq. (4.2).

$$q_{\mathrm{J}} = R_{\mathrm{AC}}(\vartheta_{\mathrm{avg}}) \cdot I^2 \tag{4.2}$$

R_{AC} symbolizes the resistance per unit length at the current conductor temperature, including a correction factor for the skin effect at standard operating frequency.

Solar heating The solar heating q_{S} depends on the conductors absorptivity α, the altitude-corrected global radiation Q_{se}, incidence angle of the sun's rays θ_{s}, and the conductors diameter D_0 [51, Eq. 8]:

$$q_{\mathrm{S}} = \alpha \cdot Q_{\mathrm{se}} \cdot \sin\theta_{\mathrm{s}} \cdot D_0. \tag{4.3}$$

A detailed location- and time-dependent calculation of the global is described in [51, Sec. 4.5]. This method is later applied in Section 6.3 to determine the solar heating for the Reliability Test System of the Grid Modernization Laboratory Consortium (RTS-GMLC) test system.

Convective cooling Convective cooling encompasses natural and forced convection. For a detailed description, the reader is directed to [51] and the associated references therein. The heat loss by forced convection is approximated by Eq. (4.4) and Eq. (4.5). [51] recommends

using the highest value of q_{C1} and q_{C2}.

$$q_{C1} = \left(1.01 + 1.35 \cdot {N_{Re}}^{0.52}\right) \cdot K_{\phi}(\phi_w) \cdot k_f \cdot (\vartheta_s - \vartheta_a) \tag{4.4}$$

$$q_{C2} = 0.754 \cdot {N_{Re}}^{0.6} \cdot K_{\phi}(\phi_w) \cdot k_f \cdot (\vartheta_s - \vartheta_a) \tag{4.5}$$

Here, N_{Re} denotes the dimensionless Reynolds number, $K_{\phi}(\phi_w)$ is the wind direction factor depending on the angle between the conductor and the wind direction ϕ_w, k_f corresponds to the thermal conductivity, ϑ_s refers to the conductor's surface temperature, and ϑ_a signifies the ambient temperature.

The heat loss due to natural convection q_n, which is predominant at low wind speeds, is described by Eq. (4.6).

$$q_n = 3.645 \cdot {\rho_f}^{0.5} \cdot {D_0}^{0.75} \cdot (\vartheta_s - \vartheta_a)^{1.25} \tag{4.6}$$

The air density is denoted by ρ_f. It is important to note that N_{Re}, ρ_f, and k_f are functions of the conductor's film temperature ϑ_{film} (Eq. (4.7)), which itself is influenced by the current I.

$$\vartheta_{film} = \frac{\vartheta_s + \vartheta_a}{2} \tag{4.7}$$

The value to be used in 4.1 is:

$$q_C = \max\{q_{C1}, q_{C2}, q_n\} \tag{4.8}$$

Radiative cooling The radiative heat transfer takes place between the conductor's surface and the surrounding, whose temperature is assumed to be the ambient temperature ϑ_a in °C. Eq. (4.9) follows the Stefan-Boltzmann law:

$$q_R = \pi \cdot \sigma \cdot D_0 \cdot \epsilon \cdot \left((\vartheta_s + 273)^4 - (\vartheta_a + 273)^4\right) \tag{4.9}$$

The Stefan-Boltzmann constant is denoted by σ and ϵ refers to the conductor's emissivity factor. As ϑ_s and ϑ_a are in °C, they are converted into K. The Permanently Admissible Transmission Loading (PATL) can be determined by solving Eq. (4.1) for I_{PATL} under steady-state conditions, i.e., for specified conductor and weather parameters and a given

conductor temperature ϑ_{avg} with $\frac{\mathrm{d}\vartheta_{\text{avg}}(t)}{\mathrm{d}t} = 0$.

$$I_{\text{PATL}} = \sqrt{\frac{q_{\text{C}} + q_{\text{R}} - q_{\text{S}}}{R_{\text{AC}}(\vartheta_{\text{avg}})}} \tag{4.10}$$

Accounting for dynamic thermal processes necessitates solving the differential equation in Eq. (4.1), which is a first-order Ordinary Differential Equation (ODE). Notably, the radiative cooling term in Eq. (4.9) introduces significant nonlinearity, and the calculation of q_{C} in Eq. (4.8) can result in discontinuities under varying weather conditions. For the determination of admissible Temporarily Admissible Transmission Loading (TATL), it is common practice to assume constant environmental parameters while the current undergoes a step change. Given a current step ΔI, a specified postfault duration τ, and an initial conductor temperature $\vartheta_{\text{avg},0}$, an approximate solution for $\vartheta_{\text{avg}}(t)$ is provided in [53]. However, to the best of the author's knowledge, a general closed-form solution to Eq. (4.1) does not exist, and numerical methods are typically employed.

4.2. Determination of line ratings

This section outlines the method for determining PATL and TATL values for OHL conductors and discusses the impact of short-circuit heating. Exemplary ratios are presented to illustrate the dependencies of TATL limitations.

4.2.1. Thermally effective current

The DC-approximation applied in this work (Section 3.2.4) implies that only active power flows are considered. Equally, the current I represents the signed active current, with positive values indicating a flow from the sending to the receiving end of a branch. Neglecting reactive power flows may lead to inaccurate results for the thermal behavior of the conductor, as the Joule heating depends on the absolute value of the apparent current $|\underline{I}|$. To account for this, active current I may be multiplied by a factor $k_{\text{Q}} \geq 1$ to obtain the thermally effective current $I_{\text{th}} \in \mathbb{R}$.

$$I_{\text{th}} = k_{\text{Q}} \cdot I \tag{4.11}$$

For clarity in the following sections, the term *loading* $l \in \mathbb{R}$ refers to the ratio of the thermally effective current to the PATL, i.e., the current I_{th} normalized by $I_{\text{PATL}} \in \mathbb{R}^{+}$.

$$l = \frac{I_{\text{th}}}{I_{\text{PATL}}} \tag{4.12}$$

4.2.2. Short-circuit heating

An important consideration for curative CM is the adiabatic heating of assets during the short-circuit. Assuming a three-phase fault-clearing time of $150\,\text{ms}$, returned a worst-case estimate for the temperature rise of $\Delta\vartheta_{\text{SC}} = 5\,\text{K}$ [54], which imposes a temperature margin for the prefault case. For consistency reasons with subsequent chapters, the prefault loading is equivalent to the loading in the base case and is denoted as l_{base}. As a consequence of the short-circuit heating, base loading must be below $100\,\%$ to ensure that the conductor temperature does not exceed the maximal temperature right after the short-circuit event. This can be proven by the example in Fig. 4.1.

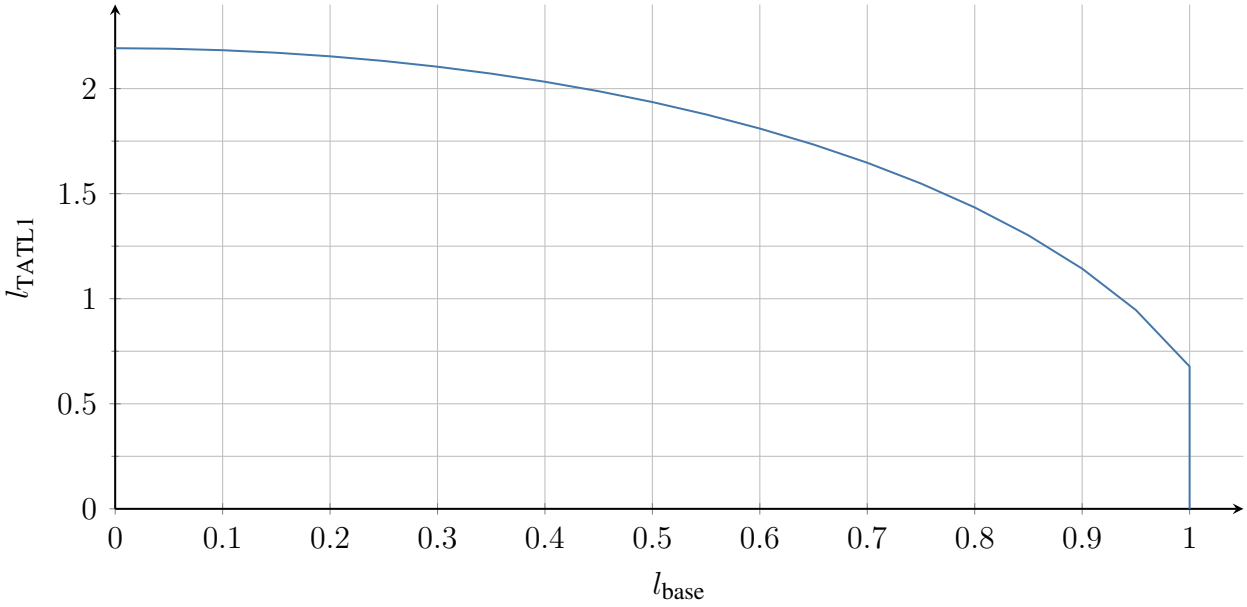

Figure 4.1.: Feasible TATL1 domain for conductor type 264-AL1/34-ST1A at standard weather conditions and a curative postfault duration of $\tau_1 = 2\,\text{min}$.

4.2.3. Calculation routines

The IEEE standard 738-2012 [51] provides an exemplary implementation for calculating steady-state and transient conductor ratings. Recent publications in [54], [55] revisit the usage of thermal conductor models to calculate dynamic line ratings. The so-called *TATL-Tool* presented in [54], [56] employs the MATLAB single-step ODE solver `ode23` [57], [58] for solving the HBE. Finding the current I_{TATL} that gives $\vartheta_{\mathrm{avg}}(\tau) = \vartheta_{\mathrm{max}}$ for a given post-contingency time τ requires iterative root-finding methods such as Bisection, Regula Falsi, or Newton's Method. For this purpose, MATLAB provides the function `fzero` based on [59]. For this work, the author implemented the package `TATLPATL.jl`, which is an equivalent version of the *TATL-Tool* [56] in Julia [60].

4.2.4. Exemplary TATL-PATL ratios

Figure 4.2 illustrates the relationship between the permissible postfault loading $l_{\mathrm{postfault}}$, the base loading l_{base}, and the duration of the postfault condition τ. The graph reveals a rapid decrease in $l_{\mathrm{postfault}}$ as τ increases, reflecting the near-exponential rise in conductor temperature following a current step. Concurrently, higher base loading values constrain the permissible postfault loading. These findings suggest that rapid response of curative CM actions is crucial to optimally leverage the thermal reserves of OHL conductors.

4.3. TATL constraints in SCOPF models

The difficulty of incorporating the conductor temperature ϑ_{avg} as a direct constraint is twofold: Firstly, its non-linearity prevents a favorable linear formulation of the overall optimization program. Secondly, there is no closed-form solution of the HBE (Eq. (4.1)) and, consequently, no functional dependency $\vartheta_{\mathrm{avg}}(t) = f\left(t, I(t)\right)$ that would allow for an evaluation of the conductor temperature at each point in time and for arbitrary current profiles during the optimization process. As a result, the curative timeframes need to be discretized, with the number of timeframes depending on the desired granularity for modeling curative RAs.

In accordance with the InnoSys 2030 project, this work chooses two consecutive curative timeframes with $\tau_1 = 2\,\mathrm{min}$ for the Temporarily Admissible Transmission Loading for the first curative timeframe (TATL1) and with $\tau_2 = 13\,\mathrm{min}$ for the Temporarily Admissible

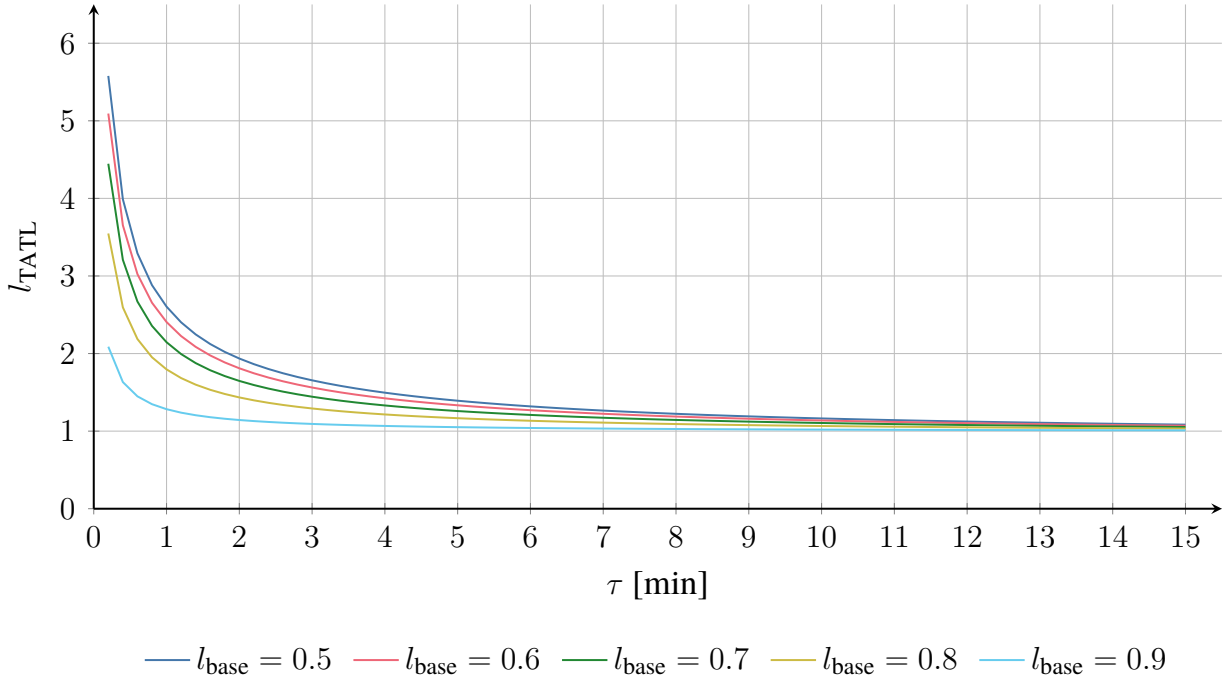

Figure 4.2.: Permissible TATL loading l_{TATL} for different base case loadings $l_{\text{base}} \in \{0.5, 0.6, \ldots, 0.9\}$ for conductor type 264-AL1/34-ST1A at standard weather conditions for curative durations $\tau \in 0.2\,\text{min}$ to $15\,\text{min}$.

Transmission Loading for the second curative timeframe (TATL2). These timeframes account for curative RAs with fast and slow response times, respectively [3].

Figure 4.3 provides an example of the conductor temperature $\vartheta_{\text{avg}}(t)$ for a 264-AL1/34-ST1A conductor at standard weather conditions (ϑ_{a}=35 °C, v_{W}=0.6 m/s, Q_{se}=900 W/m^2) for the two curative timeframes. The initial loading is set to $l_{\text{base}} = 0.75$. The short-circuit heating is approximated by a temperature step $\Delta\vartheta_{\text{SC}} = 5\,\text{K}$. The permissible loading for the first curative timeframe $0 \leq t < \tau_1$ is $l_{\text{TATL1}} = 1.47$ for which $\vartheta_{\text{avg}}(t = \tau_1) = \vartheta_{\text{max}}$. In the example, the loading of the first curative timeframe is limited to $l(0 \leq t < \tau_1) = 1.1$, which increases the conductor temperature to $\vartheta_{\text{avg}}(t = \tau_1) = 72.5\,°\text{C}$. Based on this temperature, the permissible loading for the second curative timeframe $\tau_1 \leq t < \tau_2$ is $l_{\text{TATL2}} = 1.03$. Assuming $l(\tau_1 \leq t < \tau_2) = l_{\text{TATL2}}$, the conductor temperature $\vartheta_{\text{avg}}(t = \tau_2) = \vartheta_{\text{max}}$. For $t \geq \tau_2$, the loading is limited to 1, which is the PATL for the given conductor type and weather conditions.

As the HBE is a first-order ODE, $\vartheta_{\text{avg}}(t)$ is continuous and imposes a coupling constraint in OPF programs between consecutive timestamps. Because of the nonlinear nature of the HBE, temperature changes induced by current changes cannot be superpositioned.

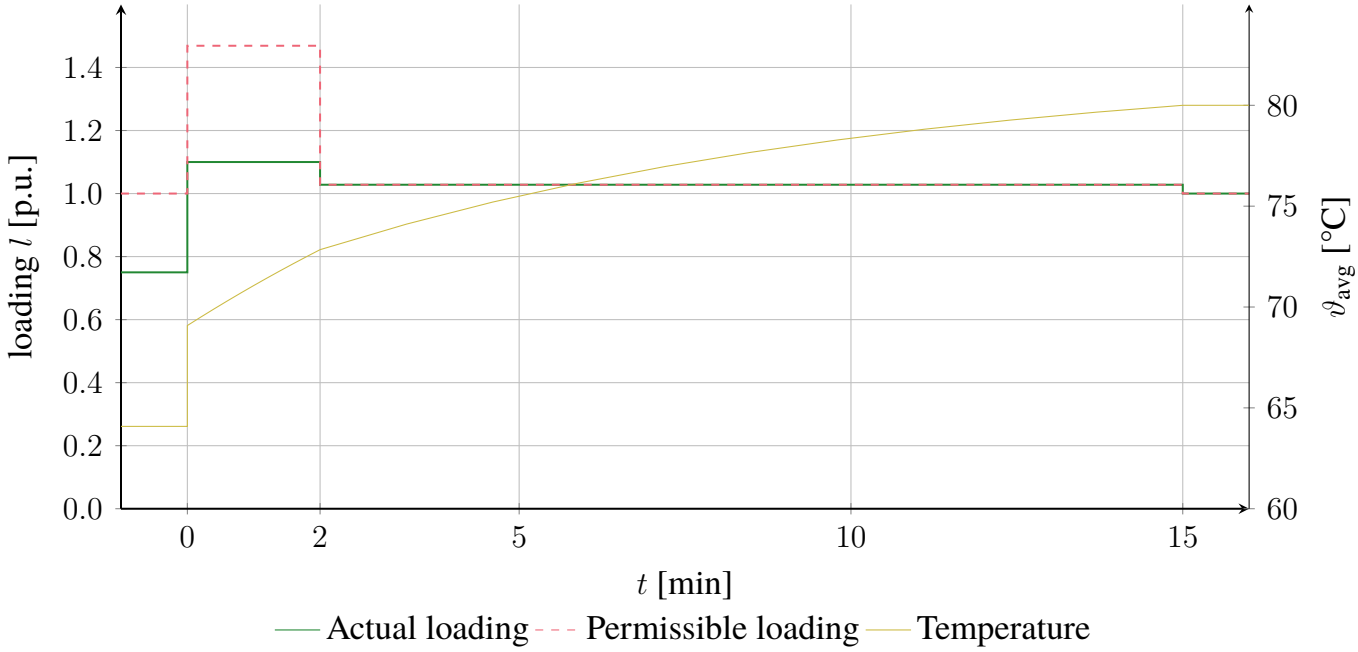

Figure 4.3.: Example for loading during curative timeframes and conductor temperature for a 264-AL1/34-ST1A conductor at standard weather conditions and an almost step-wise short-circuit heating $\Delta\vartheta_{\text{SC}} = 5\,\text{K}$.

The authors of [6] proposed three different approaches to incorporate $\vartheta_{\text{avg}}(t)$ in the CM optimization problem. The publication follows the assumptions of InnoSys 2030 on the amount and length of the curative timeframes. The first approach, denoted as *exogenous*, calculates limits for I_{TATL1} and I_{TATL2} assuming a base loading $l_{\text{base}} = 90\,\%$. Both curative timeframes are treated independently from each other. A numerical solving of the HBE for $\vartheta_{\text{avg}}(\tau_2)$ follows each CM iteration. If $\vartheta_{\text{avg}}(\tau_2) > \vartheta_{\text{max}}$, I_{TATL2} is iteratively reduced and the CM optimization is reconducted. This approach has several disadvantages: It tends to underestimate the potential of the first curative timeframe due to the assumption of $l_{\text{base}} = 90\,\%$. The focus of curative RAs is directed to the first timeframe, since the potential of the second timeframe is only used if thermal reserves are not fully exploited in the first timeframe. Performance-wise, the iterative approach is computationally expensive, since the HBE must be repeatedly solved and the CM optimization must be reconducted.

The *iterative* approach in [6] improves the incorporation of the base loading by creating a Lookup Table (LUT) for I_{TATL1} and I_{TATL2} over a range of values for the base loading. However, the disadvantages of the exogenous approach remain. Lastly, the authors of [6] draft an *endogenous* approach that incorporates the conductor temperature as a direct constraint in the CM optimization problem. However, due to the lacking closed-form solution

of the HBE, the solver would not be able to evaluate $\vartheta_{\text{avg}}(\tau)$ during the solving process. Approximate solutions may be applicable, but lack accuracy and would create nonlinear constraints that do not fit in the MILP formulation of [6].

This work proposes a novel approach to incorporate the conductor temperature in the CM optimization problem. The approach extends the work of [6] by creating a LUT for a multitude of weather scenarios, conductor types, base loadings, and postfault loadings. In contrast to [6], the permissible loading l_{TATL2} is determined depending on l_{base} and l_{TATL1}. The number of lookup values increases exponentially with each additional curative timeframe (combinatorial explosion). Hence, this approach is only feasible for a small number of curative timeframes. With a suitable partition of ambient conditions (wind speed, ambient temperature, solar irradiation, etc.), conductor types, and loading ranges, the LUT can be created with a reasonable computational effort offline.

4.3.1. TATL1 constraints

Let $\mathcal{M}_{\text{TATL1}}$ be the two-dimensional polyhedron created from the ordered vertices of the TATL1-LUT for a specific conductor type and fixed weather conditions:

$$\mathcal{M}_{\text{TATL1}} = \{\mathbf{m}_{\text{TATL1},1}, \mathbf{m}_{\text{TATL1},2}, \ldots, \mathbf{m}_{\text{TATL1},N_{\text{base}}}\}. \tag{4.13}$$

A vertex $\mathbf{m}_{\text{TATL1},i}$ is defined by the base loading $l_{\text{base},i}$ and the permissible TATL1 $l_{\text{TATL1},i}$:

$$\mathbf{m}_{\text{TATL1},i} = \left(l_{\text{base},i}, l_{\text{TATL1},i}\right)^{\top} \quad \forall i = 1, 2, \ldots, N_{\text{base}}. \tag{4.14}$$

Here, N_{base} represents the total number of discrete base loading values $l_{\text{base},i}$ in the LUT for a given conductor type and specified weather conditions, for which the corresponding permissible $l_{\text{TATL1},i}$ are determined.

The intersection of the halfspaces of the polyhedron $\mathcal{M}_{\text{TATL1}}$ defines the feasible domain for l_{base} and l_{TATL1}. The permissible loading l_{TATL1} is determined by the linear interpolation of two adjacent points in the LUT:

$$l_{\text{TATL1}} \leq \frac{l_{\text{TATL1},i+1} - l_{\text{TATL1},i}}{l_{\text{base},i+1} - l_{\text{base},i}} \cdot \left(l_{\text{base}} - l_{\text{base},i}\right) + l_{\text{TATL1},i} \quad \forall i = 1, 2, \ldots, N_{\text{base}} - 1. \tag{4.15}$$

Fig. 4.4 illustrates an example of a feasible domain for the base loading l_{base} and the permissible TATL1 loading l_{TATL1} for a 264-AL1/34-ST1A conductor.

Figure 4.4 illustrates the constraints across all four quadrants, since the loading definition in the DC power flow approximation also permits negative values. This is implemented by mirroring the LUT entries along both the x- and y-axes.

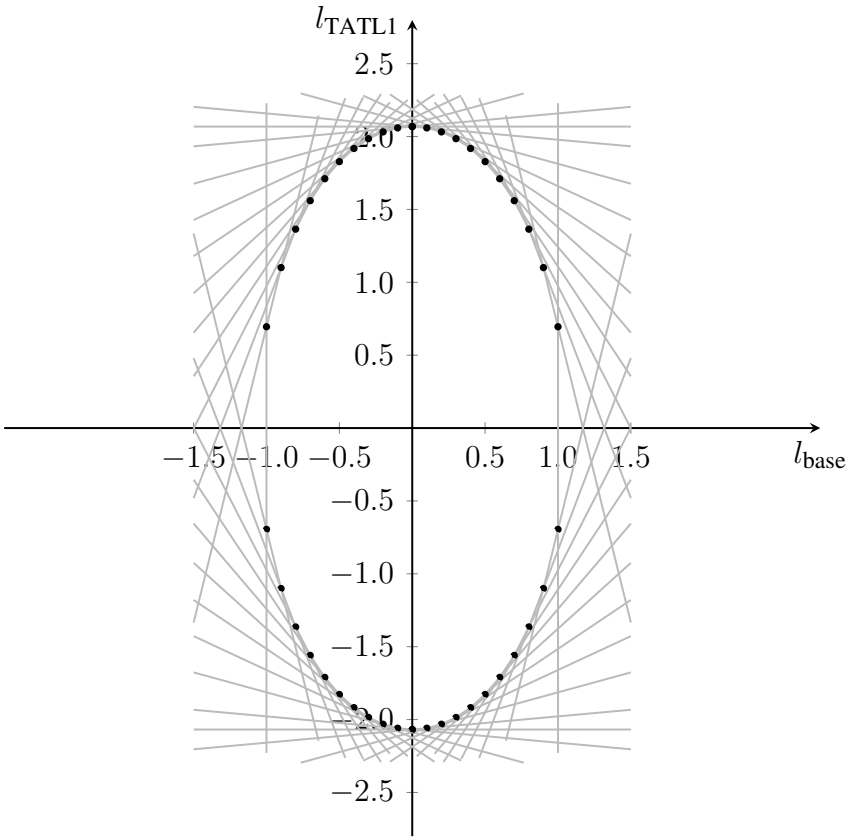

Figure 4.4.: Example of TATL1-polyhedron for a 264-AL1/34-ST1A conductor at standard weather conditions and 5 K short-circuit heating.

4.3.2. TATL2 constraints

Similarly to $\mathcal{M}_{\text{TATL1}}$, let $\mathcal{M}_{\text{TATL2}} : \mathcal{L}_{\text{base}} \times \mathcal{L}_{\text{TATL1}} \rightarrow \mathcal{L}_{\text{TATL2}}$ be the TATL2-LUT for a specific conductor type and fixed weather conditions.

The ordered sets

$$\mathcal{L}_{\text{base}} = \{l_{\text{base},1}, l_{\text{base},2}, \ldots, l_{\text{base},N_{\text{base}}}\} \tag{4.16}$$

$$\mathcal{L}_{\text{TATL1}} = \{l_{\text{TATL1},1}, l_{\text{TATL1},2}, \ldots, l_{\text{TATL1},N_{\text{TATL1}}}\} \tag{4.17}$$

denote the discrete loading values for the base case and the first curative timeframe, respectively, for which the permissible loading l_{TATL2} is determined.

The LUT $\mathcal{M}_{\text{TATL2}}$ contains the permissible loading l_{TATL2} for given base and first curative timeframe loading values:

$$\mathcal{M}_{\text{TATL2}} = \{\mathbf{m}_{\text{TATL2},1,1}, \mathbf{m}_{\text{TATL2},1,2}, \ldots, \mathbf{m}_{\text{TATL2},N_{\text{TATL2}}}\}. \tag{4.18}$$

with the tuples $\mathbf{m}_{\text{TATL2},i,j}$ defined as:

$$\begin{aligned} &\mathbf{m}_{\text{TATL2},i,j} = \left(l_{\text{base},i}, l_{\text{TATL1},j}, l_{\text{TATL2},i,j}\right)^{\top} \\ &\forall i = 1, 2, \ldots, N_{\text{base}}, j = 1, 2, \ldots, N_{\text{TATL1}}. \end{aligned} \tag{4.19}$$

Here, N_{TATL1} represents the total number of discrete TATL1 loading values $l_{\text{TATL1},j}$ in the LUT for a given conductor type and specified weather conditions, for which the corresponding permissible $l_{\text{TATL2},j}$ are determined.

Every three adjacent tuples of the LUT define a halfspace of the polyhedron $\mathcal{M}_{\text{TATL2}}$. The intersection of the halfspaces of the polyhedron $\mathcal{M}_{\text{TATL2}}$ defines the feasible domain for l_{base}, l_{TATL1}, and l_{TATL2}.

Let $\mathbf{p}_{\text{TATL2},0} = \left(l_{\text{base},i}, l_{\text{TATL1},j}, l_{\text{TATL2},i,j}\right)^{\top}$ be a location vector of the polyhedron $\mathcal{M}_{\text{TATL2}}$.

The adjacent vertices are defined as:

$$\mathbf{p}_{\text{TATL2},1} = \begin{pmatrix} l_{\text{base,i}+1} \\ l_{\text{TATL1},j} \\ l_{\text{TATL2},i+1,j} \end{pmatrix} \tag{4.20}$$

$$\mathbf{p}_{\text{TATL2},2} = \begin{pmatrix} l_{\text{base},i} \\ l_{\text{TATL1},j+1} \\ l_{\text{TATL2},i,j+1} \end{pmatrix} \tag{4.21}$$

$$\mathbf{p}_{\text{TATL2},3} = \begin{pmatrix} l_{\text{base,i}-1} \\ l_{\text{TATL1},j} \\ l_{\text{TATL2},i-1,j} \end{pmatrix} \tag{4.22}$$

$$\mathbf{p}_{\text{TATL2},4} = \begin{pmatrix} l_{\text{base},i} \\ l_{\text{TATL1},j-1} \\ l_{\text{TATL2},i,j-1} \end{pmatrix} \tag{4.23}$$

$$\forall i = 1, 2, \ldots, N_{\text{base}}, j = 1, 2, \ldots, N_{\text{TATL1}}$$

The normal form of a plane is defined by its normal vector $\mathbf{n}_{\text{TATL2}} = (a, b, c)^\top$ and a point $\mathbf{p}_{\text{TATL2},0}$ on the plane:

$$\left(\mathbf{x} - \mathbf{p}_{\text{TATL2},0}\right) \cdot \mathbf{n}_{\text{TATL2}} = 0 \tag{4.24}$$

with $\mathbf{x} = (l_{\text{base}}, l_{\text{TATL1}}, l_{\text{TATL2}})^\top$. The equivalent coordinate form of the plane is:

$$a \cdot l_{\text{base}} + b \cdot l_{\text{TATL1}} + c \cdot l_{\text{TATL2}} = d. \tag{4.25}$$

d is determined by the point $\mathbf{p}_{\text{TATL2},0}$ and the normal vector $\mathbf{n}_{\text{TATL2}}$.

The normal vectors of the four planes that contain $\mathbf{p}_{\text{TATL2},0}$ are:

$$\begin{aligned}
\mathbf{n}_{\text{TATL2},1} &= \left(\mathbf{p}_{\text{TATL2},1} - \mathbf{p}_{\text{TATL2},0}\right) \times \left(\mathbf{p}_{\text{TATL2},2} - \mathbf{p}_{\text{TATL2},0}\right) \\
\mathbf{n}_{\text{TATL2},2} &= \left(\mathbf{p}_{\text{TATL2},2} - \mathbf{p}_{\text{TATL2},0}\right) \times \left(\mathbf{p}_{\text{TATL2},3} - \mathbf{p}_{\text{TATL2},0}\right) \\
\mathbf{n}_{\text{TATL2},3} &= \left(\mathbf{p}_{\text{TATL2},3} - \mathbf{p}_{\text{TATL2},0}\right) \times \left(\mathbf{p}_{\text{TATL2},4} - \mathbf{p}_{\text{TATL2},0}\right) \\
\mathbf{n}_{\text{TATL2},4} &= \left(\mathbf{p}_{\text{TATL2},4} - \mathbf{p}_{\text{TATL2},0}\right) \times \left(\mathbf{p}_{\text{TATL2},1} - \mathbf{p}_{\text{TATL2},0}\right)
\end{aligned} \tag{4.26}$$

The normal vectors point outwards of the polyhedron $\mathcal{M}_{\text{TATL2}}$ and are normalized to unit

length for numerical stability. The halfspaces around $\mathbf{p}_{\text{TATL2},0}$ are:

$$\mathbf{n}_{\text{TATL2},k} \cdot \mathbf{x} \leq d_k \quad \forall k \in \{1, 2, 3, 4\}. \tag{4.27}$$

The total number of planes that constitute $\mathcal{M}_{\text{TATL2}}$ is:

$$N_{\text{planes}} = 8 \cdot 4 \cdot (N_{\text{base}} - 1) \cdot (N_{\text{TATL1}} - 1)\,. \tag{4.28}$$

The factor 8 in Eq. (4.28) accounts for the eight octants of $\mathbb{R}^3$ in which the tuples $(l_{\text{base}}, l_{\text{TATL1}}, l_{\text{TATL2}})^\top$ are defined. The factor 4 accounts for the four planes that are created from the LUT tuples. It is apparent, that the number of planes grows rapidly with the size of the LUT. A full inclusion of all planes in an optimization model is computationally intensive. Section 5.4 presents an iterative approach to include the TATL2-constraints during the optimization process.

A visual representation of $\mathcal{M}_{\text{TATL2}}$ in the first octant is provided by Fig. 4.5.

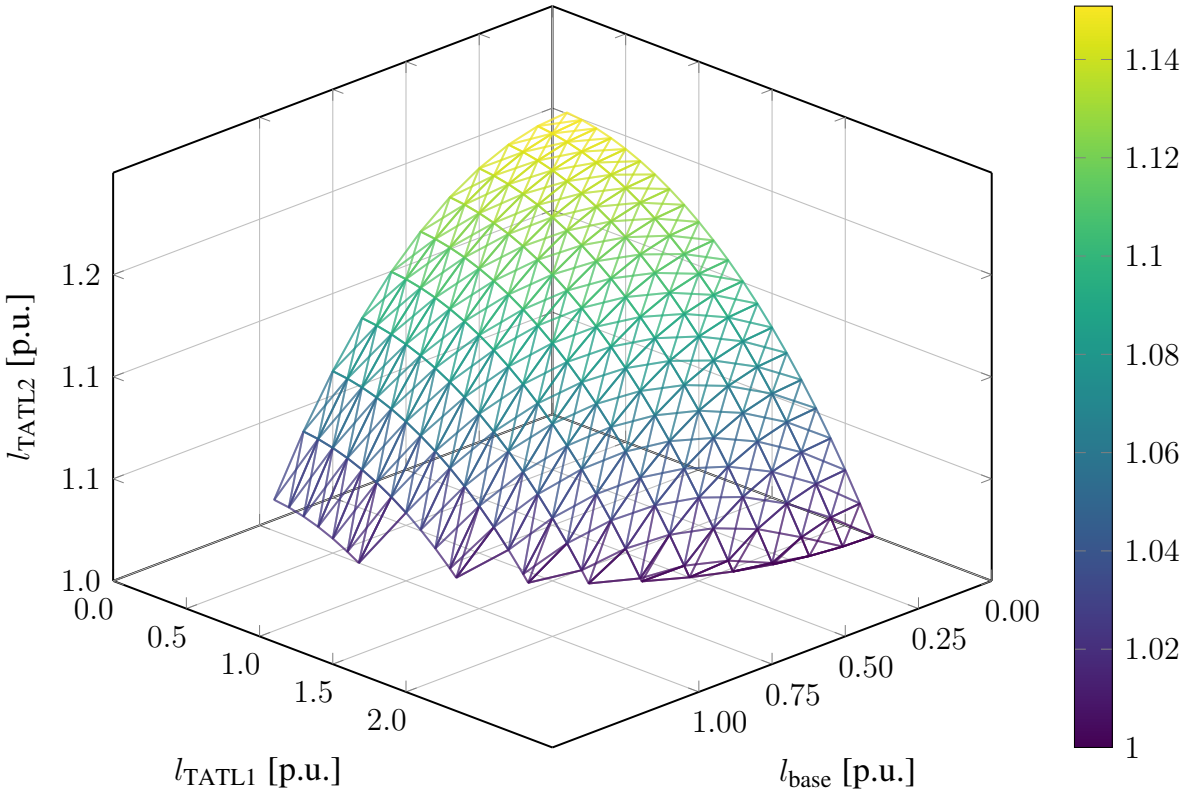

Figure 4.5.: Illustrative section of the TATL2 polyhedron in the first octant. Axes are scaled unequally for visualization purposes.

4.4. Conclusion of the chapter

This chapter analyzed the thermal behavior of OHL conductors and methods for incorporating dynamic thermal constraints into OPF models. By applying DLR and defining PATL and TATL, it showed how temporary thermal reserves can be systematically exploited to enhance grid flexibility during curative CM. The proposed LUT-based method enables practical integration of thermal constraints for OHL conductors with two curative timeframes, supporting coordinated optimization of fast and slow curative RAs.

5. Model

This chapter presents the mathematical framework of the SCOPF model designed for the PrevCurRest strategy. The formulations for the Prev and PrevCur strategies are contained as special cases within this comprehensive model. The subsequent sections detail the model design, including the objective function, decision variables, and constraints. Additionally, it explains the graph-based modeling approach used to represent and classify grid situations. This structured methodology enables a systematic analysis and comparison of different CM strategies.

5.1. Model Design Considerations

The design of the optimization model is driven by the requirements listed in Section 3.3: *Feasibility*, *Run-Time*, *Optimality*, *Interpretability*, and *Accuracy*.

This thesis adopts a modeling approach that combines binary UC variables with the DC-approximation of the PFEs, resulting in a mixed-integer linear program (MILP). This choice prioritizes the accurate representation of UC decisions over the precise modeling of the PFEs. The rationale is that, at the day-ahead operational planning stage, UC decisions for conventional power plants must be made with sufficient lead time. In contrast, the precise modeling of power flows is less critical at this point, as forecast uncertainties in load and generation can significantly alter system conditions before real-time operation. The DC-approximation is generally considered sufficiently accurate for transmission system operational planning. As long as redispatch decisions are subsequently validated using an AC power flow analysis, the DC-approximation remains a practical and accepted method. However, manual adjustments to the optimization results may still be required to ensure operational feasibility, especially regarding voltage and reactive power constraints.

SCOPF models with more accurate representations of the PFEs are in operational use (e. g. the German “Redispatch-Ermittlungs-Server” based on [32]), still, the choice of the DC-approximation in this work was necessary for *run-time* reasons. The PrevCurRest model adds another layer of complexity by requiring N–1–1 security. Preliminary tests with the MATPOWER 39-bus test grid [61] showed unacceptable run-times.

This work's prioritization of the design aspects is as follows:

1. *Run-time*: The model must be able to solve the optimization problem within a reasonable time frame.
2. *Interpretability*: The multitude of decision variables and constraints is aggregated in a graph-based model with a clear structure, which allows for a separable and interpretable model.
3. *Feasibility*: The MILP solver has to find at least one feasible solution, even if it is not optimal.
4. *Accuracy*: The binary UC and linear, DC-approximated PFE representations are sufficient for operational planning.
5. *Optimality*: Grid security always takes precedence over cost optimality. While global cost optimality is not the primary goal, it is desirable to find a solution that is close to the global optimum to lower CM costs.

The design considerations for this work prioritize *robustness*, *run-time*, *UC*, and *interpretability*. Robustness and run-time are addressed by restricting the solution process to the first step of the previously described two-step approach, which relies on the DC-approximation. This results in a MILP formulation, solved using the commercial `Gurobi` solver, renowned for its performance and reliability in large-scale mixed-integer linear programming [46].

The *interpretability* and *decomposability* of the model is enhanced through a graph-based modeling approach. This not only provides an interpretable model structure but also facilitates the application of decomposition techniques, as well as distributed and decentralized optimization algorithms.

Looking ahead, enhancing the models treatment of *voltage* and *reactive power* will be crucial for further improving the *accuracy*, *operational feasibility*, and *trustworthiness*. This can be achieved by using relaxations of the branch flow equations, which are recommended for future research. Similarly, the current model does not explicitly address *stochastic uncertainties*. Addressing this limitation could involve integrating scenario-based methods such as Monte Carlo simulations, adopting robust optimization frameworks [62], or employing chance-constrained programming techniques as demonstrated in [63]. These enhancements would allow the model to better capture real-world variability and uncertainty, thereby increasing its practical relevance and reliability. A survey of different approaches to incorporate uncertainties in SCOPF models is provided in [64].

5.2. Graph-based modeling approach

The PrevCurRest strategy involves a complex interplay of different grid situations, each representing a specific state in time and under certain contingencies. Considering N–1–1 security, including the curative restoration of N–1 security, requires a systematic approach to model these situations and their interdependencies. A graph-based modeling approach is particularly suitable for this purpose, as it allows the overall model to be separated into distinct subproblems—denoted as grid situations—and represents the relationships between them in a clear and structured manner. This approach not only enhances the interpretability of the model but also facilitates the application of decomposition techniques. Graph-based modeling was previously applied in [65], [66], [67] for decomposing and parallelizing the solution of large-scale OPF problems.

Fig. 5.1 illustrates a generic, (unreduced) grid situation graph, which will be explained in the following subsections.

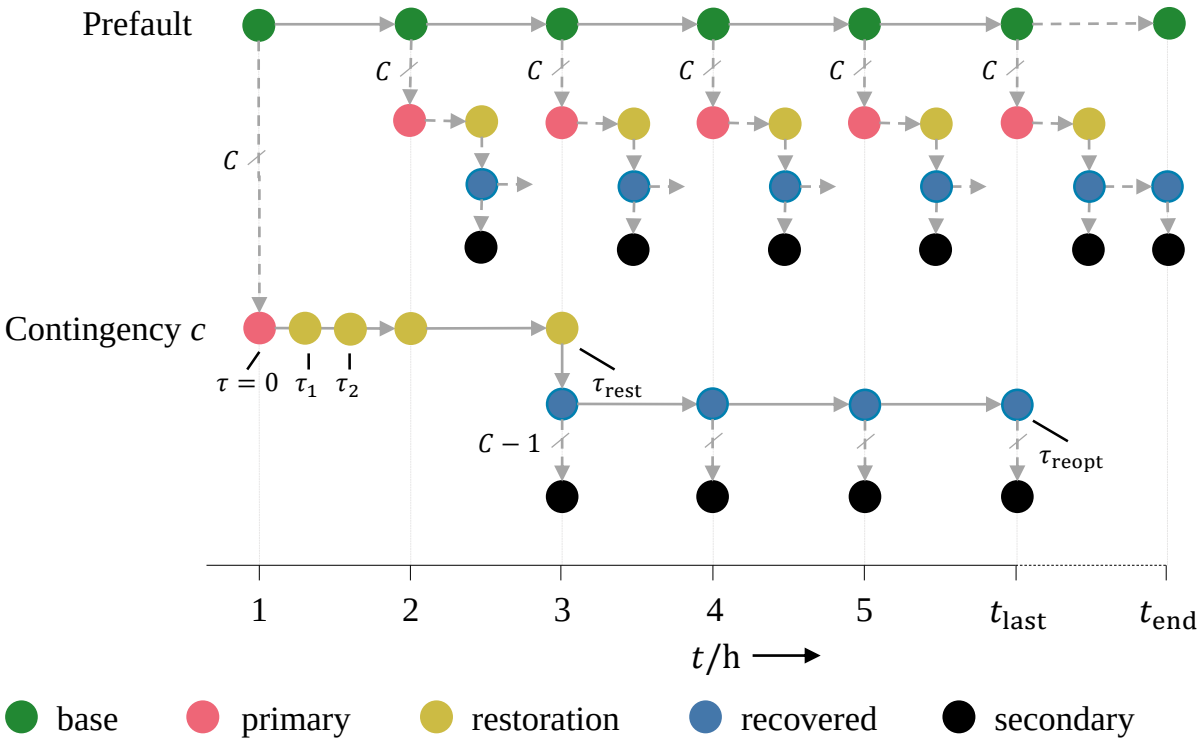

Figure 5.1.: Unreduced PrevCurRest graph with restoration, recovered, and secondary contingency situations after each primary contingency situation.

Each CM strategy focuses on specific parts of the graph:

- Prev: Base and primary contingency situations.
- PrevCur: Base, primary contingency, and restoration situations at τ_1 and τ_2.
- PrevCurRest: Full graph with base, primary contingency, restoration situations up to τ_{rest}, recovered situations, and secondary contingency situations up to τ_{reopt}.
- PrevN2: Base, primary, and secondary contingency situations. No restoration or recovery phases.

5.2.1. Classification of grid situations

The CM strategies classify grid situations into base, primary contingency, restoration, recovered, and secondary contingency situations. The SCOPF incorporates the grid situations as subproblems with coupling constraints between eachother.

The set of all grid situations is defined as

$$\Omega = \left\{ \omega = (t, c, \tau, k)^\top \in \mathcal{T}_{\text{base}} \times \mathcal{C} \times \mathcal{T}_{\text{rest}} \times \mathcal{C} \mid c \neq k \right\}. \tag{5.1}$$

The timestamp of the base situation $t \in \mathcal{T}_{\text{base}}$ is selected from the ordered set

$$\mathcal{T}_{\text{base}} = \left\{ t_i \in \mathbb{R}_0^+ \mid i = 0, 1, \ldots, N_{\text{base}};\ t_0 = 0 < t_1 < \cdots < t_{N_{\text{base}}} = t_{\text{end}} \right\} \tag{5.2}$$

The resulting set of base timestamps up to t_{end} is

$$\mathcal{T}_{\text{base}} = \{0, t_1, t_2, \ldots, t_{\text{last}}, \ldots, t_{\text{end}}\} \tag{5.3}$$

representing the reference timestamps for timeseries of unit schedules. The set of base timestamps of the business day is defined as

$$\mathcal{T}_{\text{base}}^{\text{last}} = \{ t \in \mathcal{T}_{\text{base}} \mid t \leq t_{\text{last}} \}. \tag{5.4}$$

The base timestamp t_{last} represents the end of the current business day, up to which primary contingencies are included. Beyond this, t_{end} marks the end of the planning horizon, which contains restoration, recovered, and secondary contingency situations following a primary

contingency that took place during the business day, i. e. with an initial base timestamp $t \leq t_{\text{last}}$.

Hence, the planning horizon must be extended beyond the last business day's base timestamp t_{last} to incorporate restoration and recovery phases. Restoration and recovered grid situations require reference operating points from base situations that occur after t_{last}. Therefore, the base situation graph is extended from t_{last} up to t_{end} by adding additional base situations. If base situations from the subsequent operational planning period are available, they should be used. Otherwise, the initial base situations from the current planning period can be repeated as needed. The end of the planning horizon, t_{end}, is defined as:

$$t_{\text{end}} = t_{\text{last}} + \tau_{\text{rest}} + \tau_{\text{reopt}} \tag{5.5}$$

The post-contingency duration $\tau \in \mathcal{T}_{\text{rest}}$ defines the elapsed time since the base timestamp t that encountered a primary contingency. The ordered set of timestamps for restoration situations is defined as

$$\mathcal{T}_{\text{rest}} = \mathcal{T}_{\text{base}} \cup \{\tau_1, \tau_2\} \tag{5.6}$$

with $0 < \tau_1 < \tau_2 < t_1$ representing the two consecutive restoration timestamps following a primary contingency, for which the temporary current limits I_{TATL1} and I_{TATL2} apply, respectively. The post-contingency duration τ is zero for base situations and primary contingency situations, i. e., $\tau = 0$. The set of timestamps for restoration situations is:

$$\mathcal{T}_{\text{rest}} = \{0, \tau_1, \tau_2, t_1, t_2, \ldots, t_{\text{last}}, \ldots, t_{\text{end}}\} \tag{5.7}$$

with $|\mathcal{T}_{\text{rest}}|$ being the amount of timestamps for restoration situations.

The primary contingency is identified by its index $c \in \mathcal{C}$, where

$$\mathcal{C} = \{0, 1, 2, \ldots, N_{\mathcal{C}}\} \tag{5.8}$$

contains all considered contingencies. The secondary contingency is identified by its index $k \in \mathcal{C}$. The absence of a primary and a secondary contingency is defined by $c = 0$ and $k = 0$, respectively.

A grid situation ω is thus uniquely identified by a tuple:

$$\omega = (t, c, \tau, k)^\top \tag{5.9}$$

By definition, $\omega = (0,0,0,0)^\top$ refers to the initial grid state before the operational planning period under consideration. This grid situation sets initial SoC values of storages and operating states of generators. It is not part of the SCOPF.

The actual timestamp of a grid situation t_{act} is defined as the sum of the base timestamp and the post-contingency duration associated with the grid situation $\omega = (t, c, \tau, k)^\top$. Formally, this is expressed as a function:

$$t_{\text{act}}(\omega) = t(\omega) + \tau(\omega), \tag{5.10}$$

where $t(\omega)$ and $\tau(\omega)$ denote the first and third components of ω, respectively.

Remark 1 (Time specification) *The time specification of a grid situation always denotes the beginning of a time interval. The RAs applied during the grid situation become effective at the end of the time interval. The time specification also denotes the time of the potential contingency events.*

The following paragraphs introduce the different types of grid situations and their relationships.

Base Situation A *base* situation $\omega_{\text{base}} \in \Omega_{\text{base}}$ contains no contingency. The set of base situations is denoted by

$$\Omega_{\text{base}} = \{\omega \in \Omega \mid t > 0, c = 0, \tau = 0, k = 0\}. \tag{5.11}$$

In base situations, the market schedules determine the initial dispatch for generators and loads. Preventive RAs are applied to ensure either a preventive or preventive-curative N–1 secure state, depending on the selected CM strategy. The current limits are set by I_{PATL}. The short notation of a base situation is $\omega_{\text{base}} = (t)$.

Primary contingency situation A *primary contingency* situation $\omega_{\text{prim}} \in \Omega_{\text{prim}}$ represents the grid state immediately after the occurrence and fault-clearing of a single contingency c at $\tau = 0$. The set of primary contingency situations is defined as

$$\Omega_{\text{prim}} = \{\omega \in \Omega \mid t > 0, c > 0, \tau = 0, k = 0\}. \tag{5.12}$$

During a primary contingency situation, the branch currents are limited by I_{PATL} for the Prev and PrevN2 strategies, and by I_{TATL1} for other strategies. This situation serves as the starting point for subsequent restoration actions.

Restoration situation A *restoration* situation $\omega_{\text{rest}} \in \Omega_{\text{rest}}$ is the immediate successors of a primary contingency situation. Restoration situations are only present in the PrevCur and PrevCurRest strategies. The set of restoration situations is denoted by

$$\Omega_{\text{rest}} = \{\omega \in \Omega \mid t > 0, c > 0, 0 < \tau \leq \tau_{\text{rest}}, k = 0\}\,. \tag{5.13}$$

The post-contingency duration $\tau \in (0, \tau_{\text{rest}}]$ indicates the time elapsed since the preceding primary contingency. For $\tau_1 \leq \tau \leq \tau_2$, the current limits are set to I_{TATL2}; otherwise, I_{PATL} applies. Restoration situations with $\tau \leq \tau_2$ may utilize thermal reserves and are not required to be permanently N–0 secure. From $\tau \geq \tau_2$ onward, the grid must be N–0 secure. While this suffices for the PrevCur strategy, the PrevCurRest strategy implements further curative RAs to achieve a new N–1 secure state by $\tau = \tau_{\text{rest}}$.

Recovered situation A *recovered* situation $\omega_{\text{re}} \in \Omega_{\text{re}}$ follows the sequence of restoration situations in the PrevCurRest strategy. The set of recovered situations is defined as

$$\Omega_{\text{re}} = \left\{\omega \in \Omega \mid t = 0, c > 0, \tau_{\text{rest}} \leq \tau \leq \tau_{\text{reopt}}, k = 0\right\}. \tag{5.14}$$

Once the restoration phase concludes, the grid reaches a new (preventively) N–1 secure state. In this state, the system can withstand a secondary contingency event without requiring further curative RAs for the duration $\tau_{\text{rest}} \leq \tau \leq \tau_{\text{reopt}}$.

A recovered situation is denoted as $\omega_{\text{re}} = (0, c, \tau, 0)^\top$. The timestamp is always set to $t = 0$, with the post-contingency duration τ indicating the actual time. This convention ensures consistency, as the originating base situation may not be unique (see Section 5.2.3 for details).

Secondary contingency situation A *secondary contingency* situation $\omega_{\text{sec}} \in \Omega_{\text{sec}}$ arises in the PrevCurRest strategy following a recovered situation and involves an additional contingency event affecting asset k, where $k \neq c$. The set of secondary contingency situations

is defined as

$$\Omega_{\text{sec}} = \{\omega \in \Omega \mid t = 0, c > 0, \tau \geq \tau_{\text{rest}}, k > 0, c \neq k\}\,. \tag{5.15}$$

A secondary contingency situation is represented as $\omega_{\text{sec}} = (0, c, \tau, k)^\top$. The conventions for t and τ follow those established for recovered situations.

Table 5.1 summarizes the properties of the grid situation types.

Table 5.1.: Classification of grid situations

Grid situation	**Notation**	**Contingencies**	**Current limit**	**Dispatch reference**
Base	$\omega_{\text{base}} = (t)$	$\emptyset$	I_{PATL}	market schedule
Primary	$\omega_{\text{prim}} = (t, c, 0, 0)$	c	I_{TATL1}	$\omega_{\text{base}} = (t)$
Restoration ($\tau = \tau_1$)	$\omega_{\text{rest}} = (t, c, \tau_1, 0)$	c	I_{TATL2}	$\omega_{\text{base},1} = (t)$, $\omega_{\text{base},2} = (t+1)$
Restoration ($\tau = \tau_2$)	$\omega_{\text{rest}} = (t, c, \tau_2, 0)$	c	I_{PATL}	$\omega_{\text{base},1} = (t)$, $\omega_{\text{base},2} = (t+1)$
Restoration ($\tau > \tau_2$)	$\omega_{\text{rest}} = (t, c, \tau, 0)$	c	I_{PATL}	$\omega_{\text{base}} = (t+\tau)$
Recovered	$\omega_{\text{re}} = (0, c, \tau, 0)$	c	I_{PATL}	$\omega_{\text{base}} = (t)$
Secondary	$\omega_{\text{sec}} = (0, c, \tau, k)$	c, k	I_{PATL}	$\emptyset$

The dispatch reference column in Table 5.1 specifies the grid situation to which the current grid situation applies redispatch measures. For restoration situations at $\tau = \tau_1$ and $\tau = \tau_2$, the timestamps do not coincide with the hourly base situation timestamps. Therefore, these restoration situations reference both the preceding and the subsequent base situations. This is discussed in more detail in the following section.

5.2.2. Relationships between grid situations

A graph-based representation is introduced to structure the multitude of grid situations. The grid situations, characterized by the time specification $\mathcal{T}_{\text{spec}} = (t, \tau)$ and the contingency specification $\mathcal{C}_{\text{spec}} = (c, k)$, can be viewed as the places of a Petri net. The transitions between the grid situations are time and contingency events.

The grid situations and their transitions form a directed, acyclic graph (digraph) $\Gamma(\Omega, \mathcal{E})$. The grid situations $\omega \in \Omega$ represent the graph's nodes, and the transitions $e \in \mathcal{E}$ the graph's edges. The set of edges $\mathcal{E} \subset \Omega \times \Omega$ contains ordered pairs of grid situations $(\omega_{\text{from}}, \omega_{\text{to}})$.

Table 5.2 summarizes the transition types, their conditions, and the corresponding sets of connected grid situations.

Table 5.2.: Transitions between grid situations

Transition	**Condition**	**Set**
Base → Base	time	$\mathcal{E}_{\text{base}\to\text{base}} \subset \Omega_{\text{base}} \times \Omega_{\text{base}}$
Base → Primary	contingency	$\mathcal{E}_{\text{base}\to\text{prim}} \subset \Omega_{\text{base}} \times \Omega_{\text{prim}}$
Primary → Restoration	time	$\mathcal{E}_{\text{prim}\to\text{rest}} \subset \Omega_{\text{prim}} \times \Omega_{\text{rest}}$
Restoration → Restoration	time	$\mathcal{E}_{\text{rest}\to\text{rest}} \subset \Omega_{\text{rest}} \times \Omega_{\text{rest}}$
Restoration → Recovered	time	$\mathcal{E}_{\text{rest}\to\text{re}} \subset \Omega_{\text{rest}} \times \Omega_{\text{re}}$
Recovered → Recovered	time	$\mathcal{E}_{\text{re}\to\text{re}} \subset \Omega_{\text{re}} \times \Omega_{\text{re}}$
Recovered → Secondary	contingency	$\mathcal{E}_{\text{re}\to\text{sec}} \subset \Omega_{\text{re}} \times \Omega_{\text{sec}}$

To define the sets of directly and indirectly connected grid situations, the following "neighborhood" sets of a grid situation ω are introduced.

The direct outgoing neighborhood Ω^{out} of a grid situation ω is defined as the set of all grid situations $\omega_{\text{nb}} \in \Omega$ for which there exists a directed edge from ω to ω_{nb} in the set of edges $\mathcal{E}$:

$$\Omega^{\text{out}}(\omega) = \{\omega_{\text{nb}} \in \Omega : (\omega, \omega_{\text{nb}}) \in \mathcal{E}\} \tag{5.16}$$

The extended outgoing neighborhood $\Omega^{\text{out}+}$ represents the set of grid situations that can be reached from ω within the time horizon τ_{reach}:

$$\Omega^{\text{out}+}(\omega, \tau_{\text{reach}}) = \{\omega_{\text{nb}} \in \Omega : (\omega, \omega_{\text{nb}}) \in \mathcal{E}, t_{\text{act}}(\omega_{\text{nb}}) - t_{\text{act}}(\omega) \leq \tau_{\text{reach}}\} \tag{5.17}$$

The direct incoming neighborhood Ω^{in} is defined likewise:

$$\Omega^{\text{in}}(\omega) = \{\omega_{\text{nb}} \in \Omega : (\omega_{\text{nb}}, \omega) \in \mathcal{E}\} \tag{5.18}$$

The extended incoming neighborhood $\Omega^{\text{in}+}$ is defined as:

$$\Omega^{\text{in}+}(\omega, \tau_{\text{reach}}) = \{\omega_{\text{nb}} \in \Omega : (\omega_{\text{nb}}, \omega) \in \mathcal{E}, t_{\text{act}}(\omega) - t_{\text{act}}(\omega_{\text{nb}}) \leq \tau_{\text{reach}}\}. \tag{5.19}$$

Focusing on the PrevCurRest strategy, the parameter τ_{rest} specifies the duration of the restoration phase following each primary contingency. This parameter defines the time available to re-establish a new N–1 secure state. Throughout the restoration phase, secondary contingencies are not considered. The set of restoration timestamps subsequent to a primary contingency situation are given by:

$$\mathcal{T}^{\omega}_{\text{rest}} = \{\tau \in \mathcal{T}_{\text{rest}} \mid 0 < \tau \leq \tau_{\text{rest}}\}. \tag{5.20}$$

Only after the restoration phase, during the subsequent recovery period $\tau_{\text{rest}} \leq \tau \leq \tau_{\text{reopt}}$, must the grid be robust against any secondary contingencies. The second parameter, τ_{reopt}, represents the re-optimization interval for re-running the SCOPF after a primary contingency event. It is expected that the results of a new SCOPF run can be implemented as new preventive RAs before the end of this period.

The set of timestamps in the recovery phase subsequent to a primary contingency situation are given by:

$$\mathcal{T}^{\omega}_{\text{re}} = \left\{\tau \in \mathcal{T}_{\text{base}} \mid t + \tau_{\text{rest}} \leq \tau \leq t + \tau_{\text{rest}} + \tau_{\text{reopt}}\right\}. \tag{5.21}$$

The PrevCurRest strategy requires a careful choice for the parameters τ_{rest} and τ_{reopt}. A small τ_{rest} increases the risk of encountering a potentially hazardous contingency in a weakened, N–0 secure grid state. Conversely, a larger τ_{rest} provides more time for curative RAs to establish a new N–1 secure state. Thus, an increased use of curative RAs has the potential to lower the amount of costly preventive RAs.

A larger τ_{reopt} extends the grid's preparedness against secondary contingencies but also increases the size and computational time of the optimization program. It is advisable to set τ_{reopt} to the anticipated runtime of the SCOPF optimization, plus the time required for preparing new RAs. The German intraday redispatch processes currently have a maximal duration of 2.5 h to run the SCOPF optimization, to coordinate, and to implement the RAs.

Consequently, setting $\tau_{\text{reopt}} = 4\,\text{h}$ provides a practical estimate, assuming that a new SCOPF run can be started at any point in time.

5.2.3. Reduction of the PrevCurRest graph

The amount of grid situations and their transitions in the unreduced PrevCurRest graph of Fig. 5.1 is potentially large and may be too complex to be solved in a single optimization problem. In addition, the high amount of possible transition paths may not be traceable from a human operator's perspective.

The following presents a method to reduce the size of the PrevCurRest graph. The key idea is that a primary contingency c occurring at different timestamps can lead to overlapping restoration and recovered grid situations. Specifically, restoration and recovered situations associated with the same contingency c may coincide in time, regardless of when the contingency occurred.

To exploit this, transitions are introduced from restoration situations $\omega_{\text{rest}} = (t, c, \tau_{\text{rest}}, 0)^\top$ to recovered situations $\omega_{\text{re}} = (0, c, t + \tau_{\text{rest}}, 0)^\top$. If a recovered situation ω_{re} already exists in the graph, the corresponding restoration situation is linked to this existing grid situation.

This approach merges overlapping recovered situations for the same contingency, reducing the total number of grid situations and improving graph traceability. By linking restoration situations with the same primary contingency c to a common string of recovered situations, both graph size and complexity are decreased.

However, this approach introduces indirect connections between base situations through shared recovered situations—connections that do not exist in the actual system. As a result, primary contingency situations occurring at different timestamps may influence both earlier and later base situations. In the full graph structure, each recovered situation is uniquely associated with its originating primary contingency. Despite this abstraction, the significant reduction in graph size and the resulting improvement in traceability are expected to outweigh the drawbacks of these additional indirect links between base situations.

From an operator's perspective, having a single string of recovered situations per contingency is more intuitive and simplifies the manual implementation or adjustment of RAs. The fact that RAs during the restoration phase are individual per primary contingency and reference timestamp is justifiable as automatic control systems shall activate the curative RAs, which do not require manual actions of human operators.

Fig. 5.2 illustrates a reduced graph example featuring two primary contingency situations, $\omega_{\text{prim},1} = (1, 1, 0, 0)^\top$ and $\omega_{\text{prim},2} = (4, 1, 0, 0)^\top$, both associated with the same contingency $c = 1$ but occurring at different base timestamps, $t = 1\,\text{h}$ and $t = 4\,\text{h}$. For clarity, time units are omitted in the grid situation notations; all values represent hours in this example.

After each primary contingency situation, a distinct sequence of restoration situations is generated. In the example, the recovered situations $(0, 1, \{3, \ldots, 6\}, 0)$ that follow $\omega_{\text{prim},1}$ temporally coincide with the first recovered situation $(0, 1, 6, 0)^\top$ that follows $\omega_{\text{prim},2}$. Consequently, the restoration situation $(4, 1, 2, 0)^\top$ is linked to the already existing recovered situation $(0, 1, 6, 0)^\top$. This linkage, highlighted in red in Fig. 5.2, illustrates how the reduction approach consolidates overlapping recovered situations, thereby enhancing transparency and reducing the overall graph size.

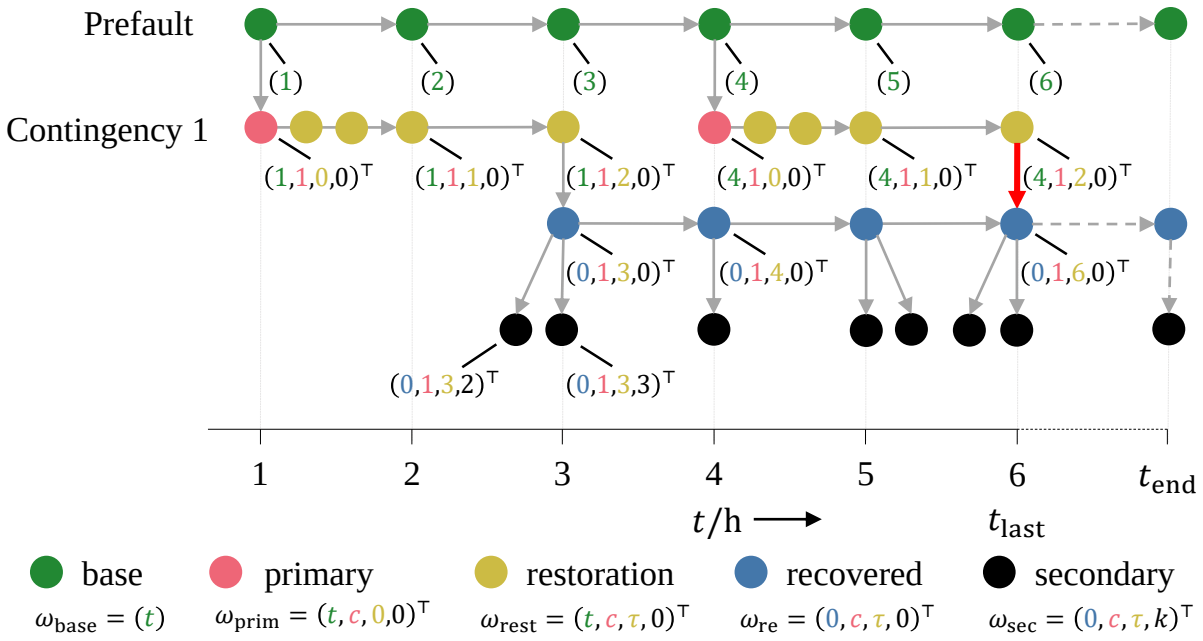

Figure 5.2.: Exemplary grid situation graph with applied reduction.

In the following, the full and reduced graph sizes are compared under the worst-case assumption that all $N_{\mathcal{C}} = |\mathcal{C}|$ primary contingencies are relevant to in each base situation. Two timestamps τ_1 and τ_2 are considered in the restoration phase. Refer to Section 5.2.1 for the definitions of the timestamp sets.

The following equations give the cardinalities (denoted by $|\cdot|$) of grid situation sets:

$$|\Omega_{\text{base}}| = |\mathcal{T}_{\text{base}}| \tag{5.22}$$

$$|\Omega_{\text{prim}}| = |\mathcal{C}| \cdot |\mathcal{T}_{\text{base}}^{\text{last}}| \tag{5.23}$$

$$|\Omega_{\text{rest}}| = |\mathcal{C}| \cdot |\mathcal{T}_{\text{base}}^{\text{last}}| \cdot |\mathcal{T}_{\text{rest}}^{\omega}| \tag{5.24}$$

The full PrevCurRest graph adds $|\mathcal{T}_{\text{re}}^{\omega}|$ recovered situations per primary contingency situation:

$$|\Omega_{\text{re}}^{\text{full}}| = |\Omega_{\text{prim}}| \cdot |\mathcal{T}_{\text{re}}^{\omega}| = |\mathcal{C}| \cdot |\mathcal{T}_{\text{base}}^{\text{last}}| \cdot |\mathcal{T}_{\text{re}}^{\omega}| \tag{5.25}$$

Assuming that each primary contingency $c \in \mathcal{C}$ is relevant at every base situation $t \in \mathcal{T}_{\text{base}}^{\text{last}}$, the reduced PrevCurRest graph introduces only one recovered situation per base timestamp and primary contingency with a completed restoration phase, linking each to the existing recovered situations with the same primary contingency. An exception applies to the final timestamp t_{last}, for which $|\mathcal{T}_{\text{re}}^{\omega}|$ recovered situations are added.

The total number of recovered grid situations in the reduced graph is:

$$|\Omega_{\text{re}}^{\text{reduced}}| = |\Omega_{\text{prim}}| + |\mathcal{C}| \cdot (|\mathcal{T}_{\text{re}}^{\omega}| - 1) = |\mathcal{C}| \cdot \left(|\mathcal{T}_{\text{base}}^{\text{last}}| + |\mathcal{T}_{\text{re}}^{\omega}| - 1\right). \tag{5.26}$$

The ratio of recovered grid situations in the reduced and the full graph size is:

$$\frac{|\Omega_{\text{re}}^{\text{reduced}}|}{|\Omega_{\text{re}}^{\text{full}}|} = \frac{|\mathcal{T}_{\text{base}}^{\text{last}}| + |\mathcal{T}_{\text{re}}^{\omega}| - 1}{|\mathcal{T}_{\text{base}}^{\text{last}}| \cdot |\mathcal{T}_{\text{re}}^{\omega}|} \tag{5.27}$$

As an illustrative example, consider an hourly resolution with $t_{\text{last}} = 24\,\text{h}$, so $|\mathcal{T}_{\text{base}}^{\text{last}}| = 24$, and let $\tau_{\text{reopt}} = 4\,\text{h}$, giving $|\mathcal{T}_{\text{re}}^{\omega}| = 4$. In this case, the ratio evaluates to $\frac{9}{32} \approx 28.1\,\%$.

The maximum number of secondary contingency situations (applicable to both the full and reduced graph structures) is given by:

$$|\Omega_{\text{sec}}| = |\Omega_{\text{re}}| \cdot (|\mathcal{C}| - 1) \tag{5.28}$$

For the full graph structure, this results in:

$$|\Omega_{\text{sec}}^{\text{full}}| = |\Omega_{\text{re}}^{\text{full}}| \cdot (|\mathcal{C}| - 1) \tag{5.29}$$
$$= |\mathcal{C}| \cdot (|\mathcal{C}| - 1) \cdot |\mathcal{T}_{\text{base}}^{\text{last}}| \cdot |\mathcal{T}_{\text{re}}^{\omega}| \tag{5.30}$$

The number of secondary contingency situations in the reduced graph is:

$$|\Omega_{\text{sec}}^{\text{reduced}}| = |\Omega_{\text{re}}^{\text{reduced}}| \cdot (|\mathcal{C}| - 1) \tag{5.31}$$
$$= |\mathcal{C}| \cdot (|\mathcal{C}| - 1) \cdot \left(|\mathcal{T}_{\text{base}}^{\text{last}}| + |\mathcal{T}_{\text{re}}^{\omega}| - 1\right) \tag{5.32}$$

The total amount of grid situations in a graph for the PrevCurRest strategy is

$$|\Omega| = |\Omega_{\text{base}}| + |\Omega_{\text{prim}}| + |\Omega_{\text{rest}}| + |\Omega_{\text{re}}| + |\Omega_{\text{sec}}|. \tag{5.33}$$

For the full graph structure, the maximum amount of grid situations is

$$|\Omega^{\text{full}}| = |\Omega_{\text{base}}| + |\Omega_{\text{prim}}| + |\Omega_{\text{rest}}| + |\Omega_{\text{re}}^{\text{full}}| + |\Omega_{\text{sec}}^{\text{full}}| \tag{5.34}$$
$$= |\mathcal{T}_{\text{base}}| + |\mathcal{C}| \cdot |\mathcal{T}_{\text{base}}^{\text{last}}| \cdot (1 + |\mathcal{T}_{\text{rest}}^{\omega}| + |\mathcal{C}| \cdot |\mathcal{T}_{\text{re}}^{\omega}|) \tag{5.35}$$
$$= |\mathcal{T}_{\text{base}}| + |\mathcal{C}| \cdot |\mathcal{T}_{\text{base}}^{\text{last}}| \cdot (1 + |\mathcal{T}_{\text{rest}}^{\omega}|) + |\mathcal{C}|^2 \cdot |\mathcal{T}_{\text{base}}^{\text{last}}| \cdot |\mathcal{T}_{\text{re}}^{\omega}|. \tag{5.36}$$

For the reduced graph structure, the maximum amount of grid situations is

$$|\Omega^{\text{reduced}}| = |\Omega_{\text{base}}| + |\Omega_{\text{prim}}| + |\Omega_{\text{rest}}| + |\Omega_{\text{re}}^{\text{reduced}}| + |\Omega_{\text{sec}}^{\text{reduced}}| \tag{5.37}$$
$$= |\mathcal{T}_{\text{base}}| + |\mathcal{C}| \cdot |\mathcal{T}_{\text{base}}^{\text{last}}| \cdot (1 + |\mathcal{T}_{\text{rest}}^{\omega}|) + |\mathcal{C}|^2 \cdot \left(|\mathcal{T}_{\text{base}}^{\text{last}}| + |\mathcal{T}_{\text{re}}^{\omega}| - 1\right). \tag{5.38}$$

Eq. (5.36) and Eq. (5.38) demonstrate that the graph size grows quadratically with the number of contingencies $|\mathcal{C}|$. This highlights the need for effective contingency filtering to maintain a tractable SCOPF problem size.

Comparing the quadratic terms in Eq. (5.36) and Eq. (5.38) shows that, in the full graph, the term is scaled by the *product* $|\mathcal{T}_{\text{base}}^{\text{last}}| \cdot |\mathcal{T}_{\text{re}}^{\omega}|$, while in the reduced graph, it is scaled by the *sum* $|\mathcal{T}_{\text{base}}^{\text{last}}| + |\mathcal{T}_{\text{re}}^{\omega}| - 1$. This reduction is particularly significant for longer planning horizons and extended restoration or recovery phases.

5.3. Optimization program

This thesis considers optimization programs in consensus form used in distributed optimization [42, P. 48]. The notation follows the one used in [41]. The optimization program is formulated as:

$$\begin{aligned} \min_{\mathbf{x}_1,\ldots,\mathbf{x}_{N_{\text{subprob}}}} \quad & \sum_{i=1}^{N_{\text{subprob}}} f_i\left(\mathbf{x}_i\right) & \\ \text{subject to} \quad & \mathbf{g}_i\left(\mathbf{x}_i\right) \leq 0 & \mid \nu_i \\ & \mathbf{h}_i\left(\mathbf{x}_i\right) = 0 & \mid \mu_i \\ & \sum_{i=1}^{N_{\text{subprob}}} \mathbf{E}_i \mathbf{x}_i = 0 & \mid \lambda_i \end{aligned} \tag{5.39}$$

Each of the N_{subprob} subproblems has its own set of decision variables $\mathbf{x}_i \in \mathbb{R}^{N_{x_i}}$, objective function $f_i : \mathbb{R}^{N_{x_i}} \to \mathbb{R}$, inequality constraints $\mathbf{g}_i : \mathbb{R}^{N_{x_i}} \to \mathbb{R}^{N_{g_i}}$, equality constraints $\mathbf{h}_i : \mathbb{R}^{N_{x_i}} \to \mathbb{R}^{N_{h_i}}$, and matrix $\mathbf{E}_i \in \mathbb{R}^{N_{x_i} \times N_{x_i}}$ for the coupling constraints in consensus form. The Lagrange multipliers are $\nu_i \in \mathbb{R}^{N_{g_i}}$, $\mu_i \in \mathbb{R}^{N_{h_i}}$, and $\lambda_i \in \mathbb{R}^{N_{x_i}}$. Note, that Lagrange multipliers are not available in MILPs.

The consensus form is common in distributed optimization and allows for a decentralized solving of the subproblems, in which only coupled subproblems need to communicate. Alternatively, a central coordinator may be applied, which is then referred to as “distributed” solving. The commonly used ADMM algorithm relies on the consensus form. For subproblems that share decision variables in their constraints, the variables are copied and linked by consensus constraints. Even though this work does not focus on distributed optimization, the consensus form provides straightforward extendability of the optimization program required in iterative solving schemes.

The following sections detail the formulation of the subproblems for each grid situation. Each subproblem corresponds to a node in the grid situation graph and is characterized by its own objective function, decision variables, and internal constraints. The coupling constraints, introduced later, connect these subproblems and ensure consistency across the overall optimization program. It is important to note that the coupling constraints are not the same as the transitions between the grid situations. Coupling constraints can also connect to subproblems that are not directly connected in the grid situation graph.

5.3.1. Objective

The objective function $f_\omega : \mathbb{R}^{N_{x_\omega}} \to \mathbb{R}$ share the same structure for all grid situations $\omega \in \Omega$ with the decision vector $\mathbf{x}_\omega \in \mathbb{R}^{N_{x_\omega}}$, the cost coefficient vector $\mathbf{c}_{\text{RD}} \in \mathbb{R}^{N_{x_\omega}}$, and the scaling factor $k_\omega \in \mathbb{R}^+$:

$$f_\omega\left(\mathbf{x}_\omega\right) = k_\omega \cdot \mathbf{c}_{\text{RD}}^\top \cdot \mathbf{x}_\omega \tag{5.40}$$

The factor k_ω scales the objective value depending on the grid situation type.

$$k_\omega = \begin{cases} 1 & : \omega \in \Omega_{\text{base}} \\ k_{\omega,\text{cur}} & : \omega \in \Omega_{\text{prim}} \cup \Omega_{\text{rest}} \cup \Omega_{\text{re}} \end{cases} \tag{5.41}$$

Since real costs for curative RAs only become relevant in the unlikely event of a primary contingency, the objective values of primary, restoration and recovered grid situations should be neglectable compared to the ones of the base situations. Hence, the condition

$$0 < k_{\omega,\text{cur}} \ll 1 \tag{5.42}$$

must be fulfilled. The choice of $k_{\omega,\text{cur}}$ requires special attention and depends on the specific grid. Very small values of $k_{\omega,\text{cur}}$ may lead to numerical issues in the optimization program. If $k_{\omega,\text{cur}}$ is chosen too large, the optimization may prefer to address several contingencies simultaneously using preventive RAs, rather than applying individual curative RAs for each contingency.

The decision vector

$$\mathbf{x}_\omega = \begin{bmatrix} \Delta\mathbf{p}_{\text{gen}}^{+} \\ \Delta\mathbf{p}_{\text{gen}}^{-} \\ \Delta\mathbf{p}^{\uparrow,+} \\ \Delta\mathbf{p}^{\uparrow,-} \\ \Delta\mathbf{p}^{\downarrow,+} \\ \Delta\mathbf{p}^{\downarrow,-} \\ \Delta\boldsymbol{\theta}^{+} \\ \Delta\boldsymbol{\theta}^{-} \end{bmatrix} \tag{5.43}$$

is constructed out of decision variable vectors according to Table 5.3.

Table 5.3.: Decision variables for redispatch and phase-angle adjustments

Positive generator redispatch	$\Delta\mathbf{p}^{+}_{\text{gen}} \in \mathbb{R}_0^{N_{\text{gen}},+}$	$= \left(\Delta P^{+}_1, \ldots, \Delta P^{+}_{N_{\text{gen}}}\right)^\top$
Negative generator redispatch	$\Delta\mathbf{p}^{-}_{\text{gen}} \in \mathbb{R}_0^{N_{\text{gen}},-}$	$= \left(\Delta P^{-}_1, \ldots, \Delta P^{-}_{N_{\text{gen}}}\right)^\top$
Positive storage charging redispatch	$\Delta\mathbf{p}^{\uparrow,+} \in \mathbb{R}_0^{N_{\text{stor}},+}$	$= \left(\Delta P^{\uparrow,+}_1, \ldots, \Delta P^{\uparrow,+}_{N_{\text{stor}}}\right)^\top$
Negative storage charging redispatch	$\Delta\mathbf{p}^{\uparrow,-} \in \mathbb{R}_0^{N_{\text{stor}},-}$	$= \left(\Delta P^{\uparrow,-}_1, \ldots, \Delta P^{\uparrow,-}_{N_{\text{stor}}}\right)^\top$
Positive storage discharging redispatch	$\Delta\mathbf{p}^{\downarrow,+} \in \mathbb{R}_0^{N_{\text{stor}},+}$	$= \left(\Delta P^{\downarrow,+}_1, \ldots, \Delta P^{\downarrow,+}_{N_{\text{stor}}}\right)^\top$
Negative storage discharging redispatch	$\Delta\mathbf{p}^{\downarrow,-} \in \mathbb{R}_0^{N_{\text{stor}},-}$	$= \left(\Delta P^{\downarrow,-}_1, \ldots, \Delta P^{\downarrow,-}_{N_{\text{stor}}}\right)^\top$
Positive phase-angle adjustments	$\Delta\boldsymbol{\theta}^{+} \in \mathbb{R}_0^{N_{\text{pst}},+}$	$= \left(\Delta\theta^{+}_1, \ldots, \Delta\theta^{+}_{N_{\text{pst}}}\right)^\top$
Negative phase-angle adjustments	$\Delta\boldsymbol{\theta}^{-} \in \mathbb{R}_0^{N_{\text{pst}},-}$	$= \left(\Delta\theta^{-}_1, \ldots, \Delta\theta^{-}_{N_{\text{pst}}}\right)^\top$

The cost coefficient vector $\mathbf{c}_{\text{RD}} \in \mathbb{R}^{N_{x_\omega}}$

$$\mathbf{c}_{\text{RD}} = \begin{bmatrix} \mathbf{c}^{+}_{\text{gen}} \\ \mathbf{c}^{-}_{\text{gen}} \\ \mathbf{c}^{+}_{\text{stor}} \\ \mathbf{c}^{-}_{\text{stor}} \\ \mathbf{c}^{+}_{\text{stor}} \\ \mathbf{c}^{-}_{\text{stor}} \\ \mathbf{c}^{+}_{\text{pst}} \\ \mathbf{c}^{-}_{\text{pst}} \end{bmatrix} \tag{5.44}$$

contains the cost coefficient vectors for redispatch of generators, storage units, and phase-angle adjustments according to Table 5.4.

Table 5.4.: Cost coefficients for redispatch and phase-angle adjustments

Positive generator redispatch	$\mathbf{c}^{+}_{\text{gen}} \in \mathbb{R}^{N_{\text{gen}},+}$	$= \left(c^{+}_{\text{gen},1}, \ldots, c^{+}_{\text{gen},N_{\text{gen}}}\right)^{\top}$
Negative generator redispatch	$\mathbf{c}^{-}_{\text{gen}} \in \mathbb{R}^{N_{\text{gen}},-}$	$= \left(c^{-}_{\text{gen},1}, \ldots, c^{-}_{\text{gen},N_{\text{gen}}}\right)^{\top}$
Positive storage redispatch	$\mathbf{c}^{+}_{\text{stor}} \in \mathbb{R}^{N_{\text{stor}},+}$	$= \left(c^{+}_{\text{stor},1}, \ldots, c^{+}_{\text{stor},N_{\text{stor}}}\right)^{\top}$
Negative storage redispatch	$\mathbf{c}^{-}_{\text{stor}} \in \mathbb{R}^{N_{\text{stor}},-}$	$= \left(c^{-}_{\text{stor},1}, \ldots, c^{-}_{\text{stor},N_{\text{stor}}}\right)^{\top}$
Positive phase-angle adjustments	$\mathbf{c}^{+}_{\text{pst}} \in \mathbb{R}^{N_{\text{pst}},+}$	$= \left(c^{+}_{\text{pst},1}, \ldots, c^{+}_{\text{pst},N_{\text{pst}}}\right)^{\top}$
Negative phase-angle adjustments	$\mathbf{c}^{-}_{\text{pst}} \in \mathbb{R}^{N_{\text{pst}},-}$	$= \left(c^{-}_{\text{pst},1}, \ldots, c^{-}_{\text{pst},N_{\text{pst}}}\right)^{\top}$

As regulatory requirement, the usage non-costly RAs is prioritized over costly RAs [68]. The cost coefficients are weighted such, that they reflect the regulatory prioritization of different RA categories:

1. **Grid-related actions** (also "non-costly RAs", e. g. switching, tap changes, HVDC set points) involve operator-owned assets and therefore have the lowest cost coefficients. The cost coefficients are small but positive to avoid arbitrary adjustments by the solver.
2. **Market-related actions** (also "costly RAs", e. g. redispatch and counter-trading) have medium cost coefficients as they involve reimbursements for market participants when generation or load schedules are affected by RAs.
3. **Emergency actions** (e. g. generation curtailment and load shedding) have high cost coefficients as they are the last resort to avoid cascading outages and should only be used in emergencies.

Consequently, the cost coefficients must satisfy the following conditions:

$$0 < \max\left(\mathbf{c}^{+}_{\text{pst}}\right) < \min\left[{\mathbf{c}^{+}_{\text{gen}}}^{\top}, {\mathbf{c}^{+}_{\text{stor}}}^{\top}\right]^{\top} \tag{5.45}$$

$$\max\left[{\mathbf{c}^{-}_{\text{gen}}}^{\top}, {\mathbf{c}^{-}_{\text{stor}}}^{\top}\right]^{\top} < \min\left(\mathbf{c}^{-}_{\text{pst}}\right) < 0 \tag{5.46}$$

In the relations of Eqs. (5.45) and (5.46), the cost vectors for generator and storage redispatch are grouped together, as they both represent market-related actions. Depending on the regulatory framework, the cost coefficients for storage units may be larger or smaller than the ones for generators.

To ensure feasibility, it is common to relax certain constraints with slack variables with high associated cost coefficients to penalize constraint violations. Typical relaxed constraints are bus balance, system balance or branch flow constraints. This documentation omits the explicit relaxation of constraints for brevity.

The generator redispatch cost coefficients $c^{+}_{\text{gen},g}$ and $c^{-}_{\text{gen},g}$ are determined as a function of the unit's marginal costs $c_{\text{gen},g} \in \mathbb{R}^{+}$ according to the following expressions:

$$c^{+}_{\text{gen},g} = c_{\text{RD}} + c_{\text{gen},g} \tag{5.47}$$

$$c^{-}_{\text{gen},g} = -\left(c_{\text{RD}} + \frac{1}{c_{\text{gen},g}}\right) \tag{5.48}$$

$$\forall g \in \{1, \ldots, N_{\text{gen}}\}.$$

The constant term $c_{\text{RD}} \in \mathbb{R}^{+}$ act as a minimum cost for all redispatch measures to ensure that grid-related actions are prioritized over market-related actions. The fraction $\frac{1}{c_{\text{gen},g}}$ in Eq. (5.48) ensures that negative redispatch of high-cost units is preferred over negative redispatch of low-cost units. The cost coefficients for HVDC converters and storage units have almost no marginal costs and are therefore set to a constant value.

Depending on the regulatory framework, a distinction between conventional units and RES may be required to prioritize the usage of RES. This prioritization may, however, lead to solutions of the SCOPF program that are optimal in terms of the objective function but not optimal regarding the total Redispatch (RD) volume. Therefore, this work assumes the same marginal costs $c_{\text{gen},g}$ for all generators.

5.3.2. Internal Constraints

This section covers the internal equality constraints g_i and inequality constraints h_i local to each grid situation's subproblem (Eq. (5.39)).

5.3.2.1. Power balance

The power balance constraints ensure that the sum of all power injections and withdrawals at a bus $n \in \mathcal{N}$ is equal to the sum of all power flows on the branches connected to the

bus:

$$\sum_{g \in \mathcal{G}_i} P_g(\omega) + \sum_{s \in \mathcal{S}_i} P_s(\omega) - \sum_{d \in \mathcal{D}_i} P_d(\omega) - \sum_{(i,k) \in \mathcal{B}^{\mathrm{E}}{}_i} P_{i,k}(\omega) = 0 \qquad \forall i \in \mathcal{N} \tag{5.49}$$

The set $\mathcal{G}_i$ contains all generators connected to bus i, $\mathcal{S}_i$ contains all storage units at bus i, and $\mathcal{D}_i$ contains all loads at bus i. $\mathcal{B}^{\mathrm{E}}{}_i$ contains all branches connected to bus i, where the branch flow is positive when flowing away from bus i.

5.3.2.2. Generators

The set of generators $\mathcal{G} = \{1, \ldots, N_{\text{gen}}\}$ includes all conventional and renewable generators as well as h converters that can be redispatched. Redispatch is a RA that modifies generator schedules relative to their market dispatch in order to alleviate congestion on grid elements. The active power output of a generator $P_g(\omega)$ after redispatch is the sum of the initial power output $P_{g,\text{init}}(\omega)$ and the positive redispatch $\Delta P_g^+(\omega) \in \mathbb{R}_0^+$ and negative redispatch $\Delta P_g^-(\omega) \in \mathbb{R}_0^-$.

$$P_g(\omega) = P_{g,\text{init}}(\omega) + \Delta P_g^+(\omega) + \Delta P_g^-(\omega) \qquad \forall g \in \mathcal{G},\ \omega \in \Omega \tag{5.50}$$

For base situations $\omega \in \Omega_{\text{base}}$, $P_{g,\text{init}}(\omega)$ is the market power schedule. For other grid situations, the initial power output is linked to the redispatch of the corresponding base situation(s) (see Section 5.3.3).

Depending on the generator type, different constraints represent its physical properties. In the following, three generator types are distinguished based on their operational flexibility.

0-state These units can be freely adjusted within their operational limits without minimum up- or down-time constraints (e. g. RES, HVDC converters). The generator set is defined as follows:

$$\mathcal{G}_{0\text{state}} = \left\{ g \in \mathcal{G} \mid P_g^{\min} \leq 0 \right\} \tag{5.51}$$

0-state units $g \in \mathcal{G}_{\text{0state}}$ are modelled without binary variables, as they can be freely adjusted within their operational limits:

$$P_g^{\min} \leq P_g(\omega) \leq P_g^{\max} \qquad \forall g \in \mathcal{G}_{\text{0state}},\ \omega \in \Omega. \tag{5.52}$$

For RES units, $P_g^{\max}$ is the maximum available power output for the current weather conditions, while for conventional units, $P_g^{\max}$ is the installed generation capacity.

2-state These units can be either on or off, have a minimum power output, and can have minimum up- and down-time constraints (e. g. gas turbines, run-of-river plants). Figure 5.3 illustrates the possible state transitions. The gradients for startup $\delta_{\text{startup},g}$ and shutdown

Figure 5.3.: State transitions of 2-state generators

$\delta_{\text{shutdown},g}$ related to the base time interval are larger than or equal to the minimum power output $P_g^{\min}$. The generator set is defined as follows:

$$\mathcal{G}_{\text{2state}} = \left\{ g \in \mathcal{G} \mid P_g^{\min} > 0, \delta_{\text{startup},g} \geq P_g^{\min}, |\delta_{\text{shutdown},g}| \geq P_g^{\min} \right\} \tag{5.53}$$

2-state units $g \in \mathcal{G}_{\text{2state}}$ have the binary variable $u_{\text{on},g} \in \{0, 1\}$ to model the on- and off-state.

$$P_g^{\min} \cdot u_{\text{on},g}(\omega) \leq P_g(\omega) \leq P_g^{\max} \cdot u_{\text{on},g}(\omega) \qquad \forall g \in \mathcal{G}_{\text{2state}},\ \omega \in \Omega \tag{5.54}$$

Explicitly modeling the on- and off-state allows for the additional modeling of minimum up- and down-times as well as penalty costs for switching the unit on or off (Fig. 5.3).

4-state These units can be on, off, in startup, or in shutdown, have a minimum power output, and can have minimum up- and down-time constraints (e. g. coal or nuclear plants).

Figure 5.4 shows the possible transitions of 4-state generators. The gradients for startup

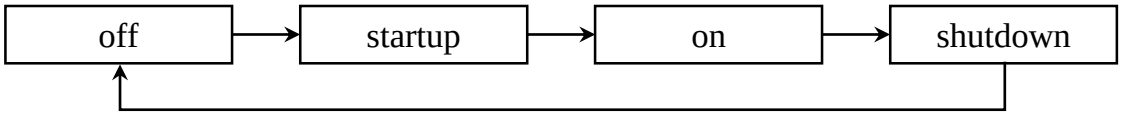

Figure 5.4.: State transitions of 4-state generators

$\delta_{\text{startup},g}$ and shutdown $\delta_{\text{shutdown},g}$ related to the base time interval are smaller than the minimum power output $P_g^{\min}$. The generator set is defined as follows:

$$\mathcal{G}_{\text{4state}} = \left\{ g \in \mathcal{G} \mid P_g^{\min} > 0, \delta_{\text{startup},g} < P_g^{\min}, |\delta_{\text{shutdown},g}| < P_g^{\min} \right\} \tag{5.55}$$

4-state units $g \in \mathcal{G}_{\text{4state}}$ require additional binary variables to model the startup state $u_{\text{startup},g} \in \{0,1\}$ and shutdown state $u_{\text{shutdown},g} \in \{0,1\}$.

$$P_g^{\min} \cdot u_{\text{on},g}(\omega) \leq P_g(\omega) \leq P_g^{\max} \cdot u_{\text{on},g}(\omega) + P_g^{\min} \cdot \left(u_{\text{startup},g}(\omega) + u_{\text{shutdown},g}(\omega) \right) \tag{5.56}$$
$$\forall g \in \mathcal{G}_{\text{4state}},\ \omega \in \Omega$$

The following constraints ensure that only one binary variable is active at a time:

$$u_{\text{on},g}(\omega) + u_{\text{startup},g}(\omega) + u_{\text{shutdown},g}(\omega) \leq 1 \tag{5.57}$$
$$\forall g \in \mathcal{G}_{\text{4state}}, \omega \in \Omega.$$

The off-status is implicitly determined by the other status variables and therefore does not require explicit modeling as a decision variable.

$$u_{\text{off},g}(\omega) = 1 - u_{\text{on},g}(\omega) - u_{\text{startup},g}(\omega) - u_{\text{shutdown},g}(\omega) \tag{5.58}$$
$$\forall g \in \mathcal{G}_{\text{4state}}, \omega \in \Omega$$

The 4-state model is applied for conventional power plants and adds intermediate states for startup and shutdown. The 4-state model allows for a distinct modeling of startup and shutdown ramp rates and thus enables a more realistic modeling of conventional power plants. This work does not further distinguish between different startup modes, such as hot-start, warm-start, and cold-start, which depend on the time since the last shutdown. By adding additional binary constraints, these startup modes could be modeled.

Figure 5.5 shows an examplary cycle of a 4-state generator. The dashed line indicates the power output of the generator, whereas the solid line indicates the discrete operating point assumed by the SCOPF model.

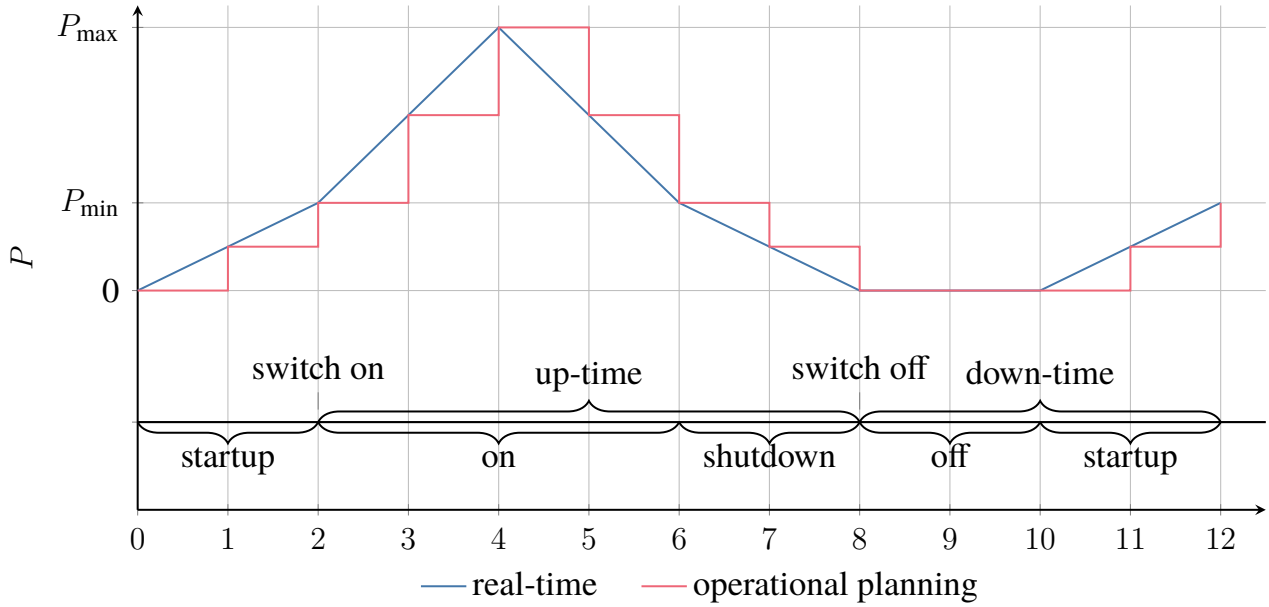

Figure 5.5.: Example of a 4-state generator cycle.

5.3.2.3. Storage

The set of storage units $\mathcal{S} = \{1, \ldots, N_{\mathcal{S}}\}$ includes all BESSs and other storages that can be redispatched. For storage units, charging $P_s^{\uparrow} \in \mathbb{R}_0^+$ and discharging $P_s^{\downarrow} \in \mathbb{R}_0^+$ are represented by separate variables. This distinction allows the application of different efficiency factors when updating the SoC W_s.

The active power output of a storage unit $s \in \mathcal{S}$ is

$$P_s(\omega) = P_s^{\downarrow}(\omega) - P_s^{\uparrow}(\omega) \qquad (5.59)$$
$$\forall s \in \mathcal{S},\ \omega \in \Omega.$$

Redispatch of storage units is considered separately by positive and negative direction, as well as for charging ($\Delta P_s^{\uparrow,+} \in \mathbb{R}_0^+$ and $\Delta P_s^{\uparrow,-} \in \mathbb{R}_0^-$) and discharging ($\Delta P_s^{\downarrow,+} \in \mathbb{R}_0^+$ and

$\Delta P_s^{\downarrow,-} \in \mathbb{R}_0^-$):

$$P_s^{\uparrow}(\omega) = P_{s,\text{init}}^{\uparrow}(\omega) + \Delta P_s^{\uparrow,+}(\omega) + \Delta P_s^{\uparrow,-}(\omega) \tag{5.60}$$

$$P_s^{\downarrow}(\omega) = P_{s,\text{init}}^{\downarrow}(\omega) + \Delta P_s^{\downarrow,+}(\omega) + \Delta P_s^{\downarrow,-}(\omega) \tag{5.61}$$

$$\forall s \in \mathcal{S},\ \omega \in \Omega$$

For base situations $\omega \in \Omega_{\text{base}}$, the initial power set points $P_{s,\text{init}}^{\uparrow}(\omega)$ and $P_{s,\text{init}}^{\downarrow}(\omega)$ are the market schedules. For other grid situations, the initial set points are linked to the redispatch of the corresponding base situation(s) (see Section 5.3.3).

The storage's operational limits are:

$$P_s^{\min} \leq P_s(\omega) \leq P_s^{\max} \tag{5.62}$$

$$0 \leq P_s^{\uparrow}(\omega) \leq P_s^{\uparrow,\max} \tag{5.63}$$

$$0 \leq P_s^{\downarrow}(\omega) \leq P_s^{\downarrow,\max} \tag{5.64}$$

$$\forall s \in \mathcal{S},\ \omega \in \Omega$$

Simultaneous charging and discharging is a well-known issue in standard OPF models that minimize generation costs. In such cases, a storage unit may charge and discharge at the same time to manipulate its SoC, for example, to reach a required final SoC at the end of the optimization horizon. Although the OPF formulation for CM penalizes all redispatch actions involving storage, making simultaneous charging and discharging unlikely, it can still occur if this appears to be the most cost-efficient solution. To prevent this, an additional binary variable v can be introduced in MILP models to explicitly prohibit simultaneous charging and discharging. Alternative continuous formulations exist, but they may reduce accuracy for the SoC over longer horizons or with low efficiency factors [69]. This work's model, use the binary variable $v_s \in \{0, 1\}$ to prevent simultaneous charging and discharging:

$$0 \leq P_s^{\uparrow}(\omega) \leq v_s \cdot P_s^{\uparrow,\max} \tag{5.65}$$

$$0 \leq P_s^{\downarrow}(\omega) \leq (1 - v_s) \cdot P_s^{\downarrow,\max} \tag{5.66}$$

$$\forall s \in \mathcal{S},\ \omega \in \Omega$$

The SoC $W_s(\omega)$ is part of the coupling constraint Eq. (5.88) (see Section 5.3.3). The

subproblem-related box constraint associated to the storage's capacity is:

$$0 \leq W_s(\omega) \leq W_s^{\max} \quad \forall s \in \mathcal{S},\ \omega \in \Omega \tag{5.67}$$

5.3.2.4. Branches

The branch flows are expressed by Eqs. (3.25) and (3.26). Due to the lossless DC-approximation, the flows at the sending and receiving end only differ in sign. It is therefore sufficient, to consider only the forward flow direction (i, k). The set of branch indexes is denoted by $\mathcal{B} = \{1, \ldots, N_{\text{branch}}\}$, the set of bus indexes is $\mathcal{B}^{\text{E}} = \{(i_1, k_1), \ldots, (i_{N_{\text{branch}}}, k_{N_{\text{branch}}})\}$. To achieve better scaling, the branch flows are expressed as loadings $l_b(\omega)$ relative to I_b^{PATL}:

$$l_b = l_{i,k} = \frac{P_{i,k}}{I_b^{\text{PATL}} \cdot V_i(\omega)} \quad \forall b \in \mathcal{B},\ (i,k) \in \mathcal{B}^{\text{E}},\ \omega \in \Omega \tag{5.68}$$

Note, that the voltage magnitude $V_i(\omega)$ and $P_{i,k}$ are expressed in p.u.

The thermally permissible loading of a branch $l_b^{\max}(\omega)$ depends on the type of the grid situation ω:

$$l_b^{\max}(\omega) = \begin{cases} I_b^{\text{TATL},1} / I_b^{\text{PATL}} & \text{if } \omega \in \Omega_{\text{prim}} \\ I_b^{\text{TATL},2} / I_b^{\text{PATL}} & \text{if } \tau(\omega) = \tau_1 \\ 1 & \text{else} \end{cases} \tag{5.69}$$

The loading constraint is expressed as:

$$-l_b^{\max}(\omega) \leq l_b(\omega) \leq l_b^{\max}(\omega) \quad \forall b \in \mathcal{B}, \omega \in \Omega \tag{5.70}$$

5.3.2.5. Phase-shift transformers

The set of PSTs indexes is denoted by $\mathcal{R} = \{1, \ldots, N_{\text{pst}}\}$. Adjusting the phase angle of PST is modelled as:

$$\theta_r(\omega) = \theta_{r,\text{init}}(\omega) + \Delta\theta_r^+(\omega) + \Delta\theta_r^-(\omega) \quad \forall r \in \mathcal{R},\ \omega \in \Omega \tag{5.71}$$

5.3.2.6. HVDC links

HVDC links are modelled as a pairs of generators $\mathcal{H} = \{(g_1, g_2) \in \mathcal{G} \times \mathcal{G} \mid g_1 \neq g_2\}$, where the first generator g_1 represents the sending end and the second generator g_2 the receiving end of the HVDC link h. Neglecting the losses, the following constraints apply:

$$P_{g_1}(\omega) = -P_{g_2}(\omega) \quad \forall (g_1, g_2) \in \mathcal{H},\ \omega \in \Omega \tag{5.72}$$

5.3.3. Coupling constraints

Coupling constraints establish the interdependencies between subproblems corresponding to different grid situations. In this framework, the dispatch of units—including preventive RAs—determined in the base situations serves as the reference point for all post-contingency grid situations with matching timestamps. Consequently, curative RAs are always modeled as adjustments relative to the preventive RAs already implemented in the base situations.

5.3.3.1. Overarching coupling constraints

The overarching coupling constraints model the interdependencies between base, restoration and recovered grid situations that are connected by the time transitions inside the grid situation graph.

As this work assumes an hourly time resolution, the ramping constraints are only applied to generators, while gradients of BESSs, HVDC links, and PST are not explicitly modeled.

They are assumed to have sufficient ramping capabilities to follow any set point changes within one hour.

The following coupling constraints are based on the grid situation ω, taking into account the neighborhood notation introduced in Section 5.2.2.

Generator state transitions While 2-state generators only switch between the on- and off-state, 4-state generators have intermediate states for startup and shutdown. The following constraints restrict the state transitions of 4-state generator in line with Fig. 5.4:

$$u_{\text{on},g}(\omega_{\text{nb}}) + u_{\text{off},g}(\omega) \leq 1 \tag{5.73}$$
$$u_{\text{on},g}(\omega_{\text{nb}}) + u_{\text{startup},g}(\omega) \leq 1 \tag{5.74}$$
$$u_{\text{off},g}(\omega_{\text{nb}}) + u_{\text{on},g}(\omega) \leq 1 \tag{5.75}$$
$$u_{\text{off},g}(\omega_{\text{nb}}) + u_{\text{shutdown},g}(\omega) \leq 1 \tag{5.76}$$
$$u_{\text{startup},g}(\omega_{\text{nb}}) + u_{\text{off},g}(\omega) \leq 1 \tag{5.77}$$
$$u_{\text{startup},g}(\omega_{\text{nb}}) + u_{\text{shutdown},g}(\omega) \leq 1 \tag{5.78}$$
$$u_{\text{shutdown},g}(\omega_{\text{nb}}) + u_{\text{on},g}(\omega) \leq 1 \tag{5.79}$$
$$u_{\text{shutdown},g}(\omega_{\text{nb}}) + u_{\text{startup},g}(\omega) \leq 1 \tag{5.80}$$
$$\forall g \in \mathcal{G}_{\text{4state}},\ \omega \in \Omega \mid \exists\, \omega_{\text{nb}} \in \Omega^{\text{in}}(\omega)$$

Generator ramping The constraints of 2-state generators with the gradients $\delta_{\text{up},g}$ and $\delta_{\text{down},g}$ are:

$$u_{\text{on},g}(\omega) \cdot \delta_{\text{down},g} \leq P_g(\omega) - P_g(\omega_{\text{nb}}) \leq u_{\text{on},g}(\omega) \cdot \delta_{\text{up},g} \tag{5.81}$$
$$\forall g \in \mathcal{G}_{\text{2state}},\ \omega \in \Omega \mid \exists\, \omega_{\text{nb}} \in \Omega^{\text{in}}(\omega)$$

The ramping constraints for 4-state units involve the gradients $\delta_{\text{up},g}$, $\delta_{\text{down},g}$, $\delta_{\text{startup},g}$, and $\delta_{\text{shutdown},g}$. Specifically, Eq. (5.82) limits generator ramping in the on-state using $\delta_{\text{up},g}$ and $\delta_{\text{down},g}$, while during startup and shutdown, the ramping is fixed by $\delta_{\text{startup},g}$ and $\delta_{\text{shutdown},g}$,

respectively.

$$\begin{aligned} & u_{\text{on},g}(\omega) \cdot \delta_{\text{up},g} + u_{\text{startup},g}(\omega) \cdot \delta_{\text{startup},g} + u_{\text{shutdown},g}(\omega) \cdot \delta_{\text{shutdown},g} \\ & \leq P_g(\omega) - P_g(\omega_{\text{nb}}) \\ & \leq u_{\text{on},g}(\omega) \cdot \delta_{\text{down},g} + u_{\text{startup},g}(\omega) \cdot \delta_{\text{startup},g} + u_{\text{shutdown},g}(\omega) \cdot \delta_{\text{shutdown},g} \\ & \qquad \forall g \in \mathcal{G}_{\text{4state}},\ \omega \in \Omega \mid \exists\, \omega_{\text{nb}} \in \Omega^{\text{in}}(\omega) \end{aligned} \tag{5.82}$$

The constraint Eq. (5.83) ensures that the generator is ramped up to at least the minimum power output $P_g^{\min}$ before the ramping limits of the on-state can be applied. ϵ_{tol} is a small tolerance value to avoid numerical issues. If this constraint was missing, the generator could be switched on before reaching the minimum power output.

$$\begin{aligned} P_g(\omega_{\text{nb}}) \geq u_{\text{on},g}(\omega) \cdot \left(P_g^{\min} - \epsilon_{\text{tol}}\right) \\ \forall g \in \mathcal{G}_{\text{4state}},\ \omega \in \Omega \mid \exists\, \omega_{\text{nb}} \in \Omega^{\text{in}}(\omega) \end{aligned} \tag{5.83}$$

Generator up/down time The minimum up- and down-times of generators are defined as the periods in which the generator may not change its on- or off-state, respectively. The indicators $u_{\text{switchon},g}$ and $u_{\text{switchoff},g}$ help to identify the beginning of up- and down-times [70]:

$$\begin{aligned} u_{\text{switchon},g}(\omega) &= u_{\text{on},g}(\omega) - u_{\text{on},g}(\omega_{\text{nb}}) \\ &= \begin{cases} 1 & \text{if switched on in } \omega \\ \{0, -1\} & \text{else} \end{cases} \end{aligned} \tag{5.84}$$

$$\begin{aligned} u_{\text{switchoff},g}(\omega) &= u_{\text{off},g}(\omega) - u_{\text{off},g}(\omega_{\text{nb}}) \\ &= \begin{cases} 1 & \text{if switched off in } \omega \\ \{0, -1\} & \text{else} \end{cases} \end{aligned} \tag{5.85}$$

$$\forall g \in \mathcal{G}_{\text{2state}} \cup \mathcal{G}_{\text{4state}},\ \omega \in \Omega \mid \exists\, \omega_{\text{nb}} \in \Omega^{\text{in}}(\omega).$$

The minimum up-time $\tau_{\text{up},g}$ of a unit creates a forward link to future grid stuations that

follow ω:

$$u_{\text{on},g}(\omega^{\text{nb}}) \geq u_{\text{switchon},g}(\omega) \quad \forall g \in \mathcal{G},\ \omega \in \Omega \mid \exists\, \omega_{\text{nb}} \in \Omega^{\text{out}+}(\omega, \tau_{\text{up},g} - 1\,\text{h}) \tag{5.86}$$

Analogously, the constraint associated with the minimum down-time constraint is expressed as:

$$u_{\text{off},g}(\omega^{\text{nb}}) \geq u_{\text{switchoff},g}(\omega) \quad \forall g \in \mathcal{G},\ \omega \in \Omega \mid \exists\, \omega_{\text{nb}} \in \Omega^{\text{out}+}(\omega, \tau_{\text{down},g} - 1\,\text{h}) \tag{5.87}$$

The constraints in Eq. (5.86) and Eq. (5.87) apply to base, restoration, and recovered grid situations. Depending on the minimum up-times, minimum down-times, and the amount of simultaneously relevant primary contingencies per base situation, the optimization program may contain many of these binary constraints. Moreover, the constraints may be highly restrictive for inflexible generators with high minimum up- and down-times.

To reduce the number of binary constraints, generator states can be enforced to be identical across base, restoration, and recovered situations that share the same timestamp. This simplification limits the application of minimum up- and down-time constraints to the base situations only. As a result, generators cannot change their operating status independently in post-contingency grid situations with the same timestamp as the base case. While this approach reduces model complexity, it also decreases operational flexibility after contingencies. Therefore, more preventive RAs may be required to ensure that the base grid state is robust enough to accommodate all relevant contingencies. This increased security margin is likely to result in higher overall CM costs.

State-of-Charge The SoC $W_s(\omega)$ of a storage s is expressed as:

$$W_s(\omega) = \begin{cases} W_{s,\text{init}} & \text{if } \Omega^{\text{in}}(\omega) = \emptyset \\ W_s(\omega_{\text{nb}}) + (t_{\text{act}}(\omega) - t_{\text{act}}(\omega_{\text{nb}})) \cdot \left(\eta_s^{\uparrow} \cdot P_s^{\uparrow}(\omega) - \frac{P_s^{\downarrow}(\omega)}{\eta_s^{\downarrow}}\right) & \text{else} \end{cases} \quad \forall s \in \mathcal{S},\ \omega \in \Omega \mid \exists\, \omega_{\text{nb}} \in \Omega^{\text{in}}(\omega) \tag{5.88}$$

with the efficiency factors $\eta_s^{\uparrow}$ for charging and $\eta_s^{\downarrow}$ for discharging. For the set of base and recovered grid situation(s) at the end of the business day, the SoC is constrained to $W_{s,\text{init}}$

to avoid discontinuities when calculating multiple OPFs for consecutive periods:

$$W_s(\omega) = W_{s,\text{init}} \tag{5.89}$$
$$\forall s \in \mathcal{S},\ \omega \in \{\omega \in \Omega_{\text{base}} \cup \Omega_{\text{re}} \mid t_{\text{act}}(\omega) = t_{\text{last}}\}$$

5.3.3.2. Type-wise coupling constraints

Type-wise coupling constraints capture the interdependencies between particular categories of grid situations. These constraints may connect grid situations that are not directly linked by an edge in the grid situation graph, but nevertheless require alignment. The following paragraphs detail the coupling constraints for each relevant pair of grid situation types.

Base-Primary coupling constraints The primary situation ω_{prim} directly succeeds the base situation ω_{base}. Therefore, the generator states (Eqs. (5.90) to (5.92)), storage state (Eq. (5.93)), generator active power outputs (Eq. (5.94)), and PST angles (Eq. (5.95)) in the primary situation are set equal to those in the corresponding base situation.

$$u_{\text{on},g}(\omega_{\text{prim}}) = u_{\text{on},g}(\omega_{\text{base}}) \qquad \forall g \in \mathcal{G}_{\text{2state}} \cup \mathcal{G}_{\text{4state}} \tag{5.90}$$
$$u_{\text{startup},g}(\omega_{\text{prim}}) = u_{\text{startup},g}(\omega_{\text{base}}) \qquad \forall g \in \mathcal{G}_{\text{4state}} \tag{5.91}$$
$$u_{\text{shutdown},g}(\omega_{\text{prim}}) = u_{\text{shutdown},g}(\omega_{\text{base}}) \qquad \forall g \in \mathcal{G}_{\text{4state}} \tag{5.92}$$
$$v_s(\omega_{\text{prim}}) = v_s(\omega_{\text{base}}) \qquad \forall s \in \mathcal{S} \tag{5.93}$$
$$P_g(\omega_{\text{prim}}) = P_g(\omega_{\text{base}}) \qquad \forall g \in \mathcal{G} \tag{5.94}$$
$$\theta_r(\omega_{\text{prim}}) = \theta_r(\omega_{\text{base}}) \qquad \forall r \in \mathcal{R} \tag{5.95}$$

$$\forall \left(\omega_{\text{base}}, \omega_{\text{prim}}\right) \in \mathcal{E}_{\text{base}\to\text{prim}}$$

The TATL1 polyhedron $\mathcal{M}_{\text{TATL1}}$ constrains the branch loading $l_b(\omega_{\text{prim}})$:

$$l_b(\omega_{\text{prim}}) \in \mathcal{M}_{\text{TATL1}} \tag{5.96}$$
$$\forall b \in \mathcal{B}, \left(\omega_{\text{base}}, \omega_{\text{prim}}\right) \in \mathcal{E}_{\text{base}\to\text{prim}}$$

Base-Restoration coupling constraints An important aspect of the restoration phase is that $\{\tau_1, \tau_2\} \notin \mathcal{T}_{\text{base}}$, this means that the grid situations $\omega_{\text{rest},1} = (t_i, c, \tau_1, 0)^\top$ and $\omega_{\text{rest},2} =$

$(t_i, c, \tau_2, 0)^\top$ do not coincide with any base situation. In this case, the operating points of generators and storages after preventive RAs are determined by linear interpolation between two base situations whose actual timestamps immediately precede and follow the timestamp of $\omega_{\text{rest},1}$ or $\omega_{\text{rest},2}$. Specifically, these are $\omega_{\text{base},1} = (t_i)$ and $\omega_{\text{base},2} = (t_{i+1})$.

$$P_{g,\text{init}}(\omega_{\text{rest}}) = P_g(\omega_{\text{base},1}) + \tau \cdot \frac{P_g\left(\omega_{\text{base},2}\right) - P_g\left(\omega_{\text{base},1}\right)}{t_{\text{act}}(\omega_{\text{base},2}) - t_{\text{act}}(\omega_{\text{base},1})} \qquad \forall g \in \mathcal{G} \tag{5.97}$$

$$P^{\uparrow}_{s,\text{init}}(\omega_{\text{rest}}) = P^{\uparrow}_s(\omega_{\text{base},1}) + \tau \cdot \frac{P^{\uparrow}_s\left(\omega_{\text{base},2}\right) - P^{\uparrow}_s\left(\omega_{\text{base},1}\right)}{t_{\text{act}}(\omega_{\text{base},2}) - t_{\text{act}}(\omega_{\text{base},1})} \qquad \forall s \in \mathcal{S} \tag{5.98}$$

$$P^{\downarrow}_{s,\text{init}}(\omega_{\text{rest}}) = P^{\downarrow}_s(\omega_{\text{base},1}) + \tau \cdot \frac{P^{\downarrow}_s\left(\omega_{\text{base},2}\right) - P^{\downarrow}_s\left(\omega_{\text{base},1}\right)}{t_{\text{act}}(\omega_{\text{base},2}) - t_{\text{act}}(\omega_{\text{base},1})} \qquad \forall s \in \mathcal{S} \tag{5.99}$$

$$\theta_{r,\text{init}}(\omega_{\text{rest}}) = \theta_r(\omega_{\text{base},1}) + \tau \cdot \frac{\theta_r\left(\omega_{\text{base},2}\right) - \theta_r\left(\omega_{\text{base},1}\right)}{t_{\text{act}}(\omega_{\text{base},2}) - t_{\text{act}}(\omega_{\text{base},1})} \qquad \forall r \in \mathcal{R} \tag{5.100}$$

$$\forall \omega_{\text{rest}} \in \Omega_{\text{rest}} \mid \tau(\omega_{\text{rest}}) \in \{\tau_1, \tau_2\}$$

For the set of restoration situations $\Omega^{\text{aligned}}_{\text{rest}} = \{\omega \in \Omega_{\text{rest}} \mid \tau(\omega) > \tau_2\}$ there exist coinciding base situations with $t_{\text{act}}(\omega_{\text{base}}) = t_{\text{act}}(\omega_{\text{rest}})$. In this case, the initial set points of generators, storages, and PSTs are equal to the base situation's set points including preventive RAs:

$$P_{g,\text{init}}(\omega_{\text{rest}}) = P_g(\omega_{\text{base}}) \qquad \forall g \in \mathcal{G} \tag{5.101}$$

$$P^{\uparrow}_{s,\text{init}}(\omega_{\text{rest}}) = P^{\uparrow}_s(\omega_{\text{base}}) \qquad \forall s \in \mathcal{S} \tag{5.102}$$

$$P^{\downarrow}_{s,\text{init}}(\omega_{\text{rest}}) = P^{\downarrow}_s(\omega_{\text{base}}) \qquad \forall s \in \mathcal{S} \tag{5.103}$$

$$\theta_{r,\text{init}}(\omega_{\text{rest}}) = \theta_r(\omega_{\text{base}}) \qquad \forall r \in \mathcal{R} \tag{5.104}$$

$$\forall \{\omega_{\text{rest}} \in \Omega^{\text{aligned}}_{\text{rest}}, \omega_{\text{base}} \in \Omega_{\text{base}}\} \mid t_{\text{act}}(\omega_{\text{base}}) = t_{\text{act}}(\omega_{\text{rest}})$$

Base-Recovered coupling constraints The timestamps of base and recovered grid situations always coincide. The initial set points of generators, storages, and PSTs in the recovered grid situations are equal to the base situation's set points including preventive

RAs:

$$P_{g,\text{init}}(\omega_{\text{re}}) = P_g(\omega_{\text{base}}) \qquad \forall g \in \mathcal{G} \tag{5.105}$$

$$P^{\uparrow}_{s,\text{init}}(\omega_{\text{re}}) = P^{\uparrow}_{s}(\omega_{\text{base}}) \qquad \forall s \in \mathcal{S} \tag{5.106}$$

$$P^{\downarrow}_{s,\text{init}}(\omega_{\text{re}}) = P^{\downarrow}_{s}(\omega_{\text{base}}) \qquad \forall s \in \mathcal{S} \tag{5.107}$$

$$\theta_{r,\text{init}}(\omega_{\text{re}}) = \theta_r(\omega_{\text{base}}) \qquad \forall r \in \mathcal{R} \tag{5.108}$$

$$\forall \{\omega_{\text{re}} \in \Omega_{\text{re}},\ \omega_{\text{base}} \in \Omega_{\text{base}}\} :\ t_{\text{act}}(\omega_{\text{base}}) = t_{\text{act}}(\omega_{\text{re}})$$

Restoration-Recovered coupling constraints The transition from the restoration phase to the recovering phase links the set points of the restoration situation to the coincident recovered situation:

$$P_g(\omega_{\text{rest}}) = P_g(\omega_{\text{re}}) \qquad \forall g \in \mathcal{G} \tag{5.109}$$

$$P^{\uparrow}_{s}(\omega_{\text{rest}}) = P^{\uparrow}_{s}(\omega_{\text{re}}) \qquad \forall s \in \mathcal{S} \tag{5.110}$$

$$P^{\downarrow}_{s}(\omega_{\text{rest}}) = P^{\downarrow}_{s}(\omega_{\text{re}}) \qquad \forall s \in \mathcal{S} \tag{5.111}$$

$$\theta_r(\omega_{\text{rest}}) = \theta_r(\omega_{\text{re}}) \qquad \forall r \in \mathcal{R} \tag{5.112}$$

$$\forall\, (\omega_{\text{rest}}, \omega_{\text{re}}) \in \mathcal{E}_{\text{rest}\to\text{re}}$$

Recovered-Secondary coupling constraints The coupling between the recovered and secondary grid situations is similar to the coupling between the base and recovered grid situations. The initial set points of generators, storages, and PSTs in the secondary grid situations are equal to the recovered situation's set points including preventive and curative RAs:

$$u_{\text{on},g}(\omega_{\text{sec}}) = u_{\text{on},g}(\omega_{\text{re}}) \qquad \forall g \in \mathcal{G}_{\text{2state}} \cup \mathcal{G}_{\text{4state}} \tag{5.113}$$

$$u_{\text{startup},g}(\omega_{\text{sec}}) = u_{\text{startup},g}(\omega_{\text{re}}) \qquad \forall g \in \mathcal{G}_{\text{4state}} \tag{5.114}$$

$$u_{\text{shutdown},g}(\omega_{\text{sec}}) = u_{\text{shutdown},g}(\omega_{\text{re}}) \qquad \forall g \in \mathcal{G}_{\text{4state}} \tag{5.115}$$

$$v_s(\omega_{\text{sec}}) = v_s(\omega_{\text{re}}) \qquad \forall s \in \mathcal{S} \tag{5.116}$$

$$P_g(\omega_{\text{sec}}) = P_g(\omega_{\text{re}}) \qquad \forall g \in \mathcal{G} \tag{5.117}$$

$$\theta_r(\omega_{\text{sec}}) = \theta_r(\omega_{\text{re}}) \qquad \forall r \in \mathcal{R} \tag{5.118}$$

$$\forall\, (\omega_{\text{re}}, \omega_{\text{sec}}) \in \mathcal{E}_{\text{re}\to\text{sec}}$$

5.4. Solving Scheme

This work implements the solving scheme of the PrevCurRest SCOPF by iteratively incorporating contingencies into the CM model. The approach builds upon the generic SCOPF scheme presented in [71] and adapts it to the specific requirements of this work. Figure 5.6 provides an overview of the solving process for the PrevCurRest model. The process begins with the generation of the TATL LUT and the initial power flow calculation. The power flow calculation is followed by a sensitivity calculation, which is used to determine the influence of nodal power injections and phase-shift angles on the branch flows. The results are then passed to the CA step, where the N–1 contingencies are analyzed. The CA results are used to filter the contingencies and extend the model with new grid situations. Finally, the optimization problem is solved using a MILP solver, which iteratively refines the model until convergence is achieved.

The remainder of this section provides implementation details of the depicted steps.

TATL LUT Generation The TATL LUT is generated by defining the ranges and granularities for expected weather conditions, including ambient temperature ϑ_{a}, wind speed v_{W}, and global radiation Q_{se}. Additionally, the ranges and granularity for the base loading l_{base} and the TATL1 loading l_{TATL1} must be provided. The TATL LUT is generated for TATL1 and TATL2 per OHL conductor type.

Power flow calculation The initial Power Flow (PF) calculation solves the PFEs for all base, restoration and recovered grid situations for the current set points of generators, storages, and PSTs, and loads. The obtained branch flows results are further processed in the CA step. Often, the PF is performed as an AC power flow calculation to account for the reactive power flows and the voltage profile. Moreover, the Jacobian matrix of the PF can be further used in the Sensitivity Calculation (SC) [32].

This work omits solving an AC power flow and instead uses the DC-approximated power flow results from the previous SCOPF iteration. Only at the beginning of the solving process is a single DC-approximated power flow calculated to initiate the first CA.

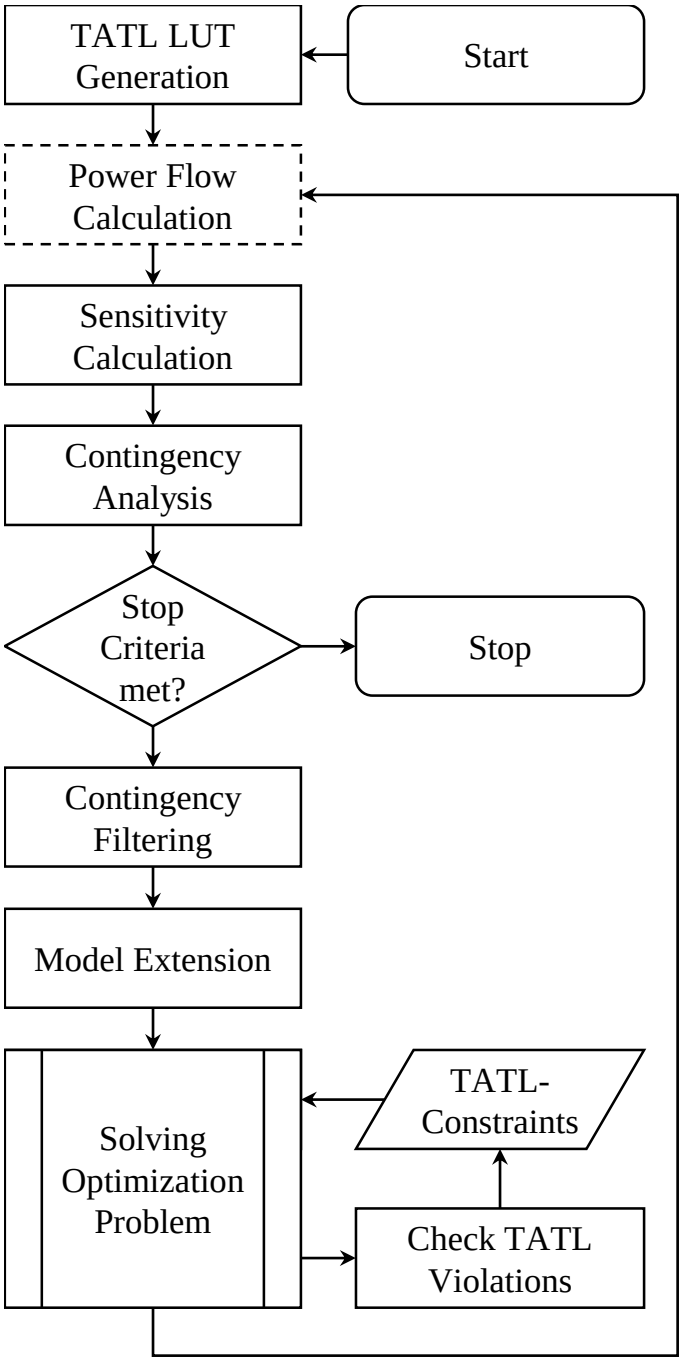

Figure 5.6.: Iterative SCOPF solving scheme.

Sensitivity Calculation Using a linearized version of the PFEs is common in OPF models to circumvent the need for including the nonconvex and nonlinear PFEs. The linearization allows for the calculation of sensitivities that map the influence of nodal power injections and phase-shift angles on the branch flows. The resulting convex LP problem can be solved efficiently.

This work's DC-approximation applies no distinct senstivity calculation, as in each iteration a full DC PF is solved per topology. To reduce the computational effort, the application of linear sensitivities such as Power Transfer Distribution Factor (PTDF), Phase Shift Distribution Factor (PSDF), and Line Outage Distribution Factor (LODF) is possible (and advisable).

Contingency Analysis The CA evaluates whether the power flows in the base case and all considered post-fault scenarios remain within the permissible current and voltage limits of the respective assets. While voltage limit violations are generally more severe — potentially causing immediate equipment damage — current limit violations are more prevalent in operational planning, particularly in Germany, where local reactive power control effectively mitigates voltage issues. Consequently, this work concentrates on current limit violations.

Typically, the CA focuses on N–1 contingencies, possibly extending the analysis to specific N–k contingencies in exceptional cases. Depending on the objective of the CA, contingencies involving transmission or generation assets may be considered. In European operational planning processes, the focus varies by context: CM processes primarily address contingencies of transmission assets, while adequacy and reserve processes emphasize generation asset contingencies. In contrast, American operational planning processes often consider both asset classes simultaneously, as SCOPF calculations determine generation schedules and reserves while accounting for asset constraints. As this work focusses on CM in the European context, it considers only N–1 contingencies of branches (OHLs and transformers).

The term Critical Network Element and Contingency (CNEC)[45] is currently used to describe relevant assets that experience limit violations during a contingency; the older term Critical Branch and Critical Outage (CBCO) referred to the same concept.

To reduce the computational effort, the set of contingencies and monitored assets is reduced to those that surpass a certain loading threshold in the base case situation. A common

assumption is a capacity factor of 0.7, which was justified by [19]. The CA makes use of parallelization to consider all contingencies simultaneously.

Stop Criterion The iterative solving scheme for the SCOPF terminates when either the predefined maximum number of iterations is reached or the most recent CA does not identify any new CNECs. In the latter case, all congestion on relevant CNECs has been resolved through RAs and, if necessary, slack variables. This work further refines the stop criterion by verifying that no additional TATL constraints were introduced during the previous optimization step, ensuring that all TATL constraint violations have been addressed.

Contingency Filtering Contingency Filtering (CF) aims to restrict the set of CNECs to those which are potentially binding in the optimization program. This restriction reduces the storage and computation requirements increasing solving process's speed. The CF is performed based on the detected limit violations during the CA. There is a trade-off between the number of included CNECs in the next SCOPF iteration and the number of iterations required to solve the SCOPF.

This work applies a filtering approach to find the non-dominated CNECs with the highest branch flow limit violations. This approach is inspired by [72]. Let

$$\mathbf{l}_c^{\text{N–1}} \in \mathbb{R}^{N_{\text{branch}}} \quad \forall c \in \mathcal{C} \tag{5.119}$$

be the branch loadings' location vectors in the N–1 contingency cases. The set of N–1 branch loading vectors is:

$$\mathcal{L}^{\text{N–1}} = \{\mathbf{l}_1^{\text{N–1}}, \ldots, \mathbf{l}_{N_\mathcal{C}}^{\text{N–1}}\} \tag{5.120}$$

To identify the set of extreme contingencies $\mathcal{C}_{\text{extreme}} \subseteq \mathcal{C}$, the convex hull of the N–1 loading vectors is computed, denoted as conv $\left(\mathcal{L}^{\text{N–1}}\right)$.

A key mathematical property of the convex hull is that it forms the smallest convex set containing all given points. For a finite set of location vectors $\mathcal{X} = \{\mathbf{x}_1, \ldots, \mathbf{x}_n\}$ in $\mathbb{R}^d$, the convex hull is defined as the set of all convex combinations of these points:

$$\text{conv}(\mathcal{X}) = \left\{ \sum_{i=1}^{n} \alpha_i \mathbf{x}_i \;\middle|\; \alpha_i \geq 0, \sum_{i=1}^{n} \alpha_i = 1 \right\}. \tag{5.121}$$

In practice, the convex hull is computed using algorithms such as Quickhull [73] or the Double Description Method [74], which identify the set of extreme points (vertices) that define the boundary of the convex polyhedron. The implementation used in this work is `CDDLib.jl` [75] in conjunction with `Polyhedra.jl` [76].

The CA's convex hull represents the minimal convex set encompassing all $\mathbf{l}_c^{\text{N}-1}$. The convex hull defined as the polyhedron created by the location vectors of extreme points of $\mathcal{L}^{\text{N}-1}$:

$$\text{conv}\mathcal{L}^{\text{N}-1} = \{\mathbf{l}_c^{\text{N}-1} \in \mathcal{L}^{\text{N}-1} \mid c \in \mathcal{C}_{\text{extreme}}\} \tag{5.122}$$

The resulting convex hull is used to filter out dominated contingencies, ensuring that only the most critical scenarios are retained for further analysis in the optimization process. The set of extreme contingencies $\mathcal{C}_{\text{extreme}}$ is further refined by excluding contingencies without limit violations and removing duplicate loading vectors. Duplicate vectors often arise in scenarios where parallel lines act as critical contingencies for one another. The filtered set of extreme contingencies retains only the non-dominated CNECs. Additional reduction is achievable by ranking contingencies based on their absolute maximum or total CNEC loading, in descending order. The highest-ranking contingencies are prioritized and incorporated into the optimization problem first. Experiments conducted during this work indicate that selecting unique extreme contingencies strikes a good balance between minimizing the number of iterations and limiting the number of contingencies added. It is worth noting that the Gurobi solver's pre-solving phase introduces an additional layer of filtering.

Figure 5.7 illustrates the CF process using a two-dimensional convex hull for an example set of two critical network elements and eight contingencies. Contingency c_2 is excluded from the set as it does not result in any limit violations. Similarly, contingency c_4 is removed because it is contained within the convex hull and is dominated by contingency c_3, as all loadings of $\overrightarrow{l}_{c_3}^{\text{N}-1}$ exceed those of $\overrightarrow{l}_{c_4}^{\text{N}-1}$.

Model Extension This step extends the SCOPF model by adding grid situations as subproblems to the graph and the optimization program. An extension is triggered if new contingencies become available after the CF step. Each new primary contingency adds a new set of grid situations consisting of a primary and multiple restoration situations. Subsequent recovered grid situations are added to the graph if they do not exist yet. Otherwise, the coupling constraints between the new restoration and the existing recovered grid situations are

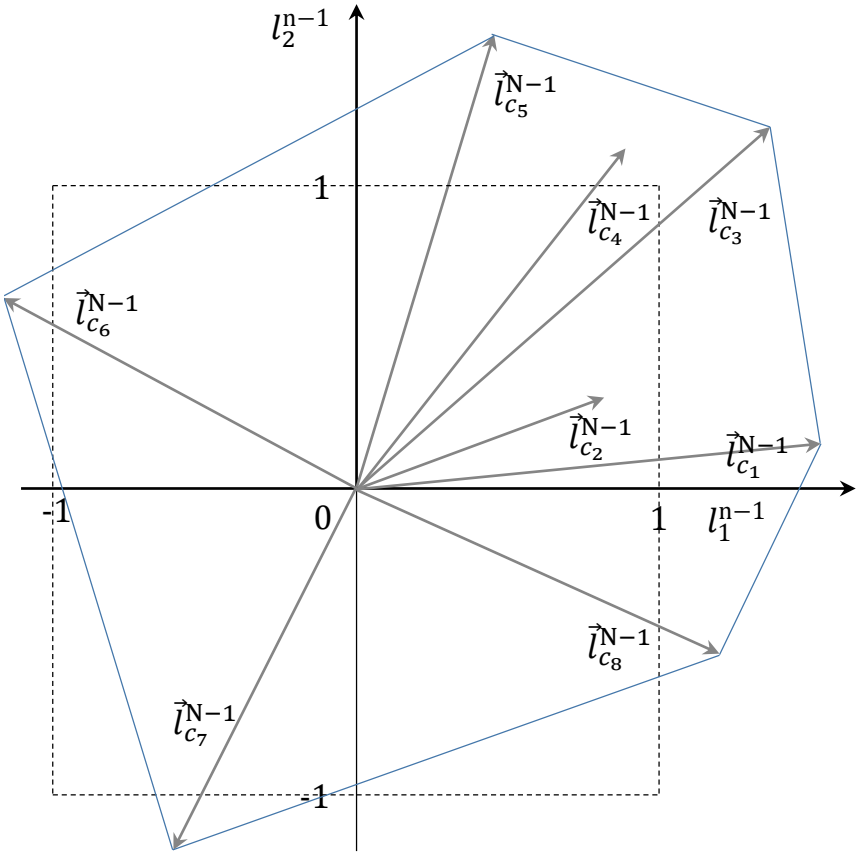

Figure 5.7.: Example of contingency filtering by convex hull.

added. Also the other coupling constraints between the new and existing grid situations are added.

In addition to the grid situations, the TATL constraints from the last iteration are added permanently to the respective grid situation subproblems.

Solving Optimization Problem The SCOPF model is handed over to the MILP solver. This work uses the Gurobi solver [46]. The solving process starts with a presolving phase, where the solver attempts to compress the problem by removing redundant constraints and variables. The challenge of MILP problems is that they are essentially nonconvex. While the linear relaxation of the problem is convex, the integer constraints introduce non-convexity. The solver uses a branch-and-bound algorithm to successively find a feasible integer solution. This algorithm starts with the root relaxation of the problem, which is an LP without integer constraints. The objective value of the root relaxation act as a lower bound for minimization problems. During the subsequent branching, the solver creates subproblems by fixing certain integer variables to specific values and solving a relaxed version of the subproblems as an LP. The branch-and-bound algorithm explores the solution space by traversing a search tree. Whenever the solver finds a feasible integer solution, the solver checks if it is better than the current best solution (incumbent solution). If it is, the incumbent solution is updated. The incumbent acts as the upper bound of the optimal solution. The lower bound of the objective function is the minimum of all relaxed node solutions found along the path to the current node. If the lower bound of a node is greater than the incumbent solution, the node is pruned from the search tree. This process continues until all nodes are explored or the gap between the lower and upper bound is sufficiently small. Gurobi uses several heuristics to quickly steer the branching process and find incumbent solutions. Moreover, it uses parallelization to solve the LP relaxation of several nodes simultaneously. [77]

Given the large number of constraints defining the TATL1 and TATL2 polyhedra, this work employs lazy constraints to incorporate TATL constraints dynamically during the optimization. The callback function evaluates intermediate node solutions and adds TATL constraints whenever a solution lies outside the corresponding polyhedron. While it is theoretically possible to implement the thermal conductor model directly within the callback—rejecting solutions where the conductor temperature exceeds its maximum—this approach is limited by the challenge of formulating constraints that directly relate decision variables to

conductor temperature. Additionally, the impact of such a strategy on solver performance remains uncertain.

An important aspect to consider is the use of lazy constraints for introducing new CNEC constraints during the optimization process. This method is only viable when curative actions are not allowed after a contingency, since adding such actions would necessitate new decision variables (column-generation), which cannot be created within callback functions for lazy constraints (row-generation). Consequently, in the context of the PrevCurRest strategy, lazy constraints for CNECs are restricted to secondary contingency scenarios. By utilizing linear sensitivities—specifically, LODFs—the branch flows in secondary contingency cases can be inferred from the branch flows in the recovered grid situations. The callback function therefore combines the CA and CF procedures, allowing new CNEC constraints to be added dynamically as required.

5.5. Implementation

The proposed model has been developed in `Julia` [60], utilizing several open-source packages, including:

- `PowerModels.jl` [30] for modeling the components of the OPF problem.
- `JuMP.jl` [78] as the optimization modeling language and interface to solvers.
- `Plasmo.jl` [66] for graph-based modeling of optimization problems.
- `Polyhedra.jl` [76] and `CDDLib.jl` [75] for polyhedral computations and constraint sets in `JuMP.jl`
- `Gurobi` [46] with `Gurobi.jl` as MILP solver.
- `Ipopt` [79] with `Ipopt.jl` as NLP-solver for testing the AC OPF formulation.

The choice of `Julia` was motivated by its high-level syntax, performance, and strong support for mathematical programming. The modular structure of the implementation allows for easy adaptation and extension of the model to accommodate future research needs.

5.6. Conclusion

This chapter presented a mathematical framework for modeling CM strategies using a graph-based approach. Grid situations are represented as nodes in a directed acyclic graph, enabling a scalable structure for preventive, curative, and restorative actions. The grid situations form subproblems connected via coupling constraints. Despite the central solving approach in this thesis, future works may use distributed or decentralized optimization algorithms such as ADMM, or distributed Sequential Quadratic Programming (SQP) or Interior Point (IP) implementations.

The DC-SCOPF formulation balances accuracy and computational efficiency, incorporating dynamic thermal ratings and an iterative solving scheme with contingency filtering to manage the complexity arising from considering N–1–1 security.

The primary contribution of this model lies in its ability to quantitatively compare different CM strategies, particularly the PrevCurRest strategy against the traditional Prev, PrevN2, and PrevCur methods. By explicitly modeling the restoration and recovery phases, the framework captures an aspect that was so far overlooked in operational planning processes, creating a more realistic and risk-prepared representation of potential post-fault scenarios.

6. Simulation

This chapter presents the simulation studies conducted to validate the proposed methods and models developed in this work. The simulations are based on the RTS-GMLC [9]. The chapter describes the test system, outlines the modifications and data sources used, details the simulation setup, and discusses the results obtained for different operational strategies.

6.1. RTS-GMLC test system

The RTS-GMLC [9] is an updated version of the IEEE Reliability Test System RTS-96 [80], designed to provide a realistic yet computationally manageable test grid for evaluating power system operations, including OPF, UC, Economic Dispatch (ED), and reliability analyses. The RTS-GMLC was chosen for its geographical mapping, the availability of consistent load and infeed time series, and the modernized generation fleet, which includes a mix of RES and conventional generation. The test system is provided in multiple formats, including formats for `MATPOWER` [29] and DigSILENT `PowerFactory` [81]. The `MATPOWER` format is used in conjunction with `PowerModels.jl` [30].

The RTS-GMLC was artificially located in the southwest of the United States, respecting the line lengths of the original RTS-96 (Fig. 6.1). The grid consists of three interconnected areas. The first digit of the bus numbers indicates the area. Branch names and directions are denoted by their bus numbers, e.g., line 318-223. To distinguish parallel branches, a suffix is added, e.g., line 318-223a. Generator names consist of the bus number, generator technology, and a suffix indicating the generator number, e.g., 101_CT_1 for the first Combustion Turbine (CT) at bus 101.

The network uses a bus-branch representation and consists of 73 buses, 120 branches, and 158 generators. The peak load is $8.9\,\text{GW}$, and the total installed generation capacity is $14.5\,\text{GW}$ across three areas. The voltage levels are $138\,\text{kV}$ and $230\,\text{kV}$. Table 6.1 shows the installed generation capacities by category.

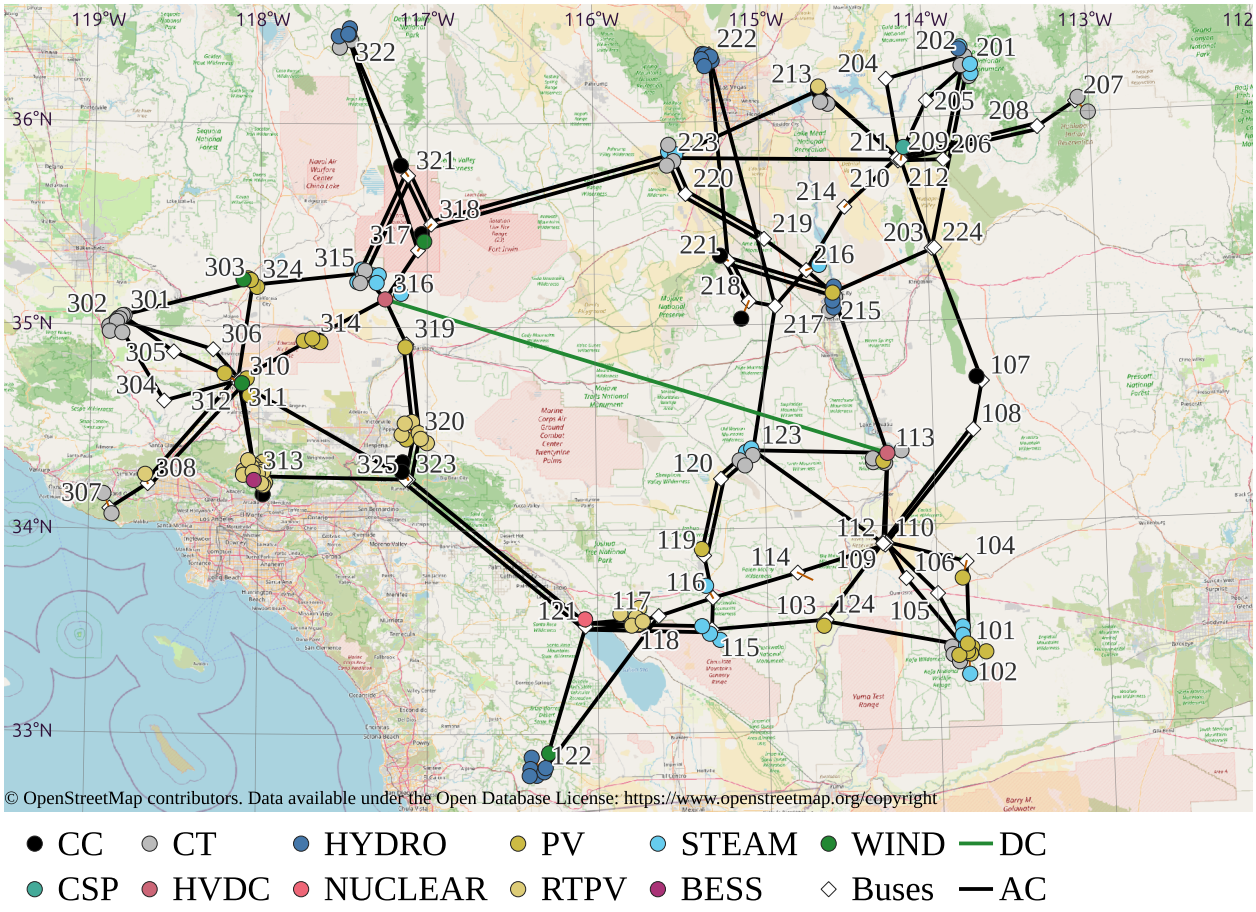

Figure 6.1.: Geographical representation of the RTS-GMLC network (grid data from [9], map data from [82]).

Table 6.1.: Installed generation capacities in the RTS-GMLC by category. (data from [9])

Category	**Unit Type Symbol**	$P_{\max}$ **[MW]**
Concentrated Solar Power (CSP)	CSP	200
Coal ST	ST	2317
Gas Combined Cycle (CC)	CC	3550
Gas Combustion Turbine (CT)	CT	1485
Hydro	HYDRO	1000
Nuclear	NUCLEAR	400
Oil Combustion Turbine (CT)	CT	240
Oil Steam Turbine (ST)	ST	84
Solar Photovoltaic (PV)	PV	1555
Solar Rooftop Photovoltaic (RTPV)	RTPV	1161
Battery Storage BESS	BESS	50
Wind	WIND	2508

6.2. Time series data and modifications

The RTS-GMLC includes time series data spanning 8760 h for Concentrated Solar Power (CSP), Photovoltaic (PV), Rooftop Photovoltaic (RTPV), hydro, wind generation, as well as for load and reserve requirements. This section describes the modifications made to the original RTS-GMLC data and the sources of the time series data used in this study.

6.2.1. Wind and solar data

The load, wind, and solar time series of the RTS-GMLC were generated using the results of the Western Wind and Solar Integration Study (WWSIS) [83]. Phase I of the WWSIS created models for wind speeds and solar radiation from 2004 to 2006 for the Western Interconnection [84]. Based on these results, Phase II of the WWSIS assumed a regional distribution of PV, wind turbine, and hydro installations in 2020. Subsequently, the power outputs of the RES were calculated for the year 2006 [85]. Unfortunately, the RTS-GMLC does not provide the original wind speed and solar radiation data, but only the power outputs of the RES. The original wind speed and solar radiation data are required to calculate the weather-dependent thermal ratings of the OHL conductors; however, these data are no longer available. During the course of WWSIS Phase II, the enhanced Wind Integration National Dataset (WIND) dataset was created, which includes temperatures and wind turbine power outputs at various heights across the continental United States for the years 2007–2013, provided on a 2 km × 2 km grid. The data can be obtained from the WIND Toolkit [86].

For this study, wind speed data at both 10 m and 100 m heights, as well as temperature data at 10 m height, for 2008 were utilized. The 10 m wind speed and temperature values served as inputs for the thermal conductor model. Wind speeds at 100 m were employed to recalculate wind turbine power outputs using an IEC Class 2 wind turbine model [86, Tab. 1], scaled according to the installed wind turbine power at each bus in the RTS-GMLC. This recalculation was necessary because the original wind turbine power output data were not available in the WIND Toolkit.

Instead of recalculating the PV and RTPV power outputs, the original 2006 time series from the RTS-GMLC was retained. Since the original solar radiation data were unavailable, they were substituted by a time- and location-dependent estimation of solar heat gain for each bus,

based on latitude, longitude, and elevation [87], and calculated under clear-sky conditions following IEEE Std. 738-2012 [51, Sec. 4.5].

For each branch, the applied weather data were selected to represent the most adverse cooling scenario from the two terminal buses. Specifically, the maximum ambient temperature, minimum wind speed, and maximum solar heat gain from either bus were used for the branch.

6.2.2. Unit commitment data

The changes in wind power generation time series required an updated UC solution for the RTS-GMLC. Benchmark datasets for OPF [34] and UC [88] are available from the IEEE PES Power Grid Lib [89], including for the RTS-GMLC. In this study, the Julia implementation of the UC model described in [90] was used. The original generation time series from the RTS-GMLC were replaced with the results from the updated UC solution. The UC solution represents the market outcome, which respects the generation and load constraints, but no grid-related constraints.

6.2.3. Topological modifications

The original RTS-GMLC includes the interconnectors 107-203, 113-215, 123-217, 318-223, and 325-121. While areas 1 and 2 are connected by three interconnectors, area 3 is linked to areas 1 and 2 by only one interconnector each. The PrevCurRest strategy requires the grid to remain interconnected under all combinations of primary and secondary contingencies. A simultaneous outage of interconnectors 318-223 and 325-121 would isolate area 3. To prevent this, these interconnectors were duplicated, resulting in branches 325-121a, 325-121b, 318-223a, and 318-223b. Additionally, the PST 323-325, which is in series with 325-121, was duplicated as 323-325a and 323-325b. The reactances and resistances of the duplicated branches were doubled to maintain the same total impedance as the original parallel branches, and their ratings were halved.

6.2.4. Modified thermal ratings

While ratings are often specified as apparent power (the product of rated current and nominal voltage), for consistency with previous chapters, all ratings in this chapter are expressed in terms of current.

The `MATPOWER` format supports three thermal ratings per branch: `RATE_A` (normal rating), `RATE_B` (emergency rating, typically up to 15 min), and `RATE_C` (long-term emergency rating). The original `MATPOWER` model of the RTS-GMLC contains only normal ratings, whereas the `PowerFactory` model includes conductor types with $\texttt{RATE\_B} = 1.25 \cdot \texttt{RATE\_A}$ and $\texttt{RATE\_C} = 1.1 \cdot \texttt{RATE\_A}$. The values for `RATE_B` and `RATE_C` in the `MATPOWER` model were adopted from the `PowerFactory` model.

The `PowerFactory` model additionally indicates whether a branch is an OHL or a cable. In total, six branches are represented as 138 kV cables; all others are modeled as OHLs or transformers. As the RTS-GMLC does not specify conductor types, OHL branches were assigned single-conductor types based on their per-unit-length resistance and nominal thermal ratings. The assumption of single, rather than bundled, conductors is appropriate for the voltage levels of 138 kV and 230 kV considered here [91, Tab. 9.8].

See Chapter A for a list of assigned conductor types.

Table 6.2 summarizes the thermal ratings for each branch type. For OHLs, ratings are derived from the generated PATL-TATL-LUT (see Section 6.3 for details). According to [92], OHLs and transformers are the most restrictive assets regarding thermal ratings, while cables and switchgear are less limiting. Due to the absence of a thermal cable model, cable ratings $I_{\text{TATL1}} = I_{\text{TATL2}} = 1.1 \cdot \texttt{RATE\_A}$ are asssumed, which may be conservative compared to [92, Fig. 3] for XLPE cables. Transformer ratings are based on IEC 60076-7 [93], which allows a normal cyclical current rating of $1.3 \cdot I_{\text{r}}$ for large power transformers, where I_{r} is the rated current [93]. In German grid operation, the permanent admissible rating is typically set to $I_{\text{PATL}} = 1.2 \cdot I_{\text{r}}$. With $\texttt{RATE\_A} = I_{\text{r}}$, $I_{\text{PATL}} = 1.2 \cdot \texttt{RATE\_A}$. The assumptions $I_{\text{TATL1}} = I_{\text{TATL2}} = 1.5 \cdot \texttt{RATE\_A}$ align with [93] and German operational practice. The American correspondent standard is IEEE Guide C57.91-20211 [94].

Table 6.2.: Thermal ratings by branch type.

Branch Type	I_{PATL}	I_{TATL1}	I_{TATL2}
OHL		PATL-TATL-LUT	
Cable	$1.0 \cdot$ `RATE_A`	$1.1 \cdot$ `RATE_A`	$1.1 \cdot$ `RATE_A`
Transformer	$1.2 \cdot$ `RATE_A`	$1.5 \cdot$ `RATE_A`	$1.5 \cdot$ `RATE_A`

6.3. Simulation setup

As outlined in Section 4.3, a precalculated PATL-TATL-LUT is one option to include dynamic thermal ratings in the SCOPF model. The range and granularity of the parameters determine the initial computation effort and the precision of the thermal modeling. For the RTS-GMLC, the ranges for the weather conditions were chosen according to the WIND Toolkit data and the calculated global radiation data. The upper limit for l_{TATL1} and l_{TATL2} is set to 1.5. It is expected that other factors, such as stability or protection device limitations, are more restrictive in these regions than thermal limitations. Table 6.3 lists the parameters used to generate the LUT with the `TATLPATL.jl` package.

Table 6.3.: Simulation setup parameters for PATL-TATL-LUT generation.

Parameter	**Value**
TATL timeframes	$\tau_1 = 2\,\text{min}$, $\tau_2 = 13\,\text{min}$
Short circuit heating	$\Delta\vartheta_{\text{SC}} = 5\,\text{K}$
OHL conductors	see Chapter A
Ambient temperature	$\vartheta_{\text{a}} = \{-10, -5, \ldots, 25, 30\}°\text{C}$
Wind speed	$v_{\text{W}} = \{0.6, 1.0, 2.0, \ldots, 20.0\}\text{m}\,\text{s}^{-1}$
Wind direction	$90°$ at $v_{\text{W}} = 0.6\,\text{m}\,\text{s}^{-1}$, $30°$ else
Solar radiation	$Q_{\text{se}} = \{0, 200, \ldots, 1400\}\text{W}\,\text{m}^{-2}$
Base loading	$l_{\text{base}} = \{0.00, 0.50, 0.55, \ldots, 1.00\}$
TATL1 loading	$l_{\text{TATL1}} = \{0.00, 0.50, 0.55, \ldots, 1.50\}$
TATL cap	$\lvert l_{\text{TATL1}}\rvert \leq 1.5$, $\lvert l_{\text{TATL2}}\rvert \leq 1.5$

The simulations are performed for a single 24-hour period, corresponding to the virtual date May 5, 2020. The contingency set consists of all branches, except for the HVDC line. The restoration duration is assumed to be $\tau_{\text{rest}} = 2\,\text{h}$, and the reoptimization duration is set to $\tau_{\text{reopt}} = 4\,\text{h}$, which are reasonable in the current system operation context. If restoration or recovered grid situations exceed the 24-hour period, these are not considered in the simulation.

The inclusion of HVDC outages and an extended simulation horizon for the PrevCurRest strategy are left for future work. Startup and shutdown costs are not considered in the simulations in order to encourage the utilization of generator flexibility.

6.4. Simulation results

The simulation conducted for this work is intended as a proof of concept for the proposed PrevCurRest strategy. In Section 6.4.1, the results are compared to the Prev, PrevCur, and PrevN2 strategies. The key indicator is the preventive RD volume, which is the absolute sum RD measures across all generators.

The curative RD volume is not used as a comparative metric between CM strategies here, since it is influenced by the number of contingencies addressed curatively in each CM strategy. This number, in turn, depends on the preventive RAs implemented and the set of contingencies deemed relevant during the CF phase. Nevertheless, Section 6.4.4 provides insights into the usage of curative RAs in the PrevCurRest strategy.

A comparative indicator is the line loading among the different CM strategies, which is analyzed in Section 6.4.2. The higher the asset loadings, the closer the grid is operated to its thermal limits, which may lead to a higher risk of line overloads if security margins are chosen improperly. On the other hand, higher asset loadings indicate more efficient use of transmission capacities, which reduces the preventive RD volumes.

The CM strategies vary significantly in model complexity. Therefore, their impact on computational effort is another important aspect, which is discussed in Section 6.4.3.

6.4.1. Preventive redispatch volume

Fig. 6.2 compares the preventive RD volumes for the different CM strategies. The PrevCur strategy achieves a substantial reduction in RD volume compared to the Prev strategy, lowering it from 16.7 GWh to 11.3 GWh. In contrast, the PrevCurRest strategy only slightly reduces the RD volume to 15.8 GWh. Nevertheless, the curative RAs in the PrevCurRest strategy still contribute to reducing preventive RD requirements. Additionally, the PrevCurRest strategy can restore an N–1 secure state curatively, which would otherwise require a

preventive RD volume of 23.7 GWh if the grid needed to be N–2 secure before the primary contingency.

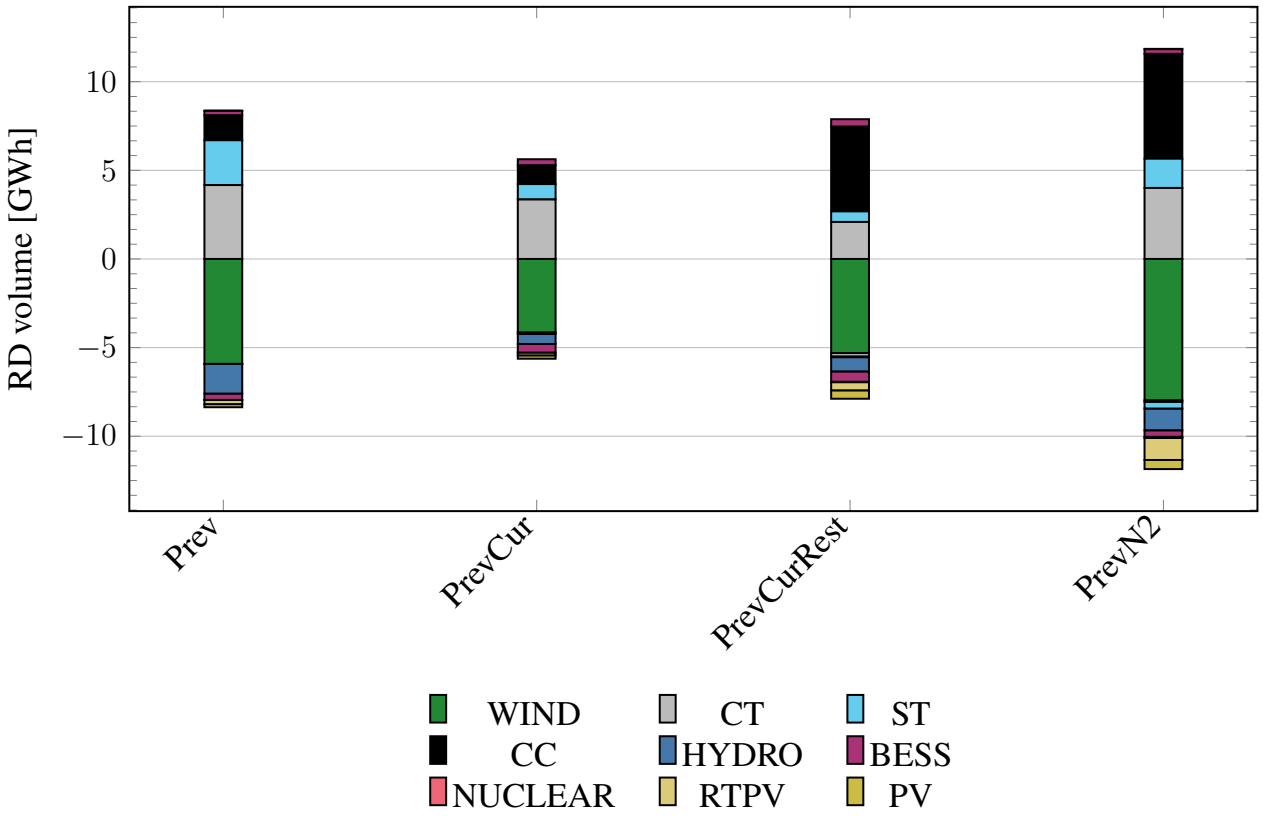

Figure 6.2.: Preventive RD volume by CM strategy and technology. CSP is ommitted due to zero RD volume.

It is important to note that the results in Fig. 6.2 are specific to the RTS-GMLC and may not generalize to all grids or time periods. For example, if the generation mix is dominated by conventional generators with limited flexibility, the PrevCurRest strategy may result in a higher RD volume than the Prev strategy, making it similar to the PrevN2 approach. In future scenarios with a greater share of RES and BESS installations, increased generation flexibility is expected to lower the RD volume for the PrevCurRest strategy – placing it between the Prev and PrevCur strategies, the latter of which does not account for preparatory RAs for potential secondary contingencies.

6.4.2. Line loading

Fig. 6.3 reveals the branch loadings in base situations for the different CM strategies. The inverse cumulated frequency plots reveal the percentage of loadings that are below the re-

spective loading value. Table 6.4 additionally lists the branch loadings at selected Inverse Cumulated Frequency (ICF) values for each strategy.

The overall base loading of all branches for during the simulation period is low, given that less than 6 % of the branches are loaded above 50 %.

In general, the deviations between the strategies are small, indicating that the base loading of the grid is not significantly affected by the different CM strategies. The median branch loading for the PrevCur strategy is 17.8 %, which is only slightly higher than the 17.3 % for the Prev strategy. Other than expected, the PrevCurRest strategy shows a slightly lower median branch loading of 16.6 % compared to the Prev strategy. This indicates the inherent preparation for secondary contingencies in the PrevCurRest strategy that partly reduces the base loading of branches.

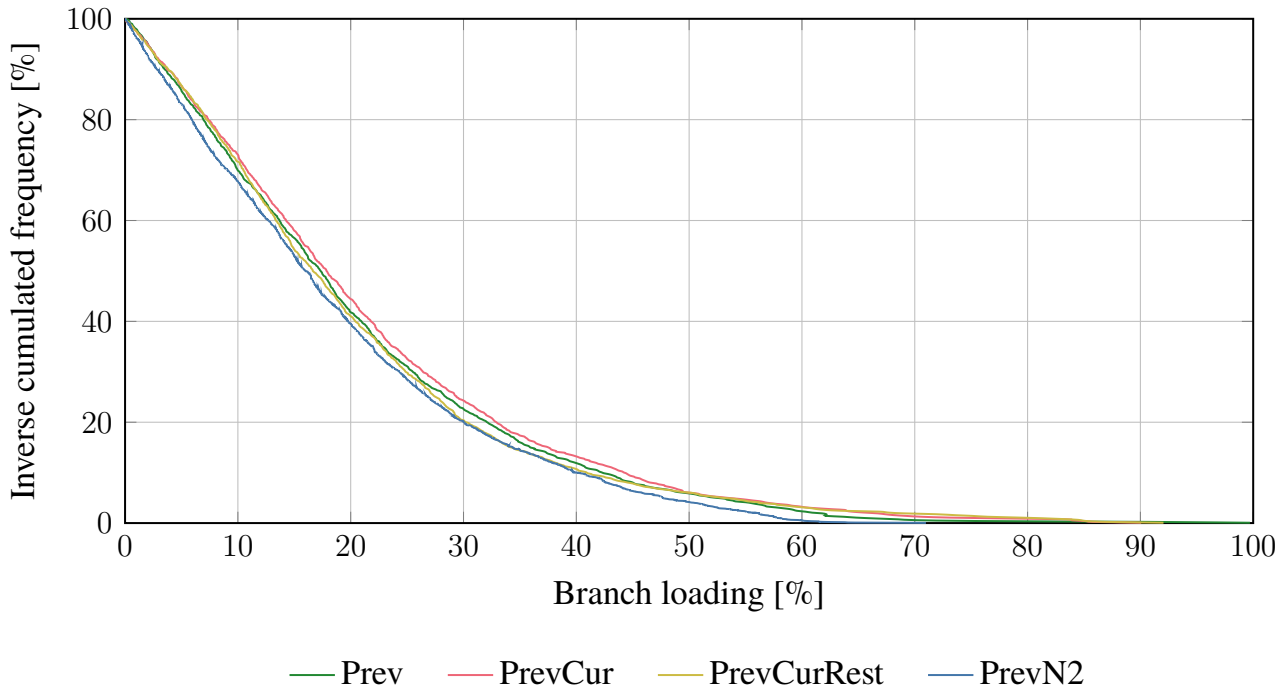

Figure 6.3.: ICF plots of the branch loading in base situations and for different CM strategies.

Fig. 6.4 and Table 6.5 show the ICF of the N–1 branch loadings during primary contingencies. Due the different number of relevant primary contingencies per hour and per CM strategy, only the maximum branch loading per hour is considered.

As expected, the PrevCur strategy shows the highest N–1 branch loadings, followed by the PrevCurRest, the Prev, and the PrevN2 strategy. The TATL1 loading is limited to 150 %, the

Table 6.4.: Branch loading in base situations at selected ICF values for each CM strategy.

ICF [%]	Prev [%]	PrevCur [%]	PrevCurRest [%]	PrevN2 [%]
75	8.5	9.2	8.9	7.3
50	17.3	17.8	16.6	16.0
25	28.5	29.4	27.6	26.9
0	99.7	90.1	93.0	71.0

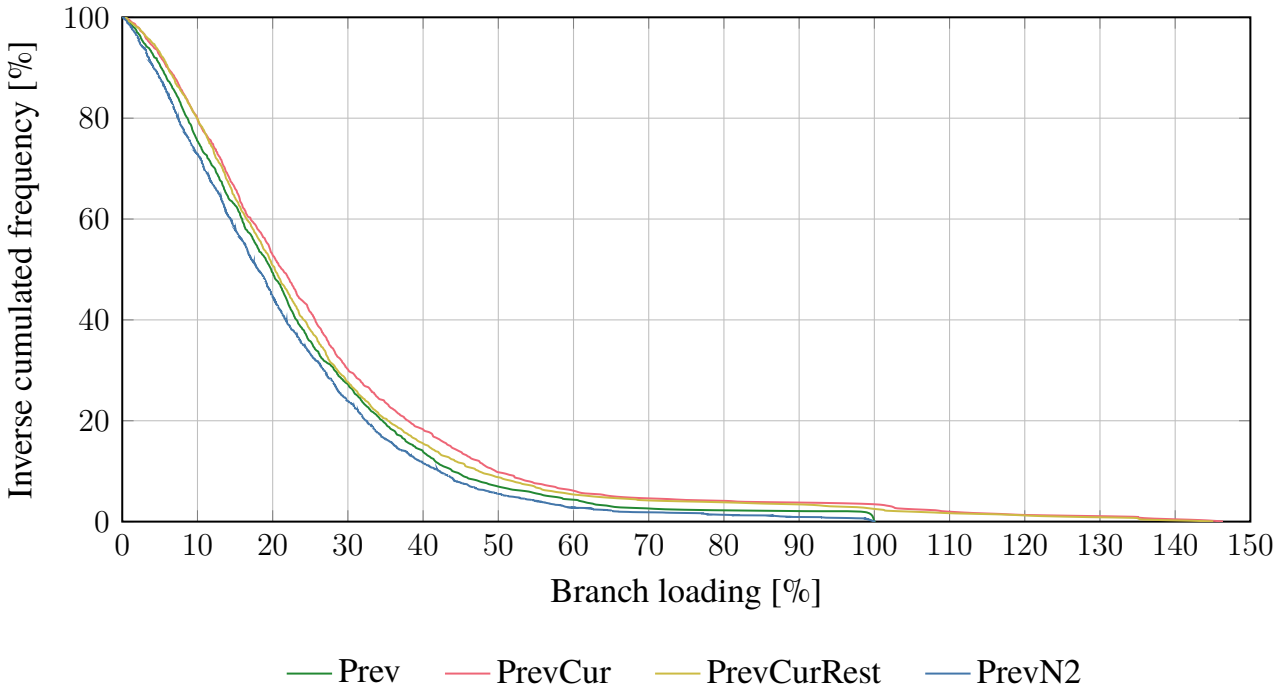

Figure 6.4.: ICF plots of the maximum branch loading in primary contingency situations per branch for different CM strategies.

highest observed N–1 branch loading is 146.4 % for the PrevCur strategy. The PrevCurRest strategy shows a maximum N–1 branch loading of 145.1 %. The occurence of N–1 branch loadings above 100 accounts for 3.4 % of the branch-timestamp combinations for the PrevCur strategy and 3.2 % for the PrevCurRest strategy. Of the 123 branches, 16 branches are loaded above 100 % at least once during the simulation period for the PrevCur strategy and 10 branches for the PrevCurRest strategy. The potential usage of thermal reserves is present for all hours of the simulation period.

The low number of branches for which thermal reserves are potentially used is connected to the low base loadings of the branches. However, this is a common pattern found in meshed power systems in which the transmission capacity of only a few branches is restricting.

Table 6.5.: Maximum loading per branch in primary contingency situations at selected ICF values for each CM strategy.

ICF [%]	Prev [%]	PrevCur [%]	PrevCurRest [%]	PrevN2 [%]
75	10.2	12.0	11.6	7.9
50	19.8	21.2	20.2	18.1
25	31.2	33.7	31.6	29.3
0	100.0	146.4	145.1	100.0

6.4.3. Computation time

The computational effort can be assessed in terms of memory usage and computation time. Due to the simulation setup, direct measurement of memory consumption and total Central Processing Unit (CPU) time is not feasible. Therefore, the reported metric is the simulation runtime of the SCOPF, broken down by the main simulation steps.

The number of grid situations solved in each CM strategy run serves as a proxy for the computational effort. The total runtime of the SCOPF run is reported, along with the number of CM iterations and the number of grid situations added in each iteration.

The workstation used for the simulations featured an AMD EPYC 12-core processor (2.79 GHz), 32 GB RAM, Windows 10 22H2, and Julia version 1.11.3.

Table 6.6 summarizes the main computational metrics for each CM strategy.

Table 6.6.: Computation metrics for different CM strategies.

Metric	Prev	PrevCur	PrevCurRest	PrevN2
Total runtime [s]	83	3346	26 316	545
SCOPF iterations	7	12	13	11
Mean runtime per iteration [s]	6	236	1809	32
Grid situations	82	355	1273	436

Simulation runtime increases sharply with the complexity of the CM strategy. The Prev strategy completes fastest and solves the fewest grid situations. The PrevCurRest strategy is the most computationally demanding, with a total runtime of $7.3\,\mathrm{h}$ and 1273 grid situations. This computation time exceeds the available window for a SCOPF rerun ($\tau_{\mathrm{reopt}} = 4\,\mathrm{h}$). The current implementation of PrevCurRest is not viable for operational use due to excessive

computation time. Reducing the number of relevant grid situations is critical for improving efficiency. The PrevCur and PrevN2 strategies require moderate computational resources, with PrevCur using more than PrevN2.

Figure 6.5 presents the number of grid situations added in each SCOPF iteration for the different CM strategies. As the simulation progresses, the number of newly added grid

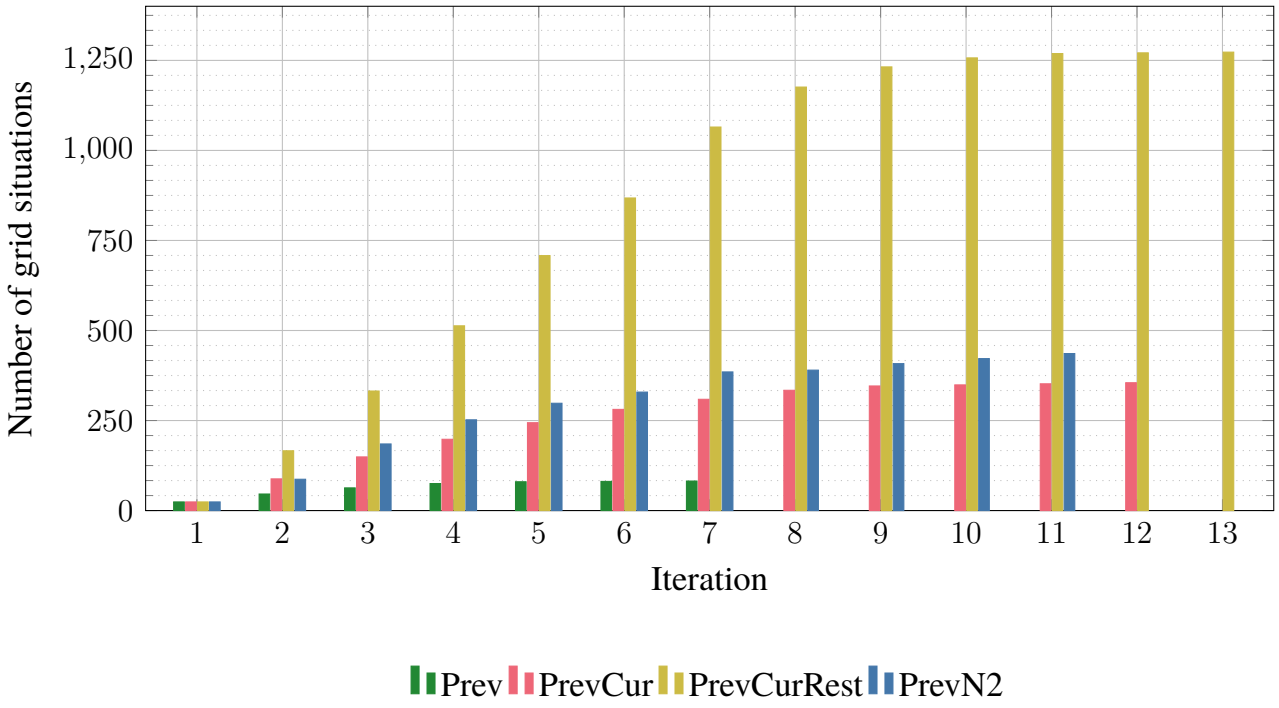

Figure 6.5.: Number of grid situations per iteration for different CM strategies.

situations per iteration declines because most grid situations with binding branch constraints have already been included. This trend is consistent across all CM strategies. The current implementation solves the entire model from scratch in each SCOPF iteration. Since the final iterations typically add only a small number of grid situations, computational efficiency could improve by reusing previous solutions rather than resolving the full problem each time. Additionally, in later iterations, the importance of CF diminishes, as including more potentially relevant contingencies does not substantially increase problem complexity but may help reduce the total number of iterations needed to reach a final SCOPF solution.

6.4.4. Details of the PrevCurRest simulation

This section offers further insights into the PrevCurRest strategy simulation, focusing on visualizing the spatial distribution of congested branches and RD measures in the RTS-GMLC test grid.

Table 6.7 summarizes the size of the optimization program in the final SCOPF iteration of the PrevCurRest simulation, both before and after presolve conducted by the `Gurobi` solver. The presolve step removes redundant variables and constraints, significantly reducing the problem size. One reason for the large number of redundant variables and constraints is the copying of variables involved in coupling constraints between the subproblems. The

Table 6.7.: Optimization program size in the last SCOPF iteration of the PrevCurRest simulation.

	Before presolve	**After presolve**	
Continuous variables	1 403 993	609 069	(−66.7 %)
Binary variables	223 146	24 604	(−89.0 %)
Constraints	2 699 812	515 066	(−80.9 %)
Non-zero elements	6 224 580	1 677 869	(−73.0 %)

following `Gurobi` solver settings were applied:

- TimeLimit: 7200 seconds (never exceeded)
- MIPGap: 0.01 (1 %)
- Method: 1 (dual simplex for root relaxation)
- Threads: 6
- LazyConstraints: 1 (enables lazy constraints)

Table 6.8 summarizes the number of grid situations and the number of branches whose flow constraints are binding after solving the SCOPF. Out of 124 branches, only a small number have binding flow constraints, with a maximum of 21 branches affected during primary contingency situations. As expected, the highest number of binding flow constraints is observed in secondary contingency situations, when the grid lacks two assets.

Figure 6.6 depicts the binding branches. Hydro generation at bus 122 in the southernmost part of the grid is a primary cause of congestion on branches 325-121a and 325-121b, the

Table 6.8.: Grid situations and binding branch constraints in the PrevCurRest simulation.

	Base	**Primary**	**Restoration**	**Recovered**	**Secondary**
Grid situations	24	116	433	186	514
Binding branches	0	21	12	13	11
Binding branch constraints	0	124	680	204	1525

duplicated interconnectors between areas 3 and 1. Additional congestion occurs around bus 303 and the single feeder connected to bus 208 in the northeastern region.

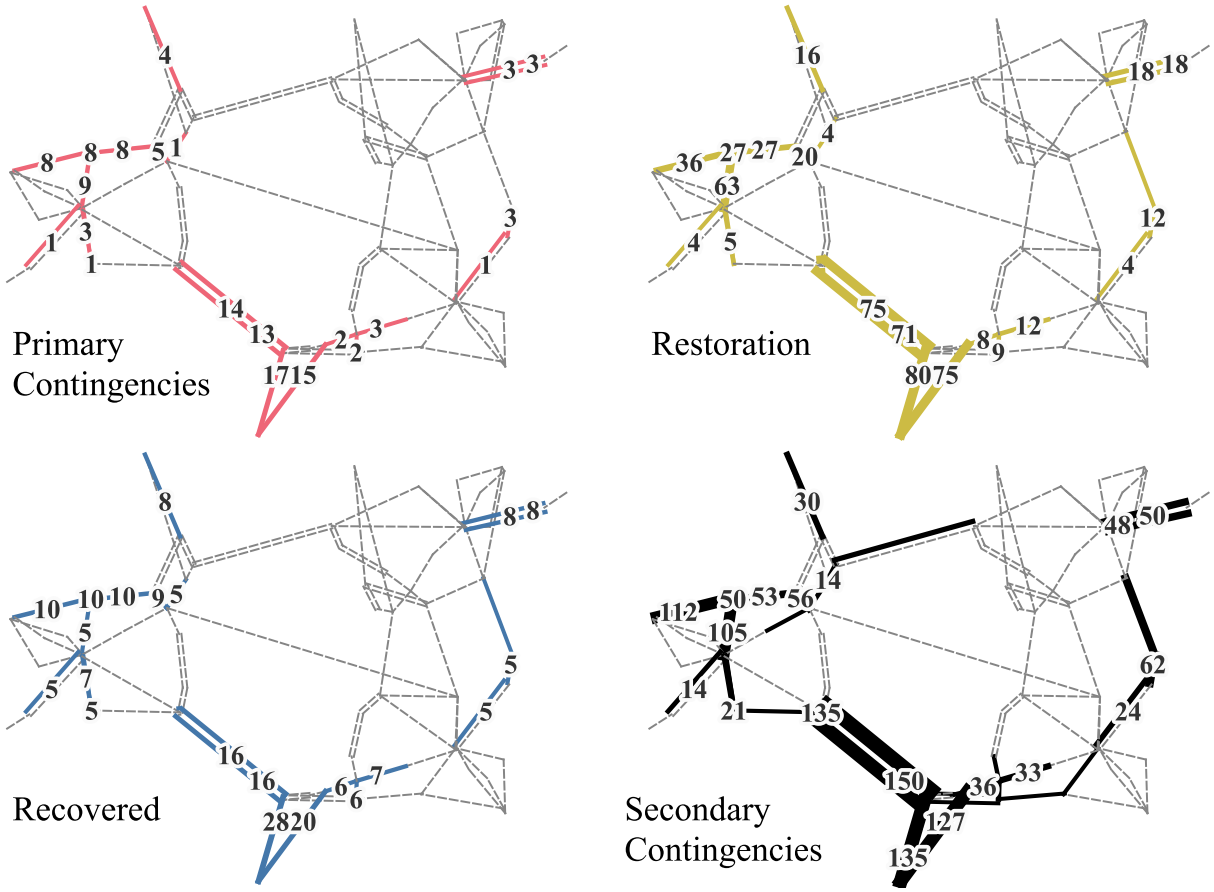

Figure 6.6.: Number of situations in which branch flow constraints are binding in the PrevCurRest simulation.

Figure 6.7 reveals the preventive RD volumes per bus and the number of primary contingency situations in which branch flow limits are limiting.

Figure 6.7 indicates that preventive curtailments are concentrated in the RES-dominated areas 1 and 3, whereas preventive ramp-up measures are primarily found in the northeastern

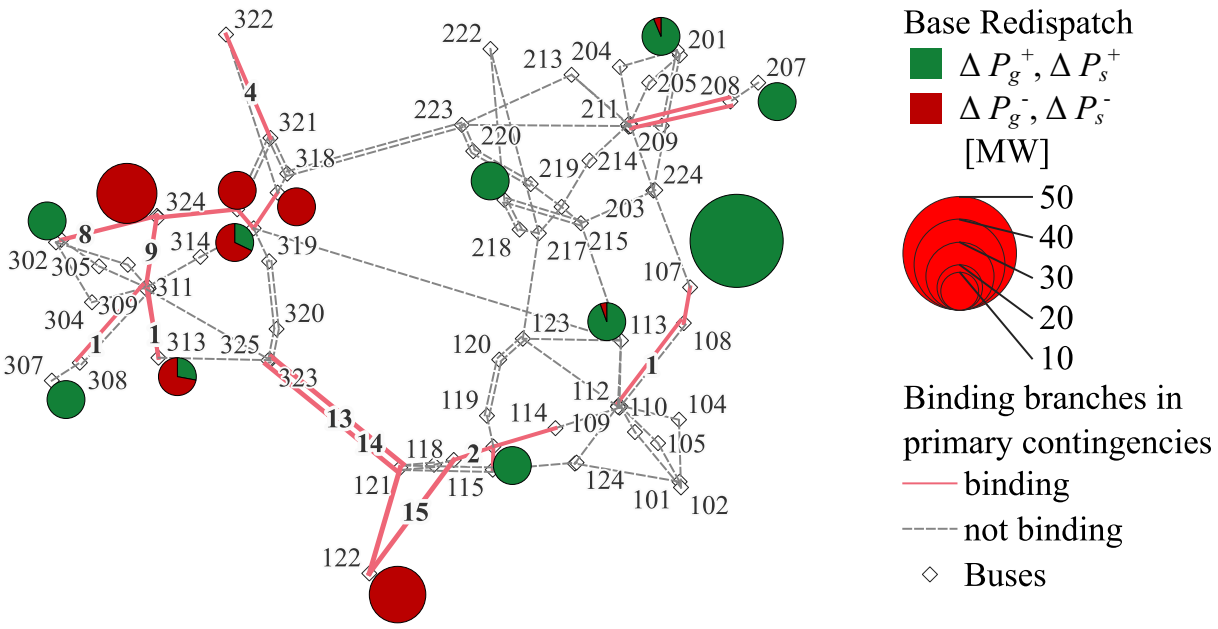

Figure 6.7.: Preventive redispatch volumes per bus and number of primary contingency situations in which branch flow limits are limiting in the PrevCurRest simulation.

part of the grid, particularly in areas 2 and 1. The high positive RD volume for generator 107_CC_1 at bus 107 is due to the long minimum up time (8 h) of the combined-cycle plant, resulting in large preventive RD volumes, even if the generator is only required for CM during a few hours.

Figure 6.8 shows the curative RD volumes per bus in restoration situations and the number of restoration situations in which branch flow limits are limiting. The pie charts illustrate the distribution of curative RD volumes across different post-fault timestamps (τ).

Interpreting absolute curative RD volumes is challenging, as these values depend on the number of contingencies considered. Comparing curative RD volumes per bus highlights areas where curative RAs are more frequently applied. Examining the direction of curative RD reveals patterns in the application of curative RAs. Buses exhibiting both positive and negative curative RD volumes are considered flexible, as they can provide a tailored response to contingency events. For example, buses 113 and 316, connected by the DC-link `DC1`, demonstrate such flexibility. Curative RAs are applied at each post-fault timestamp, with a slight preference for $\tau = 2\,\text{h}$. This timestamp marks the transition to recovered grid situations, which require an N–1 secure state. Therefore, curative RAs at this point likely serve to ensure the grid meets this security criterion before the restoration phase concludes.

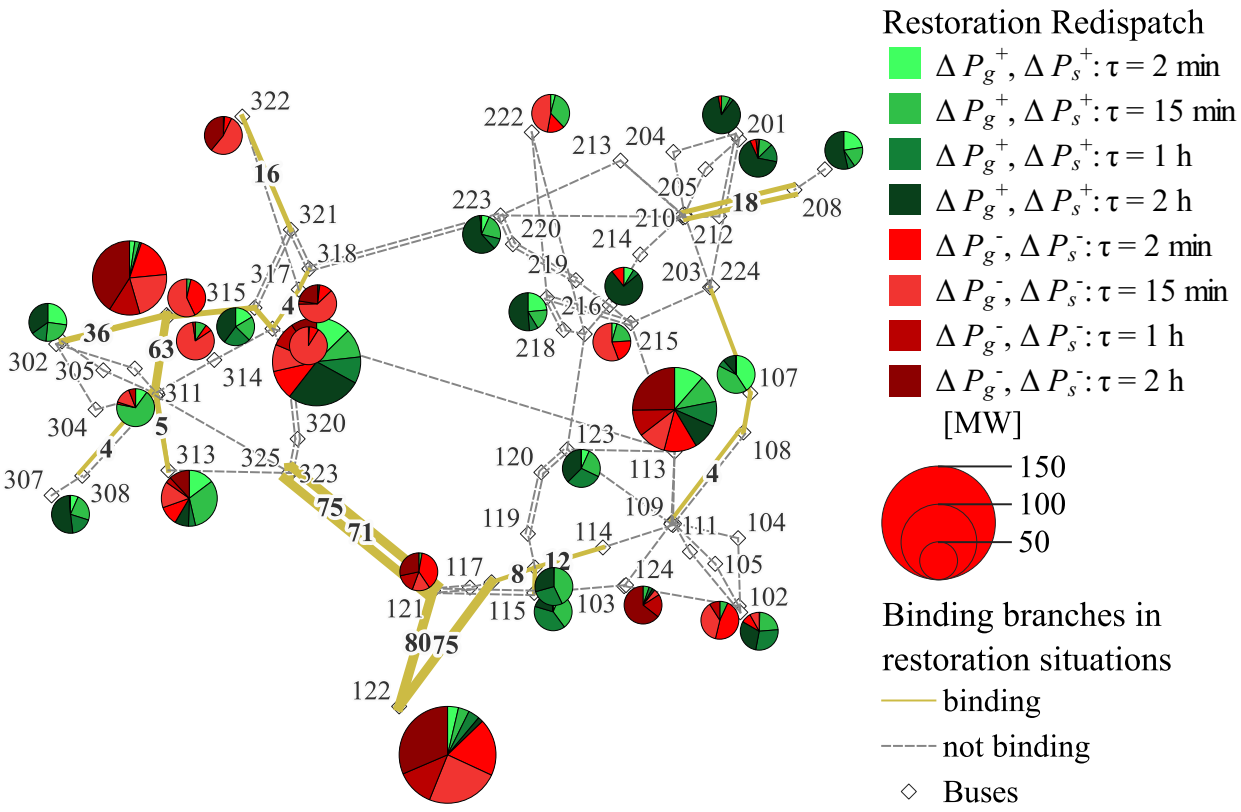

Figure 6.8.: Curative redispatch volumes per bus and number of restoration situations in which branch flow limits are limiting in the PrevCurRest simulation.

6.5. Conclusion of the chapter

The PrevCurRest strategy was successfully implemented and tested on the RTS-GMLC test system. The demonstrated results indicate that the strategy can effectively reduce the preventive RD volume compared to the Prev strategy. The reduction in RD volume is not as significant as that achieved by the PrevCur strategy, but comparison with the PrevN2 strategy highlights the potential of curative RAs to react individually to contingency events, rather than relying on preventive RAs to prepare for any N–1 or N–1–1 event.

7. Summary, conclusions and outlook

7.1. Summary

This thesis addresses the optimization of RAs for CM in transmission grids, with a particular focus on integrating curative RAs. The work introduces a graph-based model for the SCOPF problem under N–1–1 security requirements. The modeling approach is designed to facilitate the comparison of different CM strategies, including preventive (Prev), preventive-curative (PrevCur), and preventive-curative-restorative (PrevCurRest) strategies. A key contribution is the the developed scheme for the PrevCurRest strategy that allows for the explicit consideration of the N–1 security restoration phase after applying curative RAs, which has been overlooked in previous research.

The thesis also integrates polyhedral TATL constraints for two consecutive postfault timeframes into the SCOPF model, enhancing the representation of thermal reserves of OHL conductors. Including the piece-wise linear TATL constraints via callback functions (lazy constraints) in the `Gurobi` solver allows for an efficient solving of the MILP.

The results obtained from computational experiments with the RTS-GMLC test system demonstrate that the proposed PrevCurRest strategy can slightly reduce the preventive RD volume compared to the Prev strategy, while additionally providing information on how to restore N–1 security after a primary contingency. The results also show, that the restoration requirement reduces the potential cost savings of the PrevCur strategy. In practical applications, it is therefore advisded to integrate curative RA only if the N–1 restoration capabilities are sufficiently studied. Due to the long computation times in the proof-of-concept implementation, the PrevCurRest strategy is not yet suitable for real-time applications. Several points for improving the computational performance have been identified in other works, which can be applied to the proposed model:

1. **Use of sensitivity factors**: The current approach models branch flows for all grid situations using the PFE Eq. (3.23) and DC branch flow equations Eqs. (3.25) and (3.26). Alternatively, sensitivity factors such as PTDFs [95] and PSDF [96] can directly link bus power injections to branch flows. For contingency analysis, LODFs [97] can estimate post-outage power flow redistribution. This method reduces the number of variables and constraints by eliminating explicit modeling of voltage angles and individual PFE constraints for each bus. It also enables selective addition of (lazy) branch

flow constraints based on CA and CF results during iterative solving. Beyond PTDF, PSDF, and LODF, which depend on the bus admittance matrix, other techniques include using the Jacobian matrix from Newton-Raphson method for solving the AC power flow [32]. This linearization around the current operating point can be updated iteratively to improve the accuracy of the linear approximation.

2. **Relaxed LP iterations**: The current solution scheme applies a MILP formulation in each iteration (Fig. 5.6). Since the initial CM iterations focus on identifying the most critical CNECs, a relaxed LP formulation can accelerate these steps. Once no new CNECs are found in the LP iterations, the final steps can be solved as a MILP to ensure integrality of binary variables. This approach has been successfully used by [4].

3. **Omission of binary variables for BESS**: The current model introduces binary variables for each BESS and grid situation to distinguish between charging and discharging modes, preventing simultaneous charging and discharging "burning energy"). This issue typically arises in the last hours of the optimization horizon, where BESS must reach a target SoC. However, since deviations from the initial market schedule are penalized in the objective function, the solver has little incentive to select such solutions. Removing the binary variables for BESS can therefore reduce model size and computation time.

Even if the PrevCurRest model becomes suitable for real-time operation, human judgment remains essential. The automation of curative RAs implementation is limited by factors such as forecast uncertainty, system stability, and operational constraints that cannot be modeled in the static and deterministic PrevCurRest model. Human operators will therefore continue to play a key role, integrating insights from multiple support tools and making informed decisions. Their expertise is crucial for interpreting planning results and responding effectively to contingencies.

Although the proposed PrevCurRest model provides an enhanced level of security by considering N–1–1 security requirements, it is important to note that this consideration does not increase the overall resilience of the system. The application of the N–1–1 security criterion and the PrevCurRest strategy allows for studies of the system's behavior under various contingencies. This allows for a more comprehensive understanding of the system's flexibility to adapt to predefined contingencies. However, resilience concepts must also take additional scenarios into account.

7.2. Outlook

The research presented in this thesis suggests several directions for future work:

- *Distributed optimization:* Distributed optimization techniques can be applied to the graph-based SCOPF model to investigate the potential for parallelization and improved scalability in larger systems.
- *AC power flow modeling:* Incorporating exact or relaxed AC power flow equations enables a more accurate representation of voltage limits and reactive power flows in the SCOPF framework. Recent works indicate that AC SCOPF problems are solvable for large-scale systems within reasonable time frames. Although the test grid in this work is small, the number of grid situations considered leads to a large overall model size.
- *Temporal resolution:* Extending the analysis beyond hourly resolution by considering contingencies at different times within the hour can provide a more detailed understanding of system behavior.
- *Uncertainty and stochastic approaches:* Integrating stochastic methods into the optimization model addresses the increasing uncertainties associated with higher shares of RES. Additional uncertainty arises from flexible units, such as BESSs, which can respond to market signals independently of their location within the bidding zone. This includes adapting security margins and optimization models to better reflect forecast uncertainties.
- *Rolling horizon and real-time planning:* Implementing a rolling horizon approach, where the optimization is solved repeatedly with updated forecasts and a limited time window, can reduce the lead time of operational planning. This enables more dynamic and adaptive operational planning. The lead times of conventional power plants remain an important consideration and will continue to play a significant role in day-ahead decision-making.
- *System dynamics and stability:* The present work assumes quasi-static, steady-state conditions. Including stability constraints in future research is a necessary consideration to provide feasible RA for real-time operation.

These research directions can further enhance the practical applicability of decision-support tools for CM in operational planning and real-time operation. All these aspects are relevant

for the future development of CM strategies, especially in the context of increasing shares of RESs and other flexible units such as BESSs.

Operational day-ahead planning processes will order fewer binding redispatch volumes due to decreasing lead times for conventional power plants. Instead, these processes will increasingly focus on developing and evaluating probabilistic scenarios for real-time operation. RAs planned in these processes must be as flexible as possible to address a wide range of scenarios and to exclude extreme events as much as possible. In intraday operation, operational planning and real-time processes will increasingly converge to enable flexible responses to short-term congestion. CM tools, which are currently used several hours ahead of real-time operation, must be further developed to provide rapid decision support in close interaction with operators. The term "interaction" refers to the ability of support systems to present and explain decisions in a way that is understandable to humans. At the same time, operators must be able to influence optimization objectives and constraints—without detailed knowledge of the underlying optimization models—to adapt results to operational requirements. The implementation of RAs must become even more automated in the future, shifting from a controlling to a regulating mechanism. This will allow CM to automatically adapt to current power flow situations without human intervention.

In such a system, as outlined above, the forecast horizon of optimization models—such as that of the PrevCurRest strategy—will become shorter, resulting in reduced computation times. At the same time, this enables improved modeling accuracy regarding AC power flow equations and controllable grid assets. The PrevCurRest strategy could then be applied in a simplified form for real-time operation.

Use of Artificial Intelligence

The following tools and models were used throughout this work for help with wording, formatting, and styling:

Product	**Models**
OpenAI ChatGPT [98]	GPT-3.5 [99], GPT-4.0 [99], GPT-4.1 [99]
GitHub Copilot [100]	GPT-4.0 [99], GPT-4.1 [99], Claude-Sonnet 3.5 [101]
Grammarly [102]	custom
TU Dortmund Campus KI [103]	GPT o4-mini [99], GPT o4 [99]

References

[1] Bundesnetzagentur für Elektrizität, Gas, Telekommunikation, Post und Eisenbahnen, Ed., *Redispatch mit Marktkraftwerke, Mengen und Kosten von Redispatch seit Juli 2022*. Accessed: Jul. 30, 2025. [Online]. Available: https://www.smard.de/page/home/topic-article/46/213270/redispatch-mit-marktkraftwerke

[2] European Union, *Commission Regulation (EU) 2017/1485 of 2 August 2017 establishing a guideline on electricity transmission system operation*, C/2017/5310, 2017. Accessed: Dec. 5, 2024. [Online]. Available: http://data.europa.eu/eli/reg/2017/1485/oj

[3] A. Lukaschik et al., "Innovationen in der Systemführung bis 2030 : InnoSys 2030 : Abschlussbericht", *Innovationen in der Systemführung bis 2030*, DOI: 10.2314/KXP:1857908287

[4] A. Hoffrichter et al., "Simulation of Curative Congestion Management in Large-Scale Transmission Grids", in *2019 54th International Universities Power 2019*, pp. 1–6. DOI: 10.1109/UPEC.2019.8893627

[5] K. Kollenda et al., "Planungsorientierte Simulation kurativer Maßnahmen im Deutschen Übertragungsnetz", in *EnInnov2020 - 16. Symposium Energieinnovation, Kurzfassungsband ENERGY FOR FUTURE - Wege zur Klimaneutralität; 12. - 14. Februar 2020 TU Graz, Österreich*, (Graz, Feb. 12, 2020), U. Bachhiesl, Ed., Verlag der Technischen Universität Graz, 2020, pp. 207–208. DOI: 10.3217/978-3-85125-734-2

[6] K. Kollenda et al., "Curative measures identification in congestion management exploiting temporary admissible thermal loading of overhead lines", *IET Generation, Transmission & Distribution*, vol. 16, 2022. DOI: 10.1049/gtd2.12512

[7] M. Lindner et al., "Corrective Congestion Management in Transmission Grids Using Fast-Responding Generation, Load and Storage", in *2021 IEEE Electrical Power and Energy Conference (EPEC)*, (Toronto, ON, Canada, Oct. 22, 2021), IEEE, 2021, pp. 1–6. DOI: 10.1109/EPEC52095.2021.9621491

[8] InnoSys 2030, Ed., *Factsheet - InnoSys System Operation Process*, Bayreuth, 2022. Accessed: Aug. 28, 2024. [Online]. Available: https://www.innosys2030.de/wp-content/uploads/InnoSys_Factsheet_System-Operation-Process_EN.pdf

[9] C. Barrows et al., "The IEEE Reliability Test System: A Proposed 2019 Update", *IEEE Transactions on Power Systems*, vol. 35, no. 1, pp. 119–127, 2020. DOI: 10.1109/TPWRS.2019.2925557

[10] A. M. Stanković et al., "Methods for Analysis and Quantification of Power System Resilience", *IEEE Transactions on Power Systems*, vol. 38, no. 5, pp. 4774–4787, 2023. DOI: 10.1109/TPWRS.2022.3212688

[11] ENTSO-E, Ed., *Supporting document to the all TSOs' proposal for the methodology for coordinating operational security analysis*, Brussels, 2018. Accessed: May 13, 2025. [Online]. Available: https://www.entsoe.eu/Documents/nc-tasks/SOGL/SOGL_A75.1_180710_Supporting%20document%20to%20the%20CSA%20and%20RAOC%20methodologies_180914.pdf

[12] L. Huang et al., "Robust N-k Security-constrained Optimal Power Flow Incorporating Preventive and Corrective Generation Dispatch to Improve Power System Reliability", *CSEE Journal of Power and Energy Systems*, vol. 9, no. 1, pp. 351–364, 2023. DOI: 10.17775/CSEEJPES.2021.06560

[13] Y. Chen et al., "Robust N – k CCUC model considering the fault outage probability of units and transmission lines", *IET Generation, Transmission & Distribution*, vol. 13, no. 17, pp. 3782–3791, 2019. DOI: 10.1049/iet-gtd.2019.0780

[14] North American Electric Reliability Corporation, *TPL-001-5.1, Transmission System Planning Performance Requirements*, 5.1, 2023. Accessed: Oct. 28, 2024. [Online]. Available: https://www.nerc.com/pa/Stand/Reliability%20Standards/TPL-001-5.1.pdf

[15] D. Chatterjee et al., "N-1-1 AC contingency analysis as a part of NERC compliance studies at midwest ISO", in pp. 1–7. DOI: 10.1109/TDC.2010.5484209

[16] D. A. Zuniga Vazquez et al., "N-1-1 contingency-constrained unit commitment with renewable integration and corrective actions", *Annals of Operations Research*, vol. 316, no. 1, pp. 493–511, 2022. DOI: 10.1007/s10479-021-04204-y [Online]. Available: https://link.springer.com/article/10.1007/s10479-021-04204-y

[17] ENTSO-E, Ed., *ICS 2023 Annual Report*, Brussels, 2024. Accessed: May 15, 2025. [Online]. Available: https://eepublicdownloads.entsoe.eu/clean-documents/SOC%20documents/Incident_Classification_Scale/2023/ICS_report_2023.pdf

[18] S. R. Dahman, *N-1-1 Contingency Analysis using PowerWorld Simulator*, PowerWorld Corporation, Ed., 2012. Accessed: Mar. 12, 2025. [Online]. Available: https://www.powerworld.com/files/SimulatorN-1-1.pdf

[19] A. Shokri Gazafroudi, F. Neumann, and T. Brown, "Topology-based approximations for N−1 contingency constraints in power transmission networks", *International Journal of Electrical Power & Energy Systems*, vol. 137, p. 107 702, 2022. DOI: 10.1016/j.ijepes.2021.107702

[20] European Union, *Commission Regulation (EU) 2015/1222 of 24 July 2015 establishing a guideline on capacity allocation and congestion management*, OJ L 197, 2015. Accessed: Dec. 16, 2024. [Online]. Available: http://data.europa.eu/eli/reg/2015/1222/oj

[21] European Union, Ed., *Summary of Regulation (EU) 2017/1485 — guideline on electricity transmission system operation*, Brussels, 2018. Accessed: May 14, 2025. [Online]. Available: https://eur-lex.europa.eu/legal-content/EN/LSU/?uri=uriserv:OJ.L_.2017.220.01.0001.01.ENG

[22] ACER, Ed., *Methodology for coordinating operational security analysis*, Ljubljana, 2024. Accessed: May 13, 2025. [Online]. Available: https://eepublicdownloads.entsoe.eu/clean-documents/nc-tasks/ACER_Decision_07-2024_Second_CSAM_Amendment-Annex_I.pdf

[23] *Energiewirtschaftsgesetz vom 7. Juli 2005 (BGBl. I S. 1970, 3621), das zuletzt durch Artikel 41 des Gesetzes vom 23. Oktober 2024 (BGBl. 2024 I Nr. 323) geändert worden ist"*, EnWG, 2024. Accessed: Dec. 16, 2024. [Online]. Available: https://www.gesetze-im-internet.de/enwg_2005/index.html

[24] ENTSO-E, Ed., *Explanatory document to the Core Capacity Calculation Region methodology for common provisions for regional operational security coordination, in accordance with Article 76 of Commission Regulation (EU) 2017/1485 of 2 August 2017*, Brussels, 2019. Accessed: May 30, 2025. [Online]. Available: https://eepublicdownloads.entsoe.eu/clean-documents/

nc-tasks/20191219_Core%20CCR%20TSOs_Explanatory%20Note%20of%20Core%20ROSC%20Methodology.pdf

[25] C. Coffrin, *Open-source Tools for Solving Grid Optimization Problems: ARPA-e Benchmark Algorithm Overview [Slides]*, 2022. DOI: 10.2172/1894824

[26] F. Capitanescu et al., "State-of-the-art, challenges, and future trends in security constrained optimal power flow", *Electric Power Systems Research*, vol. 81, no. 8, pp. 1731–1741, 2011. DOI: 10.1016/J.EPSR.2011.04.003

[27] F. Capitanescu, "Critical review of recent advances and further developments needed in AC optimal power flow", *Electric Power Systems Research*, vol. 136, pp. 57–68, 2016. DOI: 10.1016/j.epsr.2016.02.008

[28] D. K. Molzahn and I. A. Hiskens, "A Survey of Relaxations and Approximations of the Power Flow Equations", *Foundations and Trends® in Electric Energy Systems*, vol. 4, no. 1-2, pp. 1–221, 2019. DOI: 10.1561/3100000012

[29] R. D. Zimmerman and C. E. Murillo-Sánchez, *MATPOWER User's Manual*, 2024. DOI: 10.5281/zenodo.3236519

[30] C. Coffrin et al., "PowerModels. JL: An Open-Source Framework for Exploring Power Flow Formulations", in *20th Power Systems Computation Conference, PSCC2018 Dublin : June 11-15, 2018, University College Dublin, Dublin, Ireland*, (Dublin, Ireland, Jun. 11, 2018), Institute of Electrical and Electronics Engineers, Piscataway, NJ: IEEE, 2018, pp. 1–8. DOI: 10.23919/PSCC.2018.8442948

[31] B. Stott, J. Jardim, and O. Alsac, "DC Power Flow Revisited", *IEEE Transactions on Power Systems*, vol. 24, no. 3, pp. 1290–1300, 2009. DOI: 10.1109/TPWRS.2009.2021235

[32] J. Eickmann, C. Bredtmann, and A. Moser, "Security-Constrained Optimization Framework for Large-Scale Power Systems Including Post-contingency Remedial Actions and Inter-temporal Constraints", in *Advances in Energy System Optimization, Proceedings of the first International Symposium on Energy System Optimization*, ser. Trends in Mathematics Ser, V. Bertsch et al., Eds., Cham: Springer International Publishing, 2017, pp. 47–63. DOI: 10.1007/978-3-319-51795-7_4

[33] J. Eickmann, "Simulation der Engpassbehebung im deutschen Übertragungsnetzbetrieb", IAEW, PhD Thesis, RWTH Aachen, Aachen, 2015.

[34] C. Coffrin, *Power Grid Lib - Optimal Power Flow, V23*, 2023. Accessed: Jun. 18, 2025. [Online]. Available: https://github.com/power-grid-lib/pglib-opf

[35] J. F. Benders, "Partitioning procedures for solving mixed-variables programming problems", *Numerische Mathematik*, vol. 4, no. 1, pp. 238–252, 1962. DOI: 10.1007/BF01386316

[36] M. Shahidehopour and Y. Fu, "Benders decomposition: applying Benders decomposition to power systems", *IEEE Power and Energy Magazine*, vol. 3, no. 2, pp. 20–21, 2005. DOI: 10.1109/MPAE.2005.1405865

[37] J. Martínez-Crespo, J. Usaola, and J. L. Fernández, "Optimal security-constrained power scheduling by Benders decomposition", *Electric Power Systems Research*, vol. 77, no. 7, pp. 739–753, 2007. DOI: 10.1016/j.epsr.2006.06.009

[38] Q. Wang et al., "Solving corrective risk-based security-constrained optimal power flow with Lagrangian relaxation and Benders decomposition", *International Journal of Electrical Power & Energy Systems*, vol. 75, pp. 255–264, 2016. DOI: 10.1016/j.ijepes.2015.09.001

[39] D. K. Molzahn et al., "A Survey of Distributed Optimization and Control Algorithms for Electric Power Systems", *IEEE Transactions on Smart Grid*, vol. 8, no. 6, pp. 2941–2962, 2017. DOI: 10.1109/TSG.2017.2720471

[40] A. Engelmann et al., "Toward Distributed OPF Using ALADIN", *IEEE Transactions on Power Systems*, vol. 34, no. 1, pp. 584–594, 2019. DOI: 10.1109/TPWRS.2018.2867682

[41] G. Stomberg, A. Engelmann, and T. Faulwasser, *Decentralized non-convex optimization via bi-level SQP and ADMM*, 2022. DOI: 10.48550/arXiv.2204.08786

[42] S. Boyd, "Distributed Optimization and Statistical Learning via the Alternating Direction Method of Multipliers", *Foundations and Trends® in Machine Learning*, vol. 3, no. 1, pp. 1–122, 2010. DOI: 10.1561/2200000016

[43] S. Mhanna, G. Verbic, and A. C. Chapman, "Adaptive ADMM for Distributed AC Optimal Power Flow", *IEEE Transactions on Power Systems*, vol. 34, no. 3, pp. 2025–2035, 2019. DOI: 10.1109/TPWRS.2018.2886344

[44] M. Alkhraijah et al., "PowerModelsADA: A Framework for Solving Optimal Power Flow Using Distributed Algorithms", *IEEE Transactions on Power Systems*, vol. 39, no. 1, pp. 2357–2360, 2024. DOI: 10.1109/TPWRS.2023.3318858

[45] ENTSO-E, Ed., *Explanatory note on the day-ahead and intraday common capacity calculation methodologies for the Core CCR*, Brussels, 2018. Accessed: Apr. 13, 2025. [Online]. Available: https://www.entsoe.eu/Documents/Network%20codes%20documents/Implementation/ccr/methodologies/core/cacm-deliverables/da-and-id-ccms-art-20ff/20180604-core-tsos-explanatory-note-for-core-da-id-fb-ccm-fv.pdf

[46] Gurobi Optimization LLC., Ed., *Gurobi Optimizer Reference Manual, Version 12.0*, 2025. Accessed: Apr. 14, 2025. [Online]. Available: https://docs.gurobi.com/_/downloads/optimizer/en/12.0/pdf/

[47] Deutsches Institut für Normung e.V., Ed., *EN 50182:2001 - Conductors for overhead lines - Round wire concentric lay stranded conductors*, Berlin: Beuth Verlag GmbH, 2001. Accessed: May 3, 2021.

[48] A. Webs, "Dauerstrombelastbarkeit von nach DIN 48201 gefertigten Freileitungsseilen aus Kupfer, Aluminium und Aldrey", *Elektrizitätswirtschaft*, vol. 61, pp. 861–872, 1962.

[49] V. T. Morgan, "Rating of bare overhead conductors for continuous currents", *Proceedings of the Institution of Electrical Engineers*, vol. 114, no. 10, p. 1473, 1967. DOI: 10.1049/piee.1967.0284 [Online]. Available: https://digital-library.theiet.org/content/journals/10.1049/piee.1967.0284

[50] WG B2.43, *Guide for thermal rating calculations of overhead lines, Technical Brochure 601*, CIGRE, Ed., Paris: CIGRE, 2014. Accessed: Oct. 14, 2020. [Online]. Available: https://e-cigre.org/publication/601-guide-for-thermal-rating-calculations-of-overhead-lines

[51] *IEEE standard for calculating the current-temperature relationship of bare overhead conductors*, eng. New York: Institute of Electrical and Electronics Engineers, 2013, 58 pp., ISBN: 0738188875. [Online]. Available: http://ieeexplore.ieee.org/servlet/opac?punumber=6692856

[52] 50Hertz Transmission GmbH et al., Eds., *Principles for the expansion planning of the German transmission grid*, 2024. Accessed: Aug. 18, 2025. [Online]. Available: https://www.netztransparenz.de/xspproxy/api/staticfiles/ntp-relaunch/dokumente/%5C%C3%5C%BCber%20uns/aufgaben/%5C%C3%5C%BCnb-plgrs_2024.pdf

[53] W. Black and R. Rehberg, "Simplified Model for Steady State and Real-Time Ampacity of Overhead Conductors", *IEEE Transactions on Power Apparatus and Systems*, vol. PAS-104, no. 10, pp. 2942–2953, 1985. DOI: 10.1109/TPAS.1985.319142

[54] C. Biele et al., "Simulation Tool for the Transient Temperature Behavior of Overhead Line Conductors", in *NEIS 2022, Conference on Sustainable Energy Supply and Energy Storage Systems, Hamburg, September 26 - 27, 2022*, D. Schulz, Ed., Neuerscheinung, Berlin: VDE Verlag, 2022, pp. 1–6, ISBN: 9783800759835. Accessed: Feb. 21, 2023. [Online]. Available: https://ieeexplore.ieee.org/document/10048071

[55] J. Mehlem et al., "On the influence of electro-thermal modeling of overhead lines on curative congestion management in transmission systems", in *2021 International Conference on Smart Energy Systems and Technologies (SEST)*, (Vaasa, Finland, Sep. 6, 2021), IEEE, 2021, pp. 1–6. DOI: 10.1109/SEST50973.2021.9543172

[56] C. Biele and M. Lindner. "TATL-Tool Github Repository". [Online]. Available: https://github.com/tso-martin/TATL-Tool

[57] L. F. Shampine and M. W. Reichelt, "The MATLAB ODE Suite", *SIAM Journal on Scientific Computing*, vol. 18, no. 1, pp. 1–22, 1997. DOI: 10.1137/S1064827594276424

[58] P. Bogacki and L. F. Shampine, "A 3(2) pair of Runge - Kutta formulas", *Applied Mathematics Letters*, vol. 2, no. 4, pp. 321–325, 1989. DOI: 10.1016/0893-9659(89)90079-7

[59] G. E. Forsythe, M. A. Malcolm, and C. B. Moler, *Computer methods for mathematical computations* (Prentice-Hall series in automatic computation), eng. Englewood Cliffs, NJ: Prentice-Hall, 1977, 259 pp., ISBN: 9780131653320.

[60] J. Bezanson et al., "Julia: A fresh approach to numerical computing", *SIAM Review*, vol. 59, no. 1, pp. 65–98, 2017. DOI: 10.1137/141000671

[61] G. W. Bills, *On-line stability analysis study, RP 90-1*, North American Rockwell Information Systems Co., Anaheim, CA (USA), 1970. [Online]. Available: https://www.osti.gov/biblio/5984031

[62] D. Lee et al., "Robust AC Optimal Power Flow With Robust Convex Restriction", *IEEE Transactions on Power Systems*, vol. 36, no. 6, pp. 4953–4966, 2021. DOI: 10.1109/TPWRS.2021.3075925

[63] T. Mühlpfordt, T. Faulwasser, and V. Hagenmeyer, "A generalized framework for chance-constrained optimal power flow", *Sustainable Energy, Grids and Networks*, vol. 16, pp. 231–242, 2018. DOI: 10.1016/j.segan.2018.08.002

[64] L. A. Roald et al., "Power systems optimization under uncertainty: A review of methods and applications", *Electric Power Systems Research*, vol. 214, p. 108 725, 2023. DOI: 10.1016/j.epsr.2022.108725

[65] S. Shin et al., "Graph-Based Modeling and Decomposition of Energy Infrastructures", *IFAC-PapersOnLine*, vol. 54, no. 3, pp. 693–698, 2021. DOI: 10.1016/j.ifacol.2021.08.322

[66] J. Jalving, S. Shin, and V. M. Zavala, "A graph-based modeling abstraction for optimization: concepts and implementation in Plasmo.jl", *Mathematical Programming Computation*, vol. 14, no. 4, pp. 699–747, 2022. DOI: 10.1007/s12532-022-00223-3

[67] S. Shin et al., "Scalable Multi-Period AC Optimal Power Flow Utilizing GPUs with High Memory Capacities", in *2024 Open Source Modelling and Simulation of Energy Systems (OSMSES)*, (Vienna, Austria, Sep. 3, 2024), IEEE, 2024, pp. 1–6. DOI: 10.1109/OSMSES62085.2024.10668970

[68] European Union, *Regulation (EU) 2019/943 of the European Parliament and of the Council of 5 June 2019 on the internal market for electricity*, OJ L 158, 2019. Accessed: Sep. 7, 2025. [Online]. Available: https://eur-lex.europa.eu/legal-content/EN/TXT/?uri=CELEX:32019R0943

[69] N. Nazir and M. Almassalkhi, "Guaranteeing a physically realizable battery dispatch without charge-discharge complementarity constraints", *IEEE Transactions on Smart Grid*, p. 1, 2021. DOI: 10.1109/TSG.2021.3109805

[70] J. Löfberg, *Unit commitment*, 2016. Accessed: Apr. 6, 2025. [Online]. Available: https://yalmip.github.io/example/unitcommitment/

[71] L. Platbrood et al., "A Generic Approach for Solving Nonlinear-Discrete Security-Constrained Optimal Power Flow Problems in Large-Scale Systems", *IEEE Transactions on Power Systems*, vol. 29, no. 3, pp. 1194–1203, 2014. DOI: 10.1109/tpwrs.2013.2289990

[72] F. Capitanescu and L. Wehenkel, "A New Iterative Approach to the Corrective Security-Constrained Optimal Power Flow Problem", *IEEE Transactions on Power Systems*, vol. 23, no. 4, pp. 1533–1541, 2008. DOI: 10.1109/TPWRS.2008.2002175

[73] F. P. Preparata and M. I. Shamos, *Computational Geometry : an Introduction / by Franco P. Preparata, Michael Ian Shamos* (Texts and Monographs in Computer Science, 0172-603X). New York, NY: Springer New York : Imprint : Springer, 1985, 420 pp., ISBN: 0-387-96131-3.

[74] T. S. Motzkin et al., "The double description method", *Contributions to the Theory of Games*, vol. 2, no. 28, pp. 51–73, 1953.

[75] Benoît Legat et al., *JuliaPolyhedra/CDDLib.jl: v0.10.1*, Zenodo, 2025. DOI: 10.5281/ZENODO.1214581

[76] Benoît Legat et al., *JuliaPolyhedra/Polyhedra.jl: v0.8.1*, Zenodo, 2025. DOI: 10.5281/ZENODO.1214290

[77] Gurobi Optimization LLC., Ed., *Mixed Integer Programming (MIP), A Primer on the Basics*. Accessed: Apr. 14, 2025. [Online]. Available: https://www.gurobi.com/resources/mixed-integer-programming-mip-a-primer-on-the-basics/

[78] Miles Lubin et al., "JuMP 1.0: Recent improvements to a modeling language for mathematical optimization", *Mathematical Programming Computation*, 2023. DOI: 10.1007/s12532-023-00239-3

[79] A. Wächter and L. T. Biegler, "On the implementation of an interior-point filter line-search algorithm for large-scale nonlinear programming", *Mathematical Programming*, vol. 106, no. 1, pp. 25–57, 2006. DOI: 10.1007/s10107-004-0559-y

[80] C. Grigg et al., "The IEEE Reliability Test System-1996. A report prepared by the Reliability Test System Task Force of the Application of Probability Methods Subcommittee", *IEEE Transactions on Power Systems*, vol. 14, no. 3, pp. 1010–1020, 1999. DOI: 10.1109/59.780914

[81] DigSILENT GmbH, Ed., *PowerFactory 2022 SP 3*, 2022. Accessed: Jun. 13, 2025. [Online]. Available: https://www.digsilent.de/de/powerfactory.html

[82] Openstreetmap Contributors, *OpenStreetMap*, OpenStreetMap Foundation, Ed. Accessed: Aug. 18, 2025. [Online]. Available: https://www.openstreetmap.org/

[83] A. Nagarajan, *Western Wind and Solar Integration Study*, National Renewable Energy Laboratory, Ed., Golden, CO, 2015. Accessed: Nov. 21, 2024. [Online]. Available: https://www.nrel.gov/grid/wwsis.html

[84] C. W. Potter et al., "Creating the Dataset for the Western Wind and Solar Integration Study (U.S.A.)", *Wind Engineering*, vol. 32, no. 4, pp. 325–338, 2008. DOI: 10.1260/0309-524X.32.4.325

[85] D. Lew et al., *The Western Wind and Solar Integration Study Phase 2*, National Renewable Energy Laboratory, Ed., Golden, CO, 2013. Accessed: Nov. 21, 2024. [Online]. Available: https://www.nrel.gov/docs/fy13osti/55588.pdf

[86] C. Draxl et al., "The Wind Integration National Dataset (WIND) Toolkit", *Applied Energy*, vol. 151, pp. 355–366, 2015. DOI: 10.1016/j.apenergy.2015.03.121

[87] NASA JPL, *NASA Shuttle Radar Topography Mission Global 1 arc second*, 2013. DOI: 10.5067/MEaSUREs/SRTM/SRTMGL1.003

[88] C. Coffrin, *Power Grid Lib - Unit Commitment, V19.08*, 2019. Accessed: Jun. 18, 2025. [Online]. Available: https://github.com/power-grid-lib/pglib-uc

[89] C. Coffrin, *IEEE PES Power Grid Lib*, 2025. Accessed: Jun. 18, 2025. [Online]. Available: https://power-grid-lib.github.io/

[90] B. Knueven, J. Ostrowski, and J.-P. Watson, *On Mixed Integer Porgramming Formulations for the Unit Commitment Problem*, Knoxville, TN: Department of Industrial and Systems Engineering University of Tennessee, 2018. Accessed: Jun. 18, 2025. [Online]. Available: https://optimization-online.org/?p=15513

[91] B. Valov, *Handbuch Netzintegration Erneuerbarer Energien, Netzanschluss, Stromerzeugungsanlagen und Regelung*, ger, 2. Auflage. Wiesbaden and Heidelberg: Springer Vieweg, 2022, 733 pp. DOI: 10.1007/978-3-658-37791-5

[92] J. Mehlem, M. Krüger, and A. Moser, "Thermally limiting grid assets for temporary admissible transmission loading (TATL) in curative congestion management", in *2023 IEEE PES Innovative Smart Grid Technologies - Asia (ISGT Asia)*, (Auckland, New Zealand, Nov. 21, 2023), IEEE, 2023, pp. 1–5. DOI: 10.1109/ISGTAsia54891.2023.10372604

[93] Deutsches Institut für Normung e.V., Ed., *Power Transformers, Part 7: Loading guide for mineral-oil-immersed power transformers (IEC 60076-7:2018)*, Berlin: International Electrotechnical Commission, 2023. Accessed: Jun. 17, 2025. [Online]. Available: https://www.vde-verlag.de/normen/0500246/din-iec-60076-7-vde-0532-76-7-2023-05.html

[94] Institute of Electrical and Electronics Engineers, Ed., *C57.91-2011 - IEEE Guide for Loading Mineral-Oil-Immersed Transformers and Step-Voltage Regulators*, Piscataway, NJ, USA, 2011. DOI: 10.1109/IEEESTD.2012.6166928

[95] A. J. Wood, B. F. Wollenberg, and G. B. Sheblé, *Power generation, operation, and control*, 3. ed. Hoboken, NJ: Wiley, 2014, ISBN: 9780471790556.

[96] J. Verboomen et al., "Analytical Approach to Grid Operation With Phase Shifting Transformers", *IEEE Transactions on Power Systems*, vol. 23, no. 1, pp. 41–46, 2008. DOI: 10.1109/TPWRS.2007.913197

[97] T. Guler, G. Gross, and M. Liu, "Generalized Line Outage Distribution Factors", *IEEE Transactions on Power Systems*, vol. 22, no. 2, pp. 879–881, 2007. DOI: 10.1109/TPWRS.2006.888950

[98] OpenAI OpCo, LLC, Ed., *ChatGPT*. Accessed: Aug. 1, 2025. [Online]. Available: https://chatgpt.com/

[99] OpenAI OpCo, LLC, Ed., *OpenAI Models*. Accessed: Aug. 1, 2025. [Online]. Available: https://platform.openai.com/docs/models

[100] GitHub, LLC, Ed., *GitHub Copilot*. Accessed: Aug. 1, 2025. [Online]. Available: https://docs.github.com/en/copilot

[101] Anthropic PBC, Ed., *Claude Models overview*. Accessed: Aug. 1, 2025. [Online]. Available: https://docs.anthropic.com/en/docs/about-claude/models/overview

[102] Grammarly, Inc., Ed., *Grammarly*, 2025. Accessed: Aug. 1, 2025. [Online]. Available: https://www.grammarly.com/

[103] TU Dortmund University, Ed., *Campus-KI*, Dortmund, 2025. Accessed: Sep. 24, 2025. [Online]. Available: https://campus-ki.tu-dortmund.de

Own Publications

[ML1] C. Biele et al., “Simulation Tool for the Transient Temperature Behavior of Overhead Line Conductors”, in *NEIS 2022*, D. Schulz, Ed., Berlin: VDE Verlag, 2022, ISBN: 9783800759835. Accessed: Jul. 23, 2025. [Online]. Available: https://ieeexplore.ieee.org/document/10048071

[ML2] R. Broll et al., *Digitale Systeme und Dienste für die Energiesystemtransformation*, TU Dortmund University, Ed., 2021. DOI: 10.17877/DE290R-21909

[ML3] M. Klaes et al., “State description of cyber-physical energy systems”, *Energy Informatics*, vol. 3, no. S1, 2020. DOI: 10.1186/s42162-020-00119-3

[ML4] K. Kollenda et al., “Curative measures identification in congestion management exploiting temporary admissible thermal loading of overhead lines”, *IET Generation, Transmission & Distribution*, vol. 16, 2022. DOI: 10.1049/gtd2.12512

[ML5] M. Braun et al., “Systematisierung der Autonomiestufen in der Netzbetriebsführung”, in *ETG-Fb. 163: ETG-Kongress 2021*, Energietechnische Gesellschaft im VDE, Ed., ser. ETG-Fachberichte, Berlin: VDE Verlag, 2021, pp. 65–70, ISBN: 9783800755509. Accessed: Sep. 22, 2025. [Online]. Available: https://www.vde-verlag.de/proceedings-de/455549012.html

[ML6] M. Lindner et al., “Corrective Congestion Management in Transmission Grids Using Fast-Responding Generation, Load and Storage”, in *2021 IEEE Electrical Power and Energy Conference (EPEC)*, 2021, pp. 1–6. DOI: 10.1109/EPEC52095.2021.9621491

[ML7] M. Lindner et al., “Operation strategies of battery energy storage systems for preventive and curative congestion management in transmission grids”, *IET Generation, Transmission & Distribution*, 2022. DOI: 10.1049/gtd2.12739

Supervised Thesis

[ST1] T. Hoffmann, “Systematische Analyse umfangreicher Netzdatensätze und Vergleich von Netzzuständen mittels Indikatoren”, Master Thesis, TU Dortmund University, Dortmund, 2020.

[ST2] S. Kobat, “Anwendung und Erweiterung des Verfahrens der elektro-thermischen Leistungsflussrechnung für Analysen in Höchst- und Hochspannungsnetzen”, Master Thesis, TU Dortmund University, Dortmund, 2021.

[ST3] J. Krieger, “Optimale Platzierung und Dimensionierung von Speichern zur kurativen Engpassbehebung im Transportnetz”, Master Thesis, TU Dortmund University, Dortmund, 2022.

[ST4] R. Krüßmann, “Einbindung von Netzboostern in die Betriebsplanung von Transportnetzen”, Master Thesis, TU Dortmund University, Dortmund, 2021.

[ST5] S. Mees, “Wiederherstellung der (n-1)-Sicherheit unter Verwendung von kurativen Ad-Hoc-Maßnahmen”, Master Thesis, TU Dortmund University, Dortmund, 2023.

[ST6] L. Spies, “Echtzeitsimulation kurativer Ad-hoc-Maßnahmen zur Engpassbehebung unter Einbeziehung thermischer Freiheitsgrade von Freileitungen”, Master Thesis, TU Dortmund University, Dortmund, 2022.

Acronyms

Acronym	Description
N–0	N-0
N–1–1	N-1-1
N–1	N-1
N–2	N-2
N–k	N-k
AC	Alternating Current
ACER	European Union Agency for the Cooperation of Energy Regulators
ADMM	Alternating Direction Method of Multipliers
ALADIN	Augmented Lagrangian Alternating Direction Inexact Newton
BESS	Battery Energy Storage System
C2RT	Close to real-time
CA	Contingency Analysis
CACM	Capacity Allocation and Congestion Management
CBCO	Critical Branch and Critical Outage
CC	Combined Cycle
CC	Capacity Calculation
CCR	Capacity Calculation Region
CF	Contingency Filtering
CGM	Common Grid Model
CM	Congestion Management
CNEC	Critical Network Element and Contingency
CPU	Central Processing Unit
CROSA	Coordinated Regional Operational Security Analysis
CSAM	Methodology for Coordinating Operational Security Analysis
CSP	Concentrated Solar Power
CT	Combustion Turbine
D2CF	Two Days Ahead Congestion Forecast
DA	Day Ahead
DACC	Day-Ahead Capacity Calculation
DACF	Day-Ahead Congestion Forecast

Acronym	Description
DC	Direct Current
DLR	Dynamic Line Rating
DSO	Distribution System Operator
dSQP	Distributed Sequential Quadratic Programming
ED	Economic Dispatch
EENS	Expected Energy Not Served
ENTSO-E	European Network of Transmission System Operators for Electricity
EnWG	Energiewirtschaftsgesetz
EPM	Engpassmanagement
HBE	Heat Balance Equation
HVDC	High Voltage Direct Current
ICF	Inverse Cumulated Frequency
IDCC	Intraday Capacity Calculation
IDCF	Intraday Congestion Forecast
IEEE	Institute of Electrical and Electronics Engineers
IGM	Individual Grid Model
InnoSys 2030	Innovationen in der Systemführung 2030
IP	Interior Point
ISO	Independent System Operators
LF/CA	Load Flow and Contingency Analysis
LODF	Line Outage Distribution Factor
LOLE	Loss of Load Expectation
LP	linear program
LUT	Lookup Table
MILP	Mixed-Integer Linear Program
NERC	North American Electric Reliability Corporation
NLP	Nonlinear Program
NP	Net Position
ODE	Ordinary Differential Equation
OHL	Overhead Line
OP	Operational Planning
OPF	Optimal Power Flow

Acronym	Description
PATL	Permanently Admissible Transmission Loading
PES	Power and Energy Society
PF	Power Flow
PFC	Power Flow Controlling Device
PFE	Power Flow Equation
pRD	Preventive Redispatch Process
Prev	Preventive
PrevCur	Preventive-curative
PrevCurRest	Preventive-curative-restorative
PrevN2	Preventive N–2
PSDF	Phase Shift Distribution Factor
PST	Phase-Shift Transformer
PTDF	Power Transfer Distribution Factor
PV	Photovoltaic
QP	Quadratic Program
RA	Remedial Action
RCC	Regional Coordination Center
RD	Redispatch
RES	Renewable Energy Sources
ROSC	Regional Operational Security Coordination
RSC	Regional Security Coordinator
RT	Real-time
RTPV	Rooftop Photovoltaic
RTS-GMLC	Reliability Test System of the Grid Modernization Laboratory Consortium
SAIDI	System Average Interruption Duration Index
SAIFI	System Average Interruption Frequency Index
SC	Sensitivity Calculation
SCADA	Supervisory Control and Data Acquisition
SCOPF	Security-Constrained Optimal Power Flow
SDP	Semidefinite Program
SoC	State of Charge
SOCP	Second Order Cone Program

Acronym	Description
SOGL	System Operation Guideline 17/1485
SQP	Sequential Quadratic Programming
ST	Steam Turbine
TATL	Temporarily Admissible Transmission Loading
TATL1	Temporarily Admissible Transmission Loading for the first curative timeframe
TATL2	Temporarily Admissible Transmission Loading for the second curative timeframe
TSO	Transmission System Operator
UC	Unit Commitment
WAPP	Week-ahead Planning Process
WIND	Wind Integration National Dataset
WWSIS	Western Wind and Solar Integration Study

Symbols

The symbols used in this work are denoted by the following conventions:

- **Scalars** are in italic, e.g., x.
- **Vectors** are in lower case, bold letters, e.g., $\mathbf{x}$.
- **Matrices** are in upper case, bold letters, e.g., $\mathbf{X}$.
- **Sets** are in upper case, calligraphic letters, e.g., $\mathcal{X}$.
- **Complex** variables are underlined, e.g., $\underline{x}, \underline{\mathbf{x}}$.
- **Descriptive** super- and subscripts are in normal font, e.g., x_{N}.

All current and voltage variables are treated as effective values.

Symbol	Description
B	Susceptance
C_{p}	Specific heat capacity per unit length of conductor material
$D-1$	Day before D (DA)
$D-2$	Two days before D
D_0	Conductor diameter
D	Business Day
G	Conductance
I_{r}	Rated current
I	Current
K_ϕ	Wind direction factor
N_{Re}	Reynolds number
N_{bus}	Amount of buses
N_{planes}	Number of TATL2 loading constraint planes
N	Amount
P	Active power flow on branch
P	Bus active power injection
P	Power of unit
Q_{se}	Global solar radation corrected for elevation
Q	Reactive bus power
R_{AC}	AC conductor resistance per unit length
R	Branch resistance
V	Bus Voltage
W	State of charge
X	Branch reactance
$\mathbf{\Delta p}$	Units' active power redispatch (vector)
ΔP	Unit's active power redispatch
$\boldsymbol{\Delta\theta}$	Phase-angle shifts of PSTs (vector)
$\Delta\theta$	Phase-angle shift of PST
$\Delta\vartheta_{\mathrm{SC}}$	Temperature rise during short-circuit
Γ	Graph
Ω	Set of all grid situations

Symbol	Description
α	Solar absorptivity
$\boldsymbol{\theta}$	Phase angle of PSTs
δ	Active power gradient
ϵ_{tol}	Numerical tolerance
ϵ	Emissivity factor
η	Efficiency factor
$\mathbf{B}$	Susceptance matrix
$\mathbf{E}$	Coupling constraint matrix
$\mathbf{G}$	Conductance matrix
$\mathbf{l}$	loading vector
λ	Lagrange multipliers of consensus constraints
μ	Lagrange multipliers of inequality constraints
ν	Lagrange multipliers of equality constraints
ϕ	Bus voltage angle vector
$\mathbf{c}$	Cost coefficient vector
$\mathbf{g}$	Vector of inequality constraint functions
$\mathbf{h}$	Vector of equality constraint functions
$\mathbf{m}$	Vertex of loading polyhedron
$\mathbf{n}$	Normal vector
$\mathbf{p}$	Vector of bus active power injections
$\mathbf{p}$	Power of units
$\mathbf{p}$	Location vector
$\mathbf{q}$	Reactive bus power vector
$\mathbf{v}$	Bus voltage vector
$\mathbf{x}$	Decision variable vector
$\mathcal{B}^{\text{E}}$	Set of bus indexes of branches
$\mathcal{B}$	Set of branch indexes
$\mathcal{C}_{\text{spec}}$	Contingency specification
$\mathcal{C}$	Set of contingencies
$\mathcal{D}$	Load indexes
$\mathcal{E}$	Graph edges
$\mathcal{G}$	Set of generator indexes
$\mathcal{H}$	Set of HVDC branches

Symbol	Description
$\mathcal{L}^{\text{N–1}}$	Set of N–1 loading vectors $\mathbf{l}_c^{\text{N–1}}$
$\mathcal{L}$	Set of loading values for LUT
$\mathcal{M}_{\text{TATL1}}$	Set of TATL1 LUT values
$\mathcal{M}_{\text{TATL2}}$	Set of TATL2 LUT values
$\mathcal{N}$	Set of bus indexes
$\mathcal{S}$	Set of storages
$\mathcal{T}_{\text{spec}}$	Time specification
$\mathcal{T}$	Set of timestamps
ω	Grid situation
ϕ_{w}	Wind direction angle
ϕ	Voltage angle
ρ_{f}	Air density
σ	Stefan-Boltzmann constant $5.6703\ \frac{\text{W}}{\text{m}^2\text{K}^4}$
τ_1	Postfault duration of the first curative timeframe
τ_2	Postfault duration of the second curative timeframe
τ_{reach}	Duration to reach a grid situation
τ_{reopt}	Maximum reoptimization duration
τ_{rest}	Maximum restoration duration
τ	(Postfault) Duration
θ_{s}	Angle of incidence of sun rays
θ	Transformer phase angle
$\underline{S}$	Apparent power vector
$\underline{Y}$	Admittance
$\underline{\mathbf{Y}}_{\text{branch}}$	Branch admittance matrix
$\underline{\mathbf{Y}}$	Bus admittance matrix
$\underline{\mathbf{i}}$	Bus injection current vector
$\underline{\mathbf{s}}$	Apparent bus power vector
$\underline{y}$	Branch admittance
υ	Transformer's ratio magnitude
ϑ_{a}	Ambient temperature
ϑ_{film}	Film temperature of conductor
ϑ_{s}	Surface temperature of conductor
ϑ	Temperature

Symbol	Description
c	Cost coefficient
c	Primary contingency
e	Graph edge
f	Objective function
g	Inequality constraint function
h	Equality constraint function
j	Imaginary unit ($\sqrt{-1}$)
k_f	Thermal conductivity of air
$k_{\omega,\mathrm{cur}}$	Scaling factor for objective functions of curative situation
k_ω	Scaling factor for objective function
k_Q	Scaling factor for reactive power flow
k	Secondary contingency
l	Asset loading relative to I_PATL
m	Mass per unit length of conductor material
q_C	Convective cooling per unit length
q_J	Joule heating per unit length
q_R	Radiative cooling per unit length
q_S	Solar heating per unit length
q_n	Natural convective cooling
t_act	actual timestamp of a grid situation
t_last	Last base reference timestamp
t	Time/Reference timestamp
u	Generator status
v_W	Wind speed
v	Charging/discharging status of storage
x	Decision variable of subproblem
x	Decision variable

Sub- and superscripts

Sub-/Superscript	Description
$+$	Positive direction
$-$	Negative direction
$\downarrow$	Discharging direction
$\mathcal{R}$	Set of PST indexes
0state	Generators without binary status variables
2state	generators with on and off status
4state	generators with on, off, startup and shutdown status
PATL	Permanently Admissible Transmission Loading
TATL1	First curative timeframe
TATL2	Second curative timeframe
TATL	Temporarily Admissible Transmission Loading
N–1	N–1 case
avg	Average temperature
base	Base situation
branch	Branch
down	Down
end	End of the planning horizon
gen	Generator
in+	Extended incoming
init	initial value
in	Directly incoming
last	Last timestamp of the business day
max	Maximum
min	Minimum
nb	Neighbor
off	Off
on	On
out+	Extended outgoing
out	Directly outgoing
prim	Primary contingency situation

Sub-/Superscript	Description
pst	PST
rest	Restoration situation
re	Recovered situation
sec	Secondary contingency situation
shutdown	Shutdown
startup	Startup
stor	Storage
th	Thermal
up	Up
$\uparrow$	Charging direction
b	Branch index
d	Load index
g	Generator index
h	HVDC branch
i	From bus index of branch
k	To bus index of branch
n	Bus index
r	PST index
s	Index of BESS

A. RTS-GMLC Branch Conductors

Table A.1.: Branch connections and assigned conductor types

Branch (From-To-Suffix)	Conductor Type
101-102	Cable
101-103	243-AL1/39-ST1A (240/40)
101-105	243-AL1/39-ST1A (240/40)
102-104	243-AL1/39-ST1A (240/40)
102-106	243-AL1/39-ST1A (240/40)
103-109	243-AL1/39-ST1A (240/40)
103-124	Transformer
104-109	243-AL1/39-ST1A (240/40)
105-110	243-AL1/39-ST1A (240/40)
106-110	Cable
107-108	243-AL1/39-ST1A (240/40)
107-203	243-AL1/39-ST1A (240/40)
108-109	243-AL1/39-ST1A (240/40)
108-110	243-AL1/39-ST1A (240/40)
109-111	Transformer
109-112	Transformer
110-111	Transformer
110-112	Transformer
111-113	490-AL1/64-ST1A (490/65)
111-114	490-AL1/64-ST1A (490/65)
112-113	490-AL1/64-ST1A (490/65)
112-123	490-AL1/64-ST1A (490/65)
113-123	490-AL1/64-ST1A (490/65)
113-215	490-AL1/64-ST1A (490/65)
114-116	490-AL1/64-ST1A (490/65)
115-116	490-AL1/64-ST1A (490/65)
115-121a	490-AL1/64-ST1A (490/65)
115-121b	490-AL1/64-ST1A (490/65)
115-124	449-AL1/39-ST1A (450/40)

Branch (From-To-Suffix)	Conductor Type
116-117	550-AL1/71-ST1A (550/70)
116-119	490-AL1/64-ST1A (490/65)
117-118	434-AL1/56-ST1A (435/55)
117-122	449-AL1/39-ST1A (450/40)
118-121a	550-AL1/71-ST1A (550/70)
118-121b	550-AL1/71-ST1A (550/70)
119-120a	490-AL1/64-ST1A (490/65)
119-120b	490-AL1/64-ST1A (490/65)
120-123a	434-AL1/56-ST1A (435/55)
120-123b	434-AL1/56-ST1A (435/55)
121-122	449-AL1/39-ST1A (450/40)
123-217	550-AL1/71-ST1A (550/70)
201-202	Cable
201-203	243-AL1/39-ST1A (240/40)
201-205	243-AL1/39-ST1A (240/40)
202-204	243-AL1/39-ST1A (240/40)
202-206	243-AL1/39-ST1A (240/40)
203-209	243-AL1/39-ST1A (240/40)
203-224	Transformer
204-209	243-AL1/39-ST1A (240/40)
205-210	243-AL1/39-ST1A (240/40)
206-210	Cable
207-208	243-AL1/39-ST1A (240/40)
208-209	243-AL1/39-ST1A (240/40)
208-210	243-AL1/39-ST1A (240/40)
209-211	Transformer
209-212	Transformer
210-211	Transformer
210-212	Transformer
211-213	490-AL1/64-ST1A (490/65)
211-214	490-AL1/64-ST1A (490/65)
212-213	490-AL1/64-ST1A (490/65)
212-223	490-AL1/64-ST1A (490/65)
213-223	490-AL1/64-ST1A (490/65)

Branch (From-To-Suffix)	Conductor Type
214-216	490-AL1/64-ST1A (490/65)
215-216	490-AL1/64-ST1A (490/65)
215-221a	490-AL1/64-ST1A (490/65)
215-221b	490-AL1/64-ST1A (490/65)
215-224	449-AL1/39-ST1A (450/40)
216-217	550-AL1/71-ST1A (550/70)
216-219	490-AL1/64-ST1A (490/65)
217-218	434-AL1/56-ST1A (435/55)
217-222	449-AL1/39-ST1A (450/40)
218-221a	550-AL1/71-ST1A (550/70)
218-221b	550-AL1/71-ST1A (550/70)
219-220a	490-AL1/64-ST1A (490/65)
219-220b	490-AL1/64-ST1A (490/65)
220-223a	434-AL1/56-ST1A (435/55)
220-223b	434-AL1/56-ST1A (435/55)
221-222	449-AL1/39-ST1A (450/40)
301-302	Cable
301-303	243-AL1/39-ST1A (240/40)
301-305	243-AL1/39-ST1A (240/40)
302-304	243-AL1/39-ST1A (240/40)
302-306	243-AL1/39-ST1A (240/40)
303-309	243-AL1/39-ST1A (240/40)
303-324	Transformer
304-309	243-AL1/39-ST1A (240/40)
305-310	243-AL1/39-ST1A (240/40)
306-310	Cable
307-308	243-AL1/39-ST1A (240/40)
308-309	243-AL1/39-ST1A (240/40)
308-310	243-AL1/39-ST1A (240/40)
309-311	Transformer
309-312	Transformer
310-311	Transformer
310-312	Transformer
311-313	490-AL1/64-ST1A (490/65)

Branch (From-To-Suffix)	Conductor Type
311-314	490-AL1/64-ST1A (490/65)
312-313	490-AL1/64-ST1A (490/65)
312-323	490-AL1/64-ST1A (490/65)
313-323	490-AL1/64-ST1A (490/65)
314-316	490-AL1/64-ST1A (490/65)
315-316	490-AL1/64-ST1A (490/65)
315-321a	490-AL1/64-ST1A (490/65)
315-321b	490-AL1/64-ST1A (490/65)
315-324	449-AL1/39-ST1A (450/40)
316-317	550-AL1/71-ST1A (550/70)
316-319	490-AL1/64-ST1A (490/65)
317-318	434-AL1/56-ST1A (435/55)
317-322	449-AL1/39-ST1A (450/40)
318-321a	550-AL1/71-ST1A (550/70)
318-321b	550-AL1/71-ST1A (550/70)
319-320a	490-AL1/64-ST1A (490/65)
319-320b	490-AL1/64-ST1A (490/65)
320-323a	434-AL1/56-ST1A (435/55)
320-323b	434-AL1/56-ST1A (435/55)
321-322	449-AL1/39-ST1A (450/40)
325-121a	243-AL1/39-ST1A (240/40)
325-121b	243-AL1/39-ST1A (240/40)
318-223a	243-AL1/39-ST1A (240/40)
318-223b	243-AL1/39-ST1A (240/40)
323-325a	PST
323-325b	PST